

Chapter 4

4. Sub-bottom Profiling

4.1 INTRODUCTION

Land archaeologists have successfully used many geophysical techniques as non-intrusive methods of imaging the sub-surface including electromagnetics, ground penetrating radar (GPR), magnetics and seismic techniques (Bevan, 1991, Clark, 1986). Geophysics allows the sub-surface to be imaged without causing any disturbance to the area, which is beneficial as preservation is essential in archaeological surveys. The type of geophysical technique used is dependant on the buried target. Magnetic and electromagnetic methods are mainly used to determine the location, depth and size of metallic objects, which have different magnetic signatures and conductivities to the surrounding host rock. Seismic refraction and reflection methods can detect differences in acoustic properties that correspond to sub-surface interfaces, whereas GPR uses high frequency electromagnetic waves to image subtle internal interfaces. Combinations of these methods can reveal a great deal of information useful for locating and identifying possible archaeological resources in both marine and land situations. Geophysics is therefore an extremely useful and powerful tool for gaining insight into the stratal geometries of seismic sequences and seismic facies of depositional features at outcrop and core scale.

4.1.1 Project Aims

A high-resolution geophysical survey was acquired in March 2003 to aid in the interpretation of the geomorphology of part of the submerged and buried landscape on the Northern English Channel shelf. The main objectives of the survey were to image an area of the sub bottom stratigraphy offshore Sussex in order to delineate any fluvial valley systems and other geomorphic features. Reconstructing palaeo landscapes is critical to identify possible locations of archaeological resources, primary and secondary context sites, within the study area. Since the majority of the valley systems are infilled, sub-bottom geophysical profiling was used to provide an accurate image to fully investigate the evolution of these systems and determine the palaeo-environment.

4.1.2 Survey Location

In marine settings, geophysics can provide a consistent, cost efficient approach to imaging beneath the water. The study area was located offshore Sussex, just east of the Isle of Wight (Figure 1.1, Chapter 1) and comprised of a detailed 2D seismic survey. The main fluvial system onshore in this area is the Arun River that reaches the coast at Littlehampton, identified on figure 1.1. The survey aimed to map this fluvial system offshore into the Channel, to establish its path during the last glacial maximum and determine the evolution of the river meanders. Figure 4.1 identifies the position of the seismic lines shot over a total of 86 hours and totalling 650km of new lines. The survey is concentrated in the northern region of the study area with the intention of constraining the course of the Arun river channel offshore. This can then be mapped south into the northern palaeo channel river using a less dense survey further in the area of extensive commercial seismic. Critically the new data was collected in the zone between the coast and the aggregate licence block to enable an onshore–offshore correlation not previously possible.

4.1.3 Previous Work

Previous seismic surveys have been carried out in this area, as identified on Figure 4.2. The southern region of the study area has been extensively covered with 2D seismic surveys acquired by several aggregate industries (data provided by Hanson Aggregate Marine Ltd and United Marine Dredging Ltd) over the past 15 years. These past surveys were acquired under similar conditions as this survey, but with the aim of locating gravel and sand deposits to extract for industrial use. The surveys all used a towed Boomer source with differing frequencies in order to image within the top 5m of the seabed. The dredged areas are clearly identified using the multibeam surveys (chapter 3) and do cause problems imaging beneath due to the resulting irregular sea bed.

The recorded seismic traces are all analogue, not digital (i.e. are available as paper copy only), and only have a frequency filter applied to the raw records to remove any swell noise. This means no further processing can be applied to the records once they are acquired. The surveys were also only acquired using single channel geometry (figure 4.3); therefore even if they were digital records they would not be able to provide information on velocities and AVO unlike multi-channel surveys.

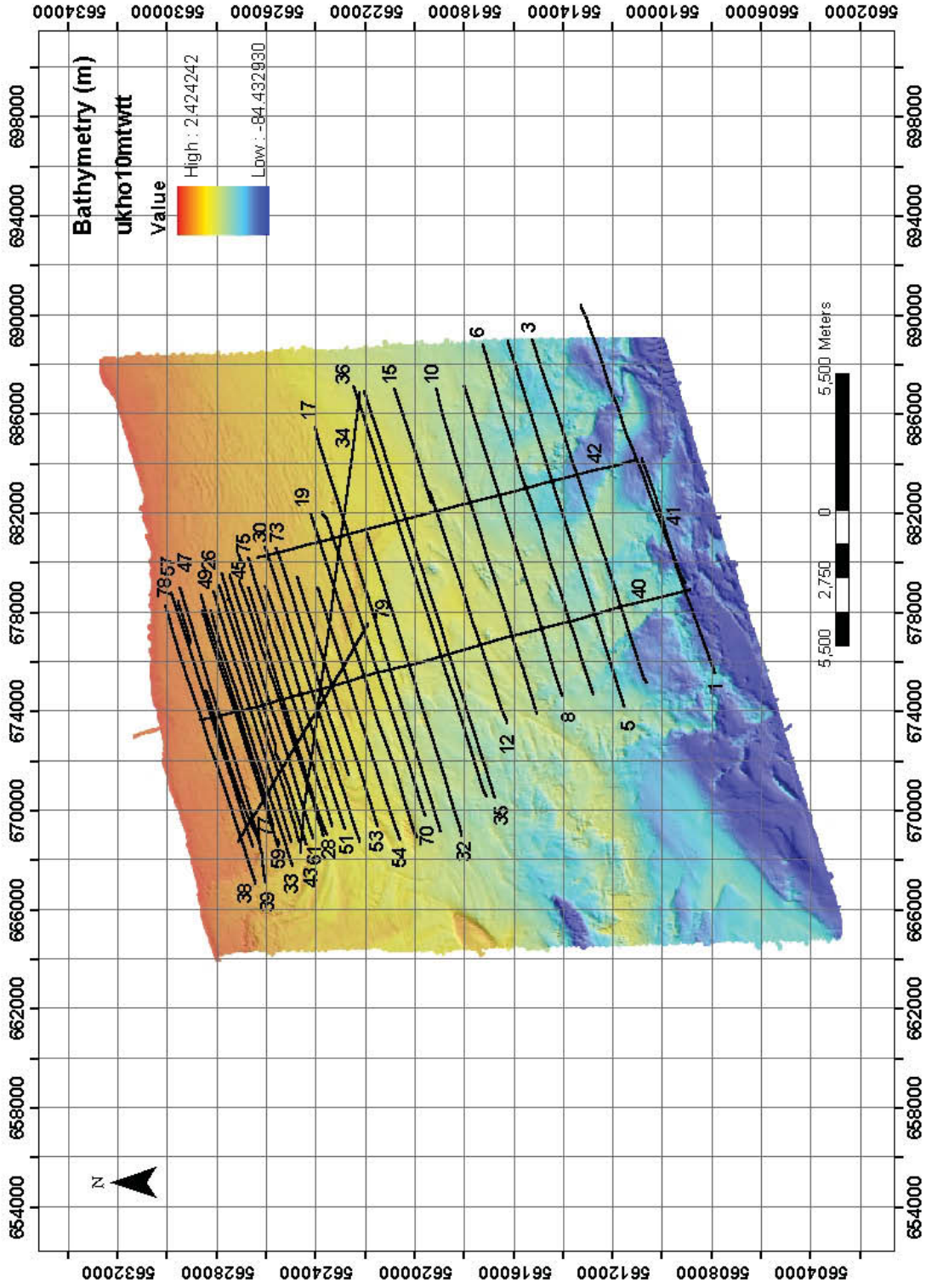


Figure 4.1: Location map of study area offshore of Littlehampton showing 2003 Boomer seismic reflection survey track lines (black) superimposed on singlebeam bathymetry data.

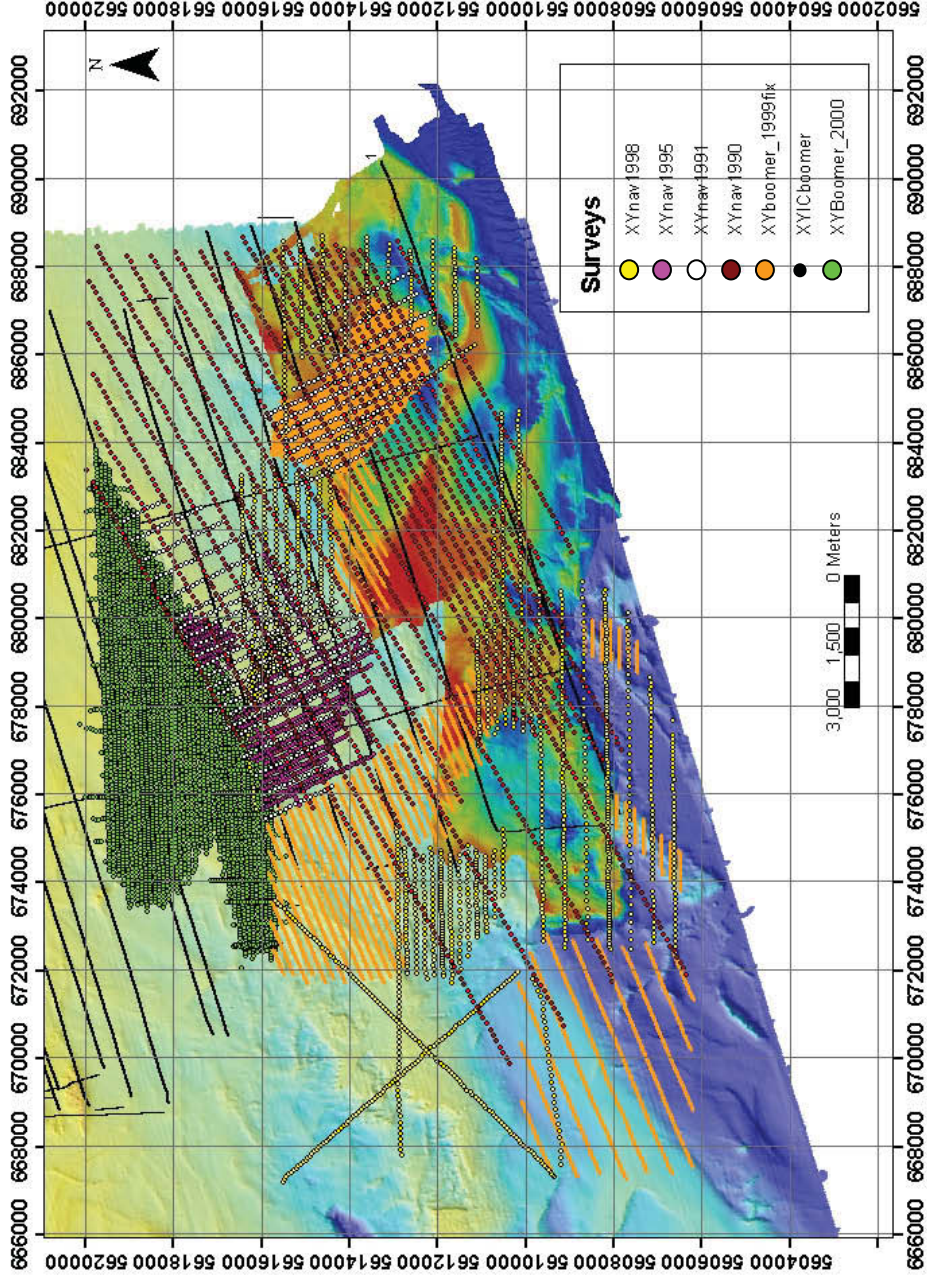


Figure 4.2: Previous seismic reflection surveys as acquired by aggregate companies (courtesy of Hanson & Marine). The key shows the different coloured track lines corresponding to the different years of surveys (XYICboomer is the 2003 survey). The lines are superimposed on both the singlebeam bathymetry data and the newly acquired multibeam bathymetry dataset (bolder colours in the SE corner).

4.2 ACQUISITION

4.2.1 Sources

A P-wave source is used to generate seismic energy throughout the subsurface. There are several different types of sources used for exploration purposes. The most ideal source to use is an implosive one, which doesn't produce any bubble pulse and therefore gives a spikier response. This is desirable since the recorded signal is a convolution of the response from the reflector and the response due to the source. If the source produces a spike response, the signal will be proportional to the reflection coefficients (earth's response) and consequently the recorded trace will give an improved account of the sub-surface. Contamination of the record can occur if bubbles are produced due to an explosive submerged source resulting in a ringing effect throughout the recorded traces. It is therefore desirable to use an implosive source if the survey requires submerged acquisition.

For this survey a Boomer source was used, which was thought to be the most suitable P-wave source. It depends on electrical energy for the sudden movement of a plate by a transducer device. The movement of the plate creates a vacuum that implodes causing a pulse of energy to be transmitted through the water. This energy then travels through the sub-surface and reflects from internal interfaces back up to the surface where it is recorded. The implosive nature means no bubble pulse is produced.

The Boomer also provided high frequencies were desirable to image shallow sub-surface detail for this survey. The plate can disperse a maximum of 300J a shot at 1 pulse per second. This corresponds approximately to a 500 – 3000Hz frequency range. The high frequencies enable an image to be formed with high vertical and lateral resolution. The large bandwidth (frequency range) creates a spikier response in the frequency domain therefore allowing the signal to more accurately model the earth's response.

4.2.1.1 Lateral Resolution

The dependence of lateral resolution on frequency can be shown using Fresnel zones or an acoustic footprint. The size of this area depends on the frequency of the transmitted ray (equation 4.1), where f is the frequency of the wave, v is the average velocity and t is the two-way travel time to the reflector.

$$radius = \frac{v}{2} \sqrt{\frac{t}{f}} \quad \text{Equation 4.1}$$

Therefore if a reflector is greater in areal extent than the radius of the Fresnel zone, the reflection shows the shape of the reflector. If however the reflector is smaller than the Fresnel zone, diffractions dominate and the reflector shape is difficult to distinguish. For this survey the radius can be calculated to be 7.3m – 17.9m (using parameters: 500-3000Hz, 250ms, 1600m/s) and within channels (50ms) of 3.2m – 8m.

4.2.1.2 Vertical Resolution

Vertical resolution is also dependant on frequency and is controlled by how thick a bed must be before a reflection from its top and bottom can be distinguished from a reflection from a single impedance boundary. For an increase in acoustic impedance with depth, reflections from the top and bottom of a thin bed will be interference free up to thickness of $\lambda/2$ (where λ is the wavelength, related to frequency by the velocity (eq. 4.8)). For thinner beds the reflections will destructively interfere until the thickness is equal to $\lambda/4$, where maximum destructive interference will occur. Below a thickness of $\lambda/8$ the wave-shape will be indistinguishable from that of a single bed. For the channel sediments ($v=1600\text{m/s}$) the vertical resolution would be between 6mm ($f = 3000\text{Hz}$) to 40cm ($f=500\text{Hz}$).

4.2.2 Receivers

The signal is recorded using hydrophones (or channels – CHAN on following plots), which are towed in a streamer behind the vessel. Unlike conventional streamers used by commercial seismic vessels, the streamer used in this survey did not have ‘birds’ to maintain the streamer below the sea surface. This had a direct impact on the system performance as a function of sea state as the streamer was subject to wave motion.

The survey is different from previous performed in the area since it uses several hydrophones in a streamer, unlike the more conventional single channel surveys used by the aggregates companies (figure 4.3 and 4.4). This should act to enhance the signal when stacking together the response for all receivers. The survey used a 60m streamer with 60 hydrophone channels and a receiver interval of 1m.

In addition to enhancing the signal, using multiple channels should also act to suppress incoherent ambient noise. Such noise should not appear in the same place on each record and therefore will destructively interfere once the records are combined together.

4.2.3 Data Recording

The field data collected was recorded on 12 DDS-4 DAT tapes in SEG-D format. The sample rate was $125\mu\text{s}$ with a record length of 250ms, although this was changed to $62\mu\text{s}$ and 125ms in the shallower regions of the study area. The SEG-D format then required translating to SEG-Y back in London. The total raw data volume was approximately 50GBytes. Table 4.1 shows the acquisition table including the date, time, exact location and weather conditions, as well as the acquisition parameters for the survey.

4.2.4 Geometry Assignment

In order to assign the geographic position of each shot and receiver the navigational (latitude, longitude, time) information recorded had to be merged with the seismic log files (shot number, time).

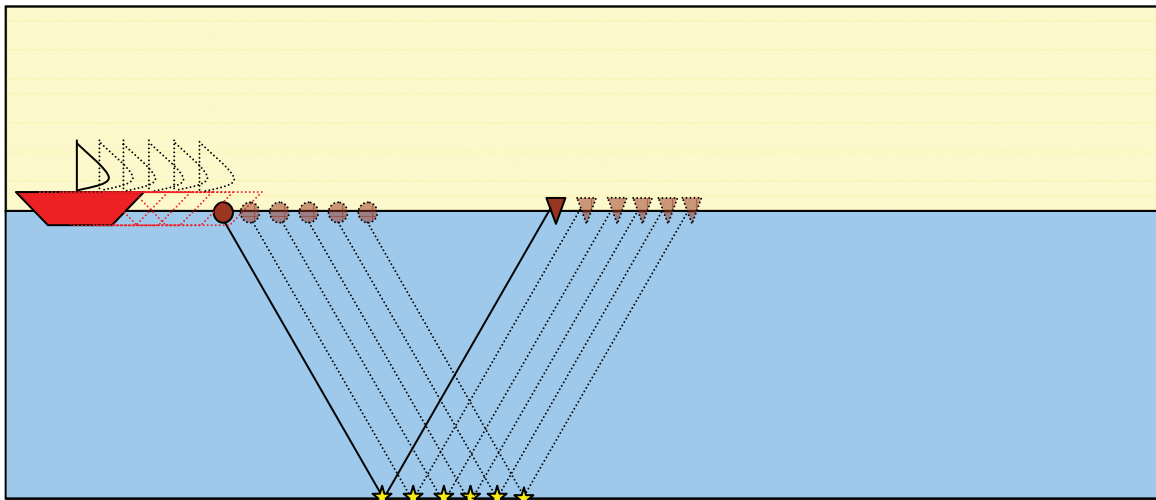


Figure 4.3: Single channel acquisition.

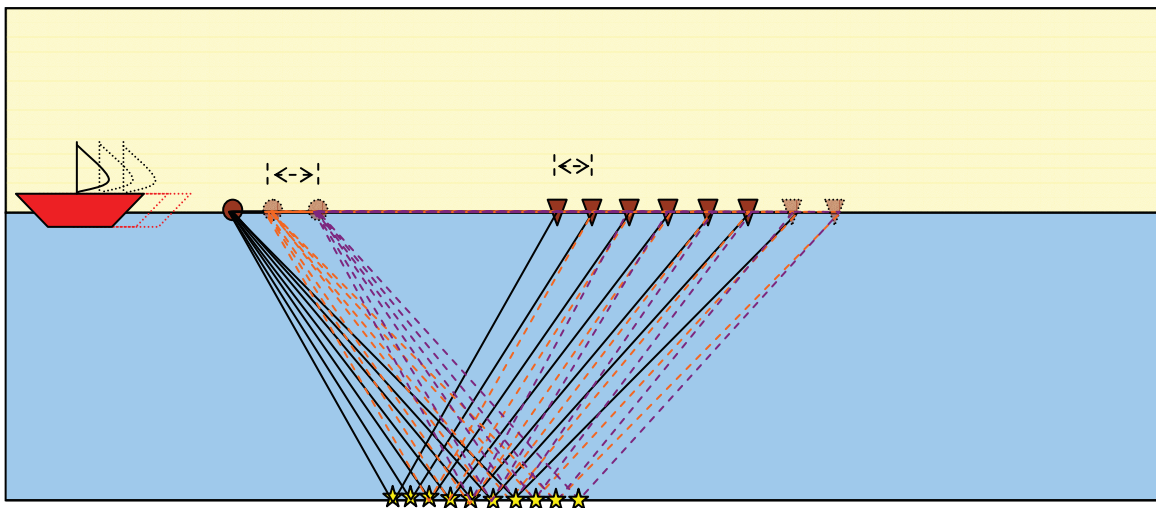


Figure 4.4: Multi-channel acquisition. The circles are the sources and the up-turned triangles are the receivers. The stars represent the position imaged on the reflector (common offset points (COP's) for 4.3, common depth points (CDP's) for 4.4). The bold source and receiver rays show the geometry for one shot, whereas the dashed equivalents show the geometry of the previous shots (5 previous shots in 4.3, 2 in 4.4).

The merging was performed using a FORTRAN program written for the task. Geometry assignment (in order to give individual shot and receiver positions) was performed in ProMAX™. The offsets between the GPS antenna and the boomer plate were initially estimated from measurements taken during acquisition and then adjusted by checking the alignment of the direct wave recorded after geometry assignment.

Date	Line No.	Start time	Shot No.	Start Lat 50° N	Start Long 0° W	End time	Shot No.	End Lat 50° N	End Long 0° W	Sample rate (µs)	Duration (ms)	Weather conditions	
04/04/2003	1	09:44:06.47	740	38.39631010	18.42347430	12.17:25.17	9553	35.76454390	31.16903060	125	250	Okay	
	2	12:19:17.77	9554	35.835940790	31.34433220	12.34:17.89	10433	37.16149400	31.42399330	125	250	Okay	
	3	12:35:37.25	10434	31.39866510	19.44139.62	14.41:39.62	17992	39.49606530	19.49642060	125	250	Okay	
	4	14:42:35.37	17993	39.52742270	19.43312980	14.48:34.47	18340	39.93748300	19.41401470	125	250	Okay	
	5	14:50:39.15	18341	40.02771870	19.57157330	16.10:44.09	23143	37.76372900	32.21990040	125	250	Okay	
05/04/2003	6	09:09:12.00	1	40.57811480	19.66427440	11.45:05.31	9298	38.42809850	31.76568850	125	250	Moderate, swell incr	
	7	11:46:57.00	9299	38.46866090	31.93005300	11.52:05.99	9608	38.91744570	32.04387120	125	250	Moderate, swell incr	
	8	11:54:34.00	9609	39.08042100	31.86127010	13.25:32.62	14939	41.01383350	21.04117640	125	250	Moderate, swell incr	
	9	13:27:27.00	14940	41.09932320	20.89342970	13.31:55.39	15209	41.45814420	20.93725390	125	250	Moderate, swell incr	
	10	13:34:38.00	15210	41.61492050	21.11619580	14.45:42.83	19436	39.66834470	32.39151080	125	250	Moderate	
	11	14:48:07.00	19437	39.71627060	32.70820580	14.54:51.48	19752	40.21347730	32.72637850	125	250	Moderate	
	12	14:57:30.00	19753	40.32709960	32.60705900	16.30:50.14	25350	41.83989570	24.59794370	125	250	Moderate	
	06/04/2003	13	10:02:00.00	1	42.09514260	24.43863400	10.11:44.40	580	41.96968320	25.28099990	125	250	Okay to moderate
		14	10:11:55.00	581	41.96587170	25.29620410	10.15:34.09	798	41.82637190	24.99132670	125	250	Okay to moderate
		15	10:15:43.00	799	41.83009650	24.96711530	10.41:00.03	2315	42.53734190	21.03713760	125	250	Okay to moderate
		16	10:43:33.00	2316	42.71766310	21.01757060	11.06:50.47	3712	44.29714510	22.06338810	125	250	Okay to moderate
		17	11:09:00.00	3713	44.28907150	22.26802310	13.11:41.87	11022	41.85590130	36.30451830	125	250	Okay to moderate
18		13:13:58.00	11023	41.98918150	36.48339510	13.17:59.54	11265	42.31957240	36.52861370	125	250	Okay to moderate	
19		13:19:26.00	11266	42.37976810	36.42885330	15.35:30.94	19396	44.46159810	25.18133820	125	250	Okay to moderate	
20		15:37:09.00	19397	44.55422760	25.19949040	15.42:33.00	19720	44.92730160	25.25538940	125	250	Okay to moderate	
21		15:44:52.00	19721	44.96245680	25.54325280	16.36:30.00	22812	43.52869430	33.33405960	125	250	Okay to moderate	
09/04/2003		22	09:18:53.00	1	44.43795510	27.02823150	10.38:46.00	4778	42.74518360	36.13638660	125	250	Okay
		23	10:40:55.00	4779	42.85638150	36.26120400	10.52:46.92	5491	43.76622970	36.24075600	125	250	Moderate
	24	10:54:14.00	5492	43.81285090	36.07061910	11.08:21.59	6339	44.08053350	34.35853990	125	250	Rapid decrease	
	10/04/2003	25	08:48:55.00	1	45.25378750	27.47914210	08.56:30.07	456	45.09396550	28.44170350	62.5	125	Moderate to okay
26		09:46:18.00	457	46.43378480	27.21116350	11.06:23.00	5246	44.37920250	31.30117290	62.5	125	Moderate to okay	
27		11:11:11.00	5247	44.31319520	30.70954590	11.15:51.32	5528	44.24563960	30.13256200	62.5	125	Okay to good	
28		11:22:41.00	5529	44.15034270	29.28385560	12.33:27.00	9747	46.06167850	26.52366430	62.5	125	Okay to good	
29		12:35:28.00	9748	45.96318070	26.35167500	12.40:08.92	10029	45.58542290	26.23104920	62.5	125	Okay to good	
30		12:42:25.00	10030	45.47195830	26.35030250	14.17:35.00	15703	43.62138150	36.55363300	62.5	125	Okay to good	
31		14:19:41.00	15704	43.48429170	36.63301410	14.46:22.70	17304	41.45608590	36.61430380	62.5	125	Okay to good	
32		14:48:17.00	17305	41.41517190	36.42230900	16.17:00.70	22618	43.24623180	25.92311650	62.5	125	Okay to good	
11/04/2003	33	09:10:42.00	2	46.69910610	28.46276940	10.15:40.63	3778	45.10440090	37.33134450	62.5	125	Okay to good	
	34	10:21:03.00	3779	44.92846480	36.83379300	12.27:15.62	11326	43.29338950	21.12135900	62.5	125	Okay to good	
	35	12:32:42.00	11327	43.19074010	21.12175870	14.39:55.00	18934	40.65109450	35.18572330	62.5	125	Okay to good	
	36	14:43:45.00	18935	40.83397550	35.12034040	16.30:39.00	25292	43.42154830	20.89074550	62.5	125	Okay to good	
12/04/2003	37	10:01:25.00	1	46.73089100	28.30519020	10.53:05.00	3068	45.49469110	35.39497070	62.5	125	Poor	

15/04/2003	38	08.38:46.00	1	47.69082060	28.22118230	09.46:33.00	4047	45.92488040	37.89026900	125	Moderate to okay
	39	09.50:59.00	4048	45.70347370	37.82209550	10.56:39.00	7979	46.77710540	31.70373380	125	Moderate to okay
	40	11.05:49.00	7980	47.01786480	32.19152700	13.26:45.39	16398	36.23831950	28.27615660	125	Moderate to okay
	41	13.30:38.00	16399	36.33376140	28.04404230	14.29:19.00	19915	37.19812640	23.7278580	125	Moderate to okay
	42	14.31:56.00	19916	37.36093050	23.77743260	16.22:23.00	26542	45.64740920	26.66481590	125	Moderate to okay
16/04/2003	43	08.33:17.00	1	46.32774210	28.11250170	09.56:53.00	4168	45.11779230	36.47954520	125	Good
	44	09.58:47.00	4169	44.97872510	36.54967400	10.06:18.00	4620	44.40118460	36.57821150	125	Good
	45	10.09:47.00	4621	44.41916580	36.29431440	11.52:52.00	10809	46.06761560	27.42577660	125	Good
	46	11.54:39.00	10810	46.18898450	27.42387460	12.04:13.00	11384	46.91281140	27.56041210	125	Good
	47	12.06:29.00	11385	46.90738960	27.91098330	13.03:33.25	14807	45.37946240	36.55815820	125	Good
	48	13.05:39.00	14808	45.21579100	36.63654780	13.08:38.00	14987	44.96148880	36.61486600	125	Good
	49	13.10:34.00	14988	44.95362230	36.44712880	14.37:21.00	20196	46.50312950	27.58626540	125	Good
	50	14.39:24.00	20197	46.39216200	27.47112360	14.48:36.00	20747	45.59397420	27.48088310	125	Good
	51	14.50:31.00	20748	45.49700730	27.68900920	15.50:36.00	24350	43.94016610	36.11644180	125	Good
	52	15.53:07.00	24351	43.79030230	36.28682370	15.59:25.04	24729	43.23291410	36.26115250	125	Good
	53	16.01:54.00	24730	43.22839310	36.01034370	17.11:49.54	28920	44.79860140	27.374110530	125	Good
17/04/2003	54	08.50:41.00	1	44.35763960	27.80148810	10.12:45.00	4905	42.74582850	36.52265260	125	Good
	55	10.17:13.00	4906	42.99080770	36.45018900	10.50:45.00	6918	43.75404050	32.67185270	125	Good
	56	10.52:28.00	6919	43.90203190	32.75977880	11.21:57.00	8688	46.36284540	33.68688110	125	Good
	57	11.24:53.00	8689	46.46601670	33.45744070	12.20:46.00	12042	47.40481910	28.04562810	125	Good
	58	12.23:05.00	12043	47.23888820	27.96191290	12.27:09.00	12287	46.92861220	27.87315090	125	Good
	59	12.30:56.00	12288	46.89644070	28.46036980	13.20:56.00	15286	45.40349360	36.64452590	125	Good
	60	13.23:08.00	15287	45.21887910	36.71156610	13.29:46.32	15685	44.64083460	36.63126660	125	Good
	61	13.32:56.00	15686	44.64656670	36.33844830	15.01:34.00	21002	46.26862310	27.21865940	125	Good
18/04/2003	62	09.55:22.00	1	45.64917030	24.89911660	11.33:40.00	5898	43.57058140	36.28206110	125	Moderate
	63	11.42:58.00	5899	43.76600140	35.74657840	12.15:10.00	7832	44.78192870	33.27666110	125	Rapid decrease
21/04/2003	64	10.06:05.00	1	45.58793990	36.50104720	11.12:25.00	3979	47.31799030	26.92123750	125	Moderate to okay
	65	11.17:52.00	3980	47.00260540	26.83180360	11.30:02.00	4710	46.25894750	27.06798420	125	Moderate to okay
	66	11.33:15.00	4711	46.16734490	27.29771570	11.48:27.00	5623	45.62435520	28.32925110	125	Moderate to okay
	67	11.50:57.00	5624	45.76275590	28.48140020	12.12:22.00	6904	47.50766390	29.09304240	125	Moderate to okay
	68	14.27:11.00	6905	46.06945710	36.45568620	15.50:45.00	11917	47.47928540	28.54306690	125	Moderate to okay
	69	15.54:04.00	11918	47.49754080	28.83353600	16.13:29.00	13084	46.46749160	31.14501140	125	Moderate to okay
22/04/2003	70	08.07:24.00	1	44.19857280	25.21038740	09.34:03.00	5199	42.18096430	35.75165600	125	Okay to good
	71	09.35:36.00	5200	42.27192250	35.84914610	09.50:49.00	6113	43.51456080	36.32082930	125	Okay to good
	72	09.52:33.00	6114	43.58343320	36.11559480	10.01:06.00	6627	43.81078820	34.86055950	125	Okay to good
	73	10.05:29.00	6628	43.82557800	34.20928490	10.54:38.00	9549	45.23664620	26.34506830	125	Good
	74	10.56:14.00	9550	45.35967680	26.31759780	11.02:36.00	9932	45.86280620	26.47759520	125	Good
	75	11.04:50.00	9933	45.84786470	26.67842130	12.40:53.00	15695	44.21016910	36.02072540	125	Good
	76	12.42:39.00	15696	44.31302720	36.13855250	12.58:40.77	16656	45.70435650	36.64174260	125	Good
	77	13.00:57.00	16657	45.81438370	36.38475380	14.08:59.00	20749	47.36512990	27.58928210	125	Good
	78	14.12:46.39	20750	47.55052770	27.78737920	15.15:19.12	24485	45.95804720	36.59844950	125	Good
	79	15.23:48.46	24486	46.27942260	36.40959220	16.45:04.56	29351	43.28999290	29.06703600	125	Good
24/04/2003	80	08.33:29	1	47.21419500	27.44721990	09.48:20.01	4489	45.39656500	37.37504250	125	Moderate to poor

Table 4.1: Observation Log for 2003 boomer seismic reflection survey, displaying the date, time, line number, shot numbers, position, acquisition parameters and weather observations. Weather scale; Good – Okay – Moderate – Poor, with increases or decreases in weather quality also occurring during a day.

4.3 METHODS

4.3.1 Seismic Theory

Seismic methods of geophysical exploration utilize the fact that elastic waves travel with different velocities through different lithologies within the Earth. These elastic waves propagate through the subsurface until they encounter an abrupt change in elastic properties. At this discontinuity part of the energy is reflected and remains in the same medium as the incident energy. The balance of the energy is refracted into the other medium with an abrupt change in the direction of propagation occurring at the interface (figure 4.5). The direction of propagation in both media can be related to the angle of incidence using Snell's law, where θ_1 is the angle of incidence, θ_2 is the angle of refraction, v_1 is the velocity in the incident layer, and v_2 is the velocity in the lower medium.

$$\frac{\sin \theta_1}{v_1} = \frac{\sin \theta_2}{v_2} \quad \text{Equation 4.2}$$

The seismic reflection technique is used ubiquitously in shallow sub-seafloor profiling. A P-wave source is used to produce the seismic waves that are reflected and returned to the surface where they can be recorded. By observing the amplitudes and travel-times of these arrivals, information can be determined about the lithology from which they were reflected.

4.3.2 Noise

Seismic reflection records also contain undesirable events known as noise. This noise can occur in two forms; ambient or coherent.

4.3.2.1 Ambient Noise

Ambient noise is also known as random noise such as swell noise or background noise. This is very variable across the survey and depends on the surrounding conditions. For the surface towed streamer used here, ambient noise depends largely on the sea-state.

4.3.2.2 Coherent Noise

Coherent noise is energy that appears regularly on the records such as diffractions, multiples and linear events. Figure 4.6 shows occurrence of such noise on a shot record. Although the first seabed reflection is easily identified, it is difficult to pick many other reflection events. Diffractions occur due to an abrupt change in seismic properties of the ground, which can cause major problems by contaminating the recorded traces and affecting interpretation. Multiples occur due to reverberations between interfaces before the energy is recorded. There are many different types of multiples, some more problematic than others. The challenging multiples in this survey are identified in section 4.4, where digital processing is used to suppress such noise events.

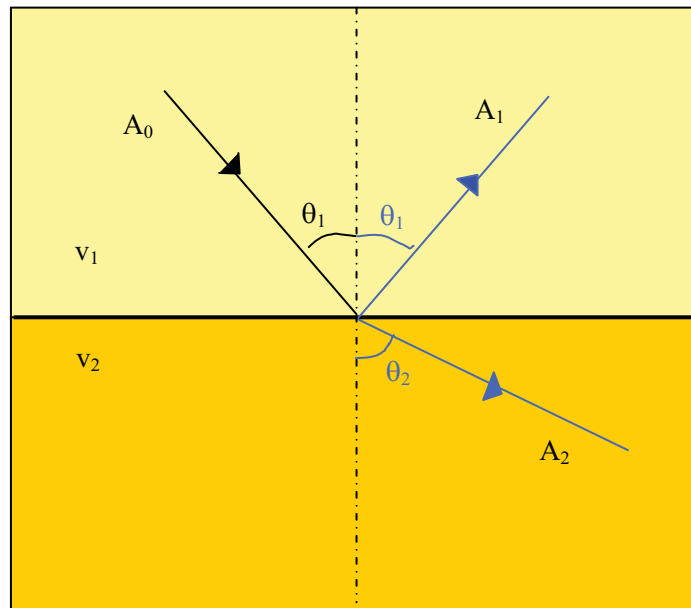


Figure 4.5: Partitioning of energy at an interface. A_0 is the incident ray, which splits into a reflected component A_1 and a refracted component A_2 .

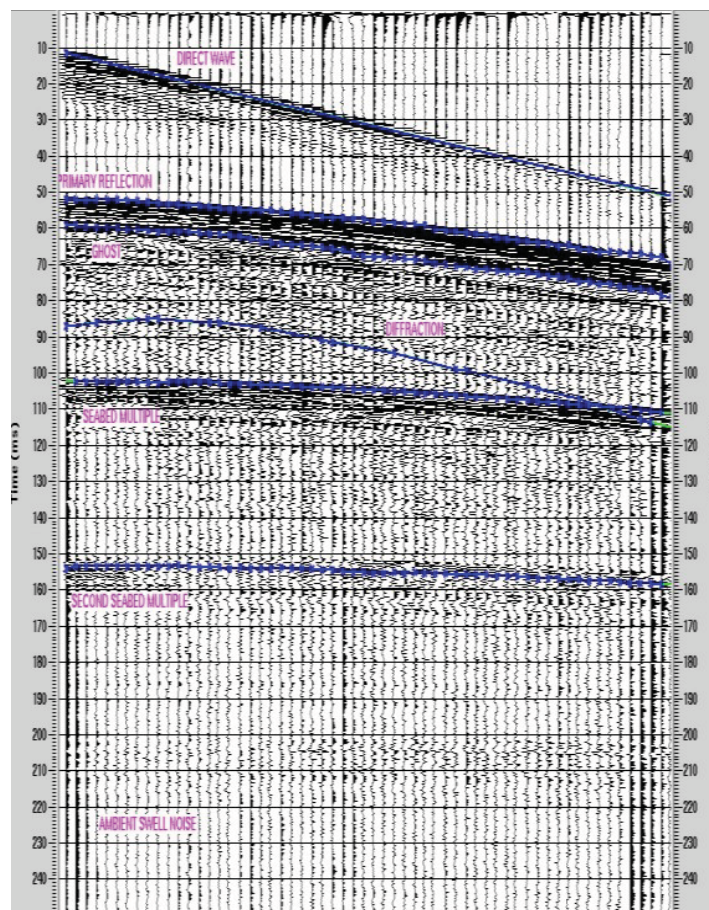


Figure 4.6: Shot record showing undesirable noise contaminating the primary reflection including the direct wave, the ghost arrival, diffractions, ambient noise and the seabed multiple. The record shows the output of each of the 60 hydrophone receivers for a single shot.

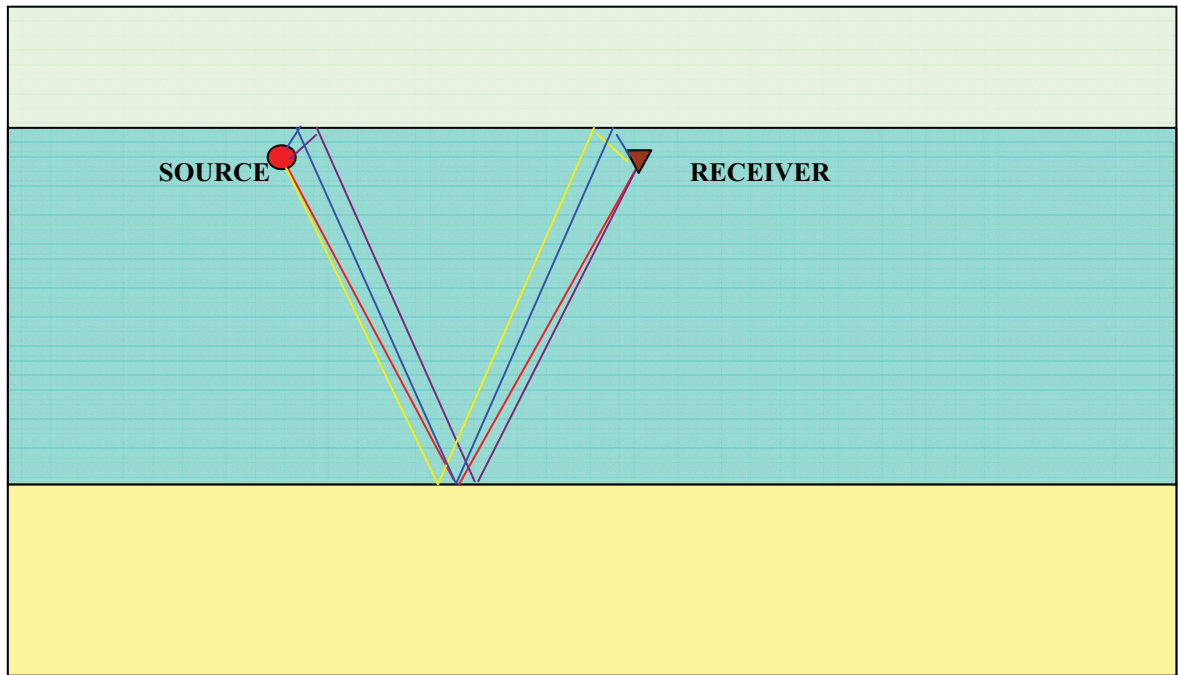


Figure 4.7 Ghost arrivals generated at the source (purple ray) or at the receiver (yellow ray) or both (blue ray). These arrivals appear just after the primary arrival (red ray) on the recorded record.

4.3.2.3 Ghost Arrivals

The ghost arrivals are a form of coherent noise, especially problematic in marine surveys using submerged sources and receivers. They are short path multiples caused by the additional reflection from the sea surface either above the source or the receiver, or both (figure 4.7). These arrivals can be high in amplitude and could mask any near surface reflectors.

The time lag (Δt) that the ghost arrivals appear behind the primary arrivals at the near and far offsets can be calculated using equation 4.3, assuming a water velocity (v_w) of 1500m/s, a source and receiver depth (d) of 1m and a seabed depth of 35m.

$$\Delta t = \frac{2d \cos \theta}{v_w} \quad \text{Equation 4.3}$$

For the near offset trace (30m), the angle of incidence (θ) is 23.2° , which gives a time lag of 1.22ms for a single ghost reflection either at the source or receiver. The time lag is doubled to 2.44ms if there is a ghost reflection at both the source and receivers. For the far offset trace (90m), the incident angle is 18.4° , which leads to a lag time of 1.27ms for a single ghost or 2.54ms for a double.

An important aspect of the sea surface ghost is that it has the reverse polarity to the primary downward energy and so causes a notch in the frequency spectrum at $1/\Delta t$ (750Hz - figure 4.12A).

4.4 PROCESSING TECHNIQUES

The principle limitation of the reflection technique is the difficulty of enhancing reflections, which can be masked by other arrivals such as multiples and diffractions, as mentioned previously. Reducing this consequence involves a large amount of processing after acquisition. ProMAX™ seismic processing software was used in this study to apply these post-acquisition processes with the aim of increasing the signal to noise ratio and therefore enhancing the desired energy.

Some caution needs to be applied when applying processing techniques to high frequency surveys. The high frequencies are needed to resolve fine structures, as mentioned previously, but they can be destroyed by inappropriate acquisition parameters or processing techniques (e.g. incorrect NMO causes destructive interference of higher frequency arrivals (Nissen, 1999)). High-resolution surveys are therefore more sensitive to processing techniques (high frequencies have a much smaller velocity error than low frequencies) and care needs to be taken when applying post-acquisition processes.

4.4.1 Amplitude Losses

There are several factors that can act to reduce the amplitude of the incoming seismic energy (figure 4.8). Some of these factors can be corrected for with the use of post acquisition processing. The desired energy must be able to survive various loss mechanisms, such as geometrical divergence, transmission and reflection losses, and absorption losses, while propagating back to the receivers to be recorded. Geometrical spreading causes the energy to be spread over a larger area as it propagates through the earth, which causes a reduction in amplitude, but not a loss of energy. Energy is however lost within the Earth due to absorption. Higher frequencies are attenuated due to absorption more quickly than lower frequencies and therefore there is a loss in the high frequency content for the recorded signal from deeper horizons. This can lead to a reduction in resolution as discussed in chapter 4.2.1. Additionally, rugged relief at the incident interface may prevent the downward propagating energy to be phase coherent. This may cause energy reflected to destructively interfere and not appear as coherent arrivals on the record. These arrivals would then be attenuated when the records are stacked together.

4.4.2 Pre-stack Processing

There are various techniques that can be applied to the digital dataset in order to enhance the desired image, giving the digital data an advantage over the previously acquired analogue data collected by the aggregates companies. Figure 4.9 shows a raw shot of the data before any processes have been applied. Problematic arrivals are highlighted on this figure that would obscure the signal and make interpretation arduous. Pre-processes are applied to reduce this unwanted energy and improve the imaging of target reflectors.

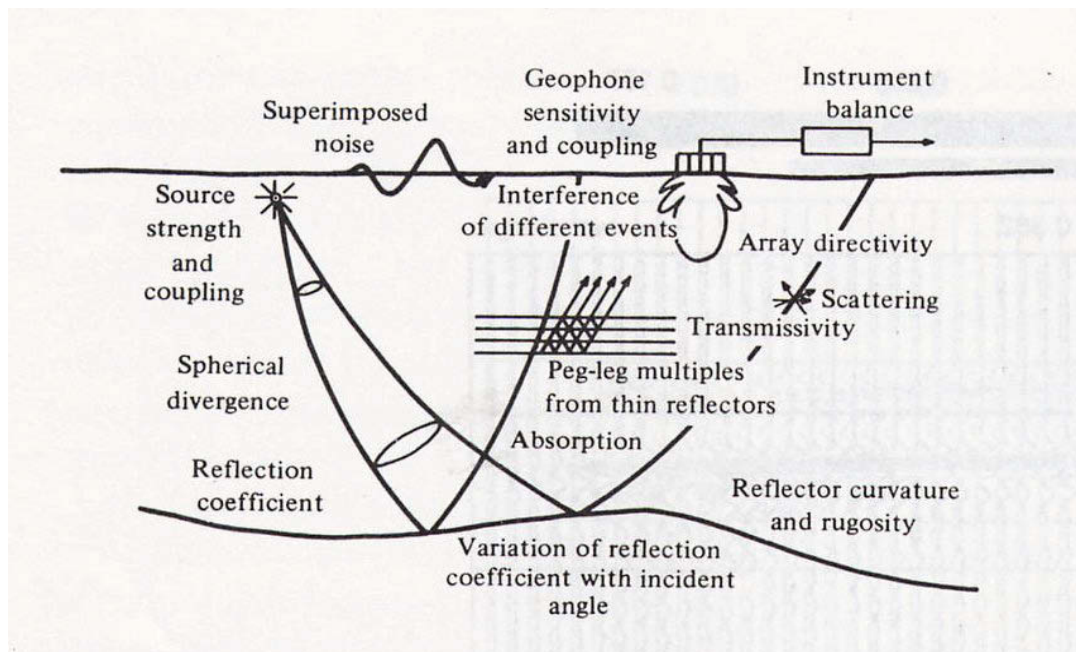


Figure 4.8: Factors affecting the amplitude of a recorded wave (Diagram after Sheriff and Geldart, 1995). The problematic factors for this survey were absorption, reflector curvature, scattering and interference from multiples. All these factors act to suppress the recorded reflection from the internal interface.

4.4.2.1 Trace Muting

A top mute can be applied to the shot records to remove the linear direct wave energy. This is energy that has not been reflected, but travels directly from the shot to the receiver through the water. The top mute is positioned just above the seabed reflection so as to remove any energy that arrives before this first reflection (figure 4.10). The resulting shot records can be seen in figure 4.11, which show that this linear energy has been sufficiently removed.

4.4.2.2 Bandpass Filtering

Frequency filtering is required to remove low frequency noise such as swell noise derived from the seastate. It may also be used to filter out any high frequency ambient noise that may be present in the record. The frequency content of the data can be found by taking a Fourier transform of the time-offset ($t-x$) domain to transform it into the frequency domain.

The sample rate is an important consideration when imaging within the frequency domain. Using equation 4.4, if samples are taken at a time interval of Δt , any frequency above $1/(2\Delta t)$ will appear as a lower frequency in the reconstruction of the wave (aliasing).

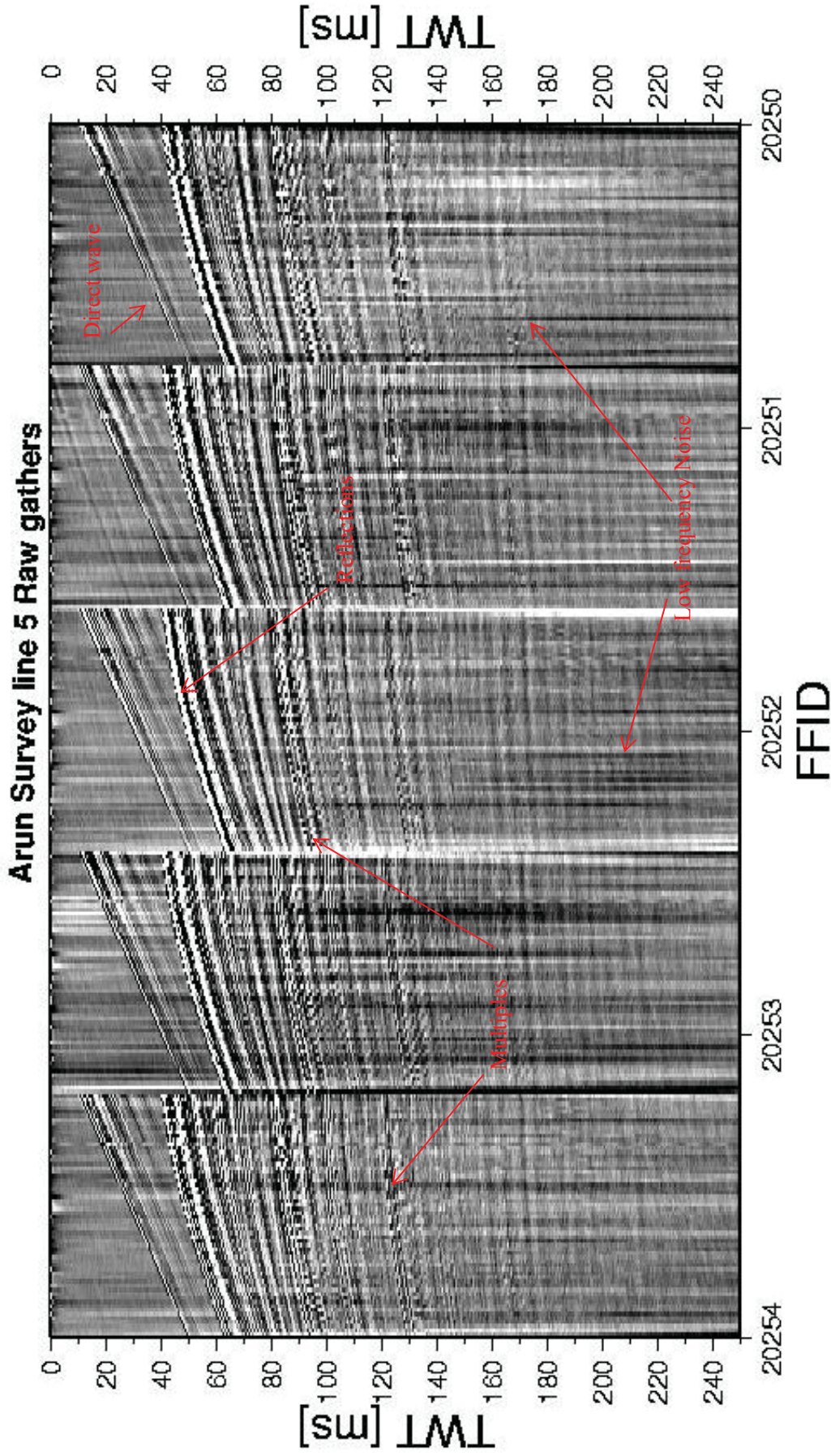


Figure 4.9: Raw gathers for an example seismic line identifying the direct wave, primary reflections, multiples and low frequency ambient noise. There are five shot gathers (FFID's) shown, with the horizontal axis for each panel being the source-receiver offset, which varies from 15m to 75m.

The frequency $1/(2\Delta t)$ is known as the Nyquist frequency (f_{nq}). For this survey the Nyquist frequency was 4000Hz (125 μ s sample rate) for the deeper areas and 8000Hz (62 μ s sample rate) for the shallower areas of the study grid. Since there wasn't any signal expected over 3000Hz for the boomer system used, there should be no aliased energy and therefore all energy imaged within the frequency domain should appear in its correct position.

$$f_{nq} = \frac{1}{2\Delta t} \quad \text{Equation 4.4}$$

Figure 4.12 displays the frequency spectrum for a single shot. This shows the low frequency spike corresponding to the swell noise (at about 1 Hz), which causes contamination of the record. The frequency range of the signal is also identified, being predominantly between 150 and 2000Hz. A Butterworth bandpass filter can be used to filter out any unwanted frequencies outside this range. Parameter tests were used to determine the most appropriate parameters for the filter. Several factors needed to be taken into account when choosing the ideal frequencies. The bandwidth must be kept broad since the broader the bandwidth the more compressed the filter operator, hence the more resolved the response. Also, to avoid Gibbs phenomenon (ringing effects), tapered edges needed to be applied to the filter design. The final parameters used were 24-150-3500-36 (slope-corner-corner-slope), as shown schematically in figure 4.13. The resulting shot record after frequency filtering can be observed in figure 4.14. This diagram displays the original record (A), the filtered record (B), and the difference the filtering has made to the data (C). As is evident the low frequency noise that contaminates A is suppressed in B without alteration to the desired signal.

Figure 4.15 shows the frequency spectrum again after the filter has been applied. It is clear that although the low frequency spike is not completely removed, it is significantly attenuated.

4.4.2.3 Amplitude Recovery

Amplitudes are reduced with the propagation of seismic waves within the Earth due to several different phenomena such as spherical spreading, absorption, and partitioning at interfaces (as discussed in 4.4.1). Energy for spherical waves (i.e. generated at a point source) reduces by $1/r$, where r is the distance propagated. The resulting effect is that deeper reflections have greatly reduced amplitudes compared to the shallower structure. To correct for this occurrence, true amplitude recovery (TAR) can be used. However in this survey the target areas are the shallow regions of the record so it is advantageous not to scale these regions down compared to the deeper sections, which are contaminated with multiples. Additionally, applying an amplitude correction without knowledge of the velocity field causes information about the true amplitudes to be lost. Hence an amplitude correction was not applied in this instance, since the reduction in amplitude was not considered significant in the depths of interest.

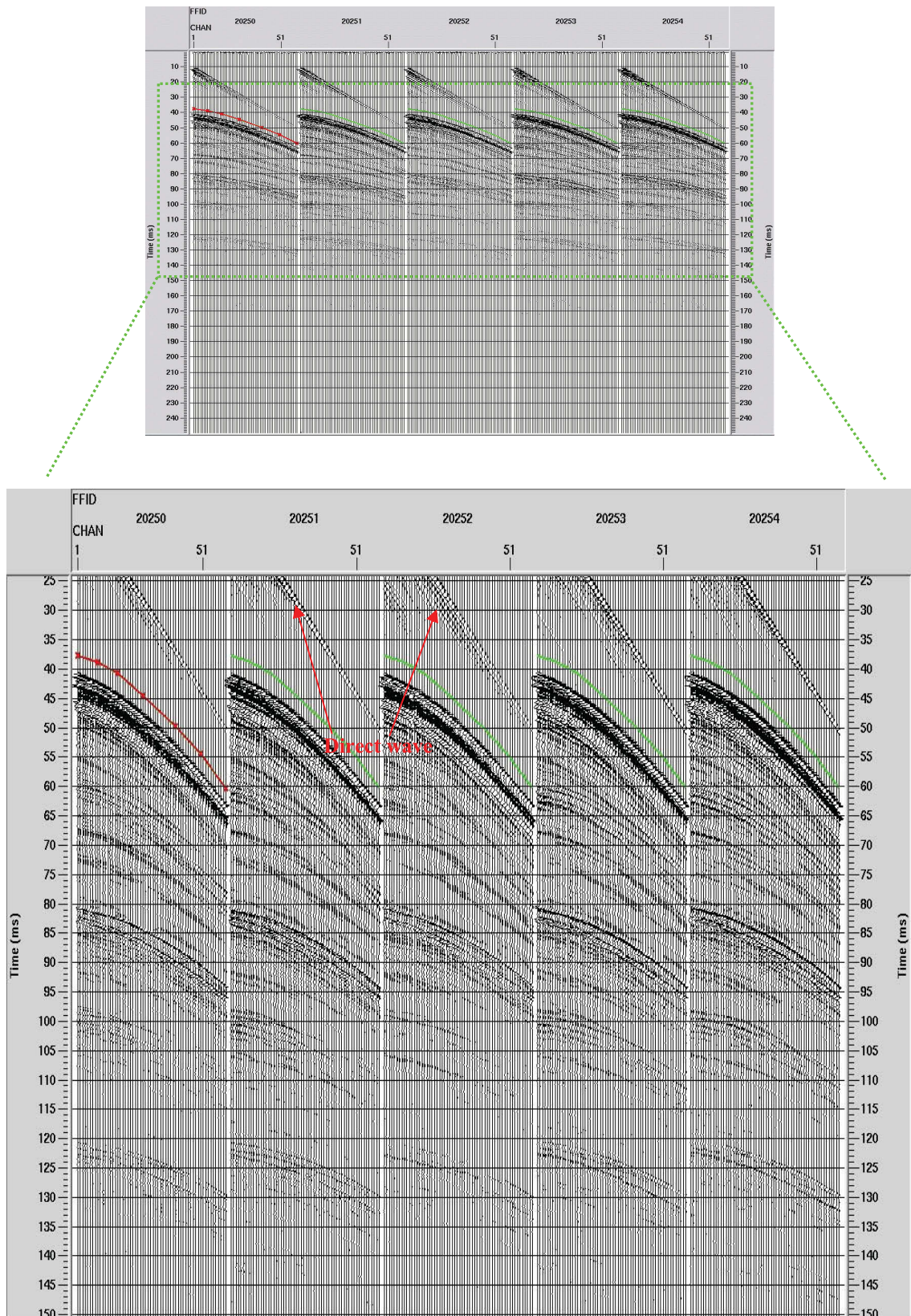


Figure 4.10: Design of Top mute within the t-x domain. The red line shows the picked mute, which is extrapolated across the following shots (green line). This is designed to remove the identified direct wave energy, whilst not affecting the primary reflections. The horizontal axis are the individual recording channels (hydrophones).

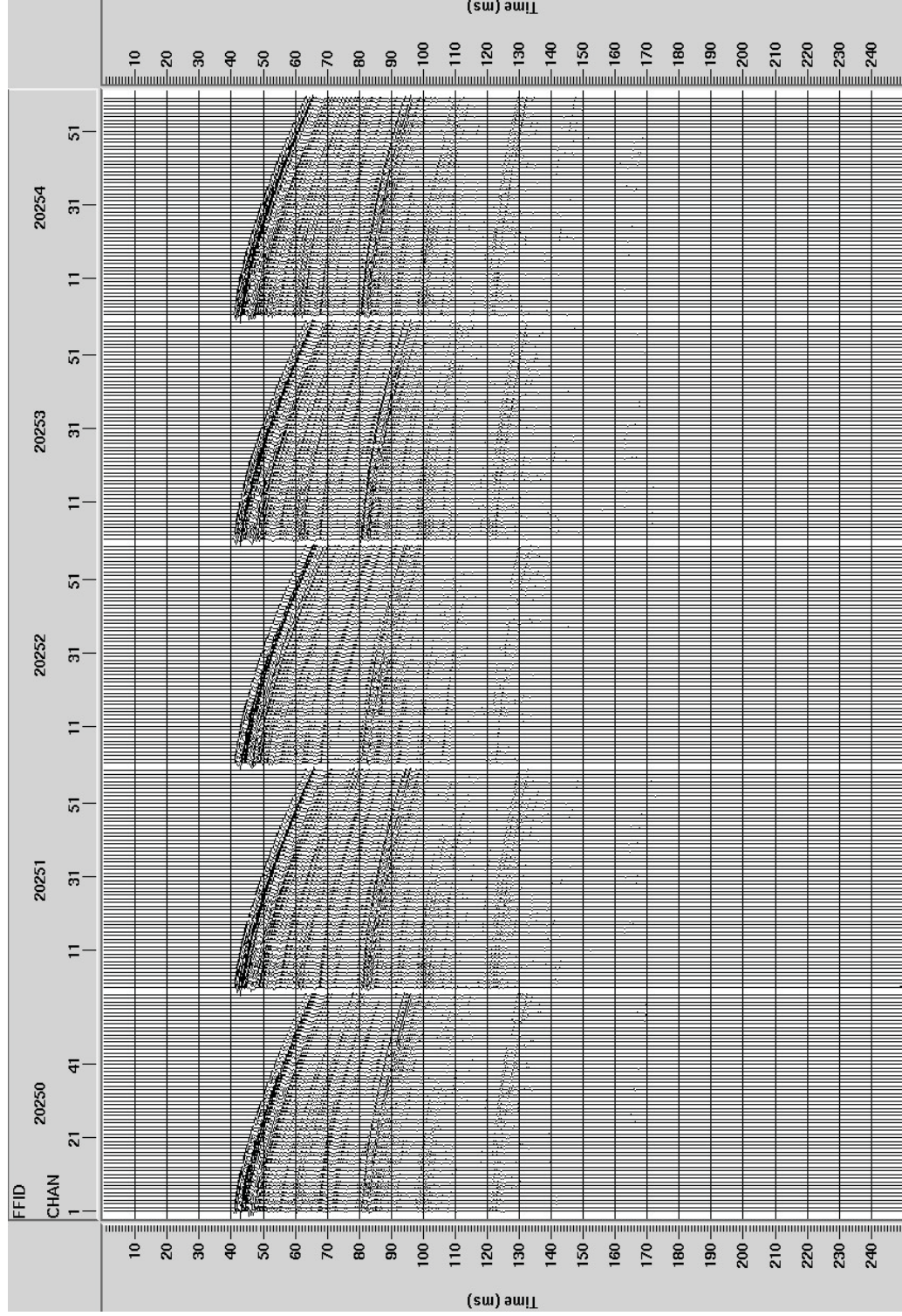
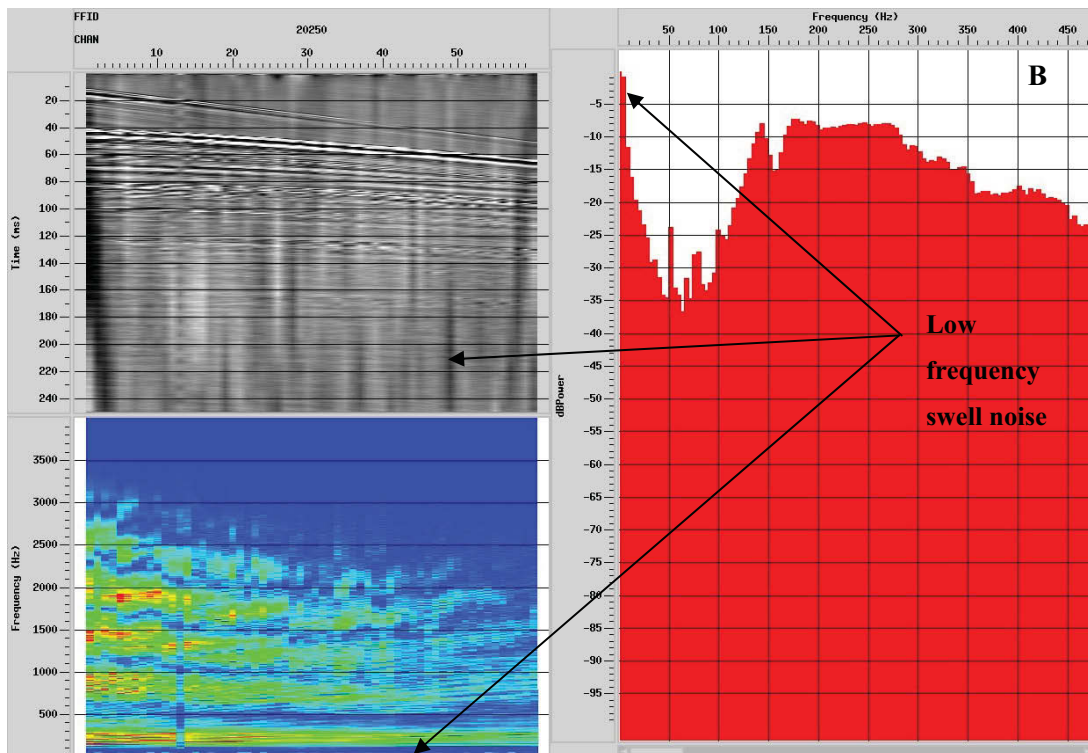
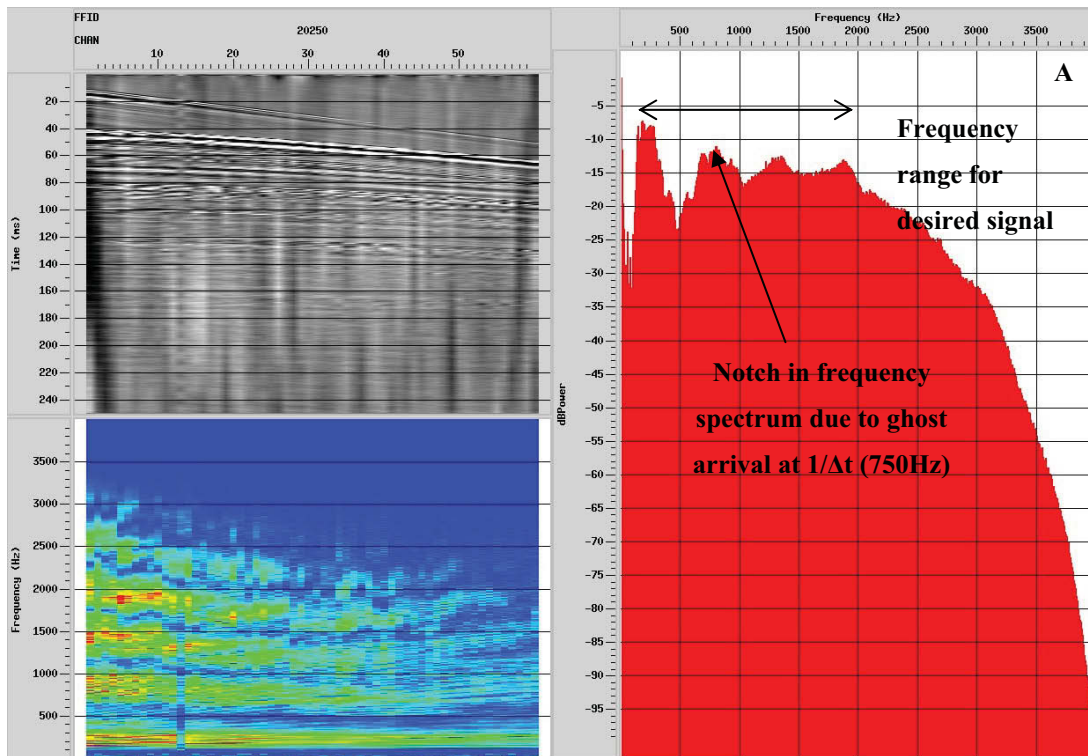


Figure 4.11: Resulting shot records from figure 4.9, after the application of the top mute. The direct wave energy has successfully been removed without destroying any primary energy.



4.12 A) Frequency spectrum for a single shot (red plot). B) Zoomed in to observe the low frequency spike. Also shown on the figures are the raw gathers (top left) and the frequency as a function of source-receiver offset (bottom left). Highlighted on Figure A is the notch in the spectrum due to the ghost arrival (as discussed in 4.3.2.3).

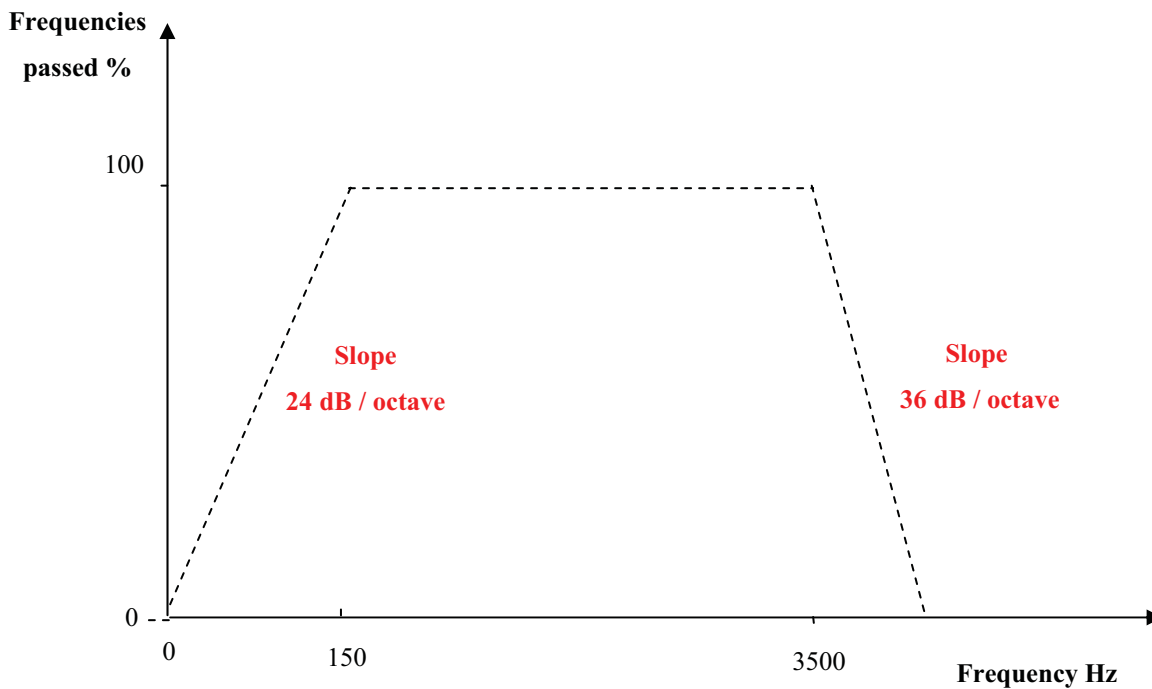


Figure 4.13: Schematic diagram of frequency filter design. The sloped edges reduce ringing artefacts (Gibbs phenomena).

4.4.2.4 Predictive Deconvolution

Deconvolution is applied to pre-stacked data to compress the recorded source wavelet and therefore improve the temporal resolution of the trace. Predictive deconvolution also has the advantage of removing any ghosting effects caused by both the receiver and the source, which arrive at a predictable distance behind the primary arrival.

The autocorrelation function can be used to design parameters for the predictive deconvolution operator. The autocorrelation is a special case of correlation where the dataset is correlated with itself. This results in a peak value at zero time shifts since the data is most like itself before it is time shifted. Any large value at some non-zero time shift indicates periodic arrivals, with the period equal to the time shift. Periodic arrivals can be assumed to be non-geological events (i.e. not real) and therefore can be suppressed using this process. The autocorrelation function can therefore be thought of as a measure of the repetitiveness of a function. The prediction distance is the time length of the wavelet, and is therefore omitted from the deconvolution operator. This usually corresponds to the time length of the second zero crossing in the autocorrelation. Making the distance too small could damage the wavelet, whereas making the distance too large could include short period multiples, which would then not be removed by deconvolution. The lag distance determines how much of the autocorrelation to use and is the length of time to be included in the deconvolution. This should be the time corresponding to the period of the multiples that are to be eliminated. This is shown schematically in figure 4.16 with a simple trace.

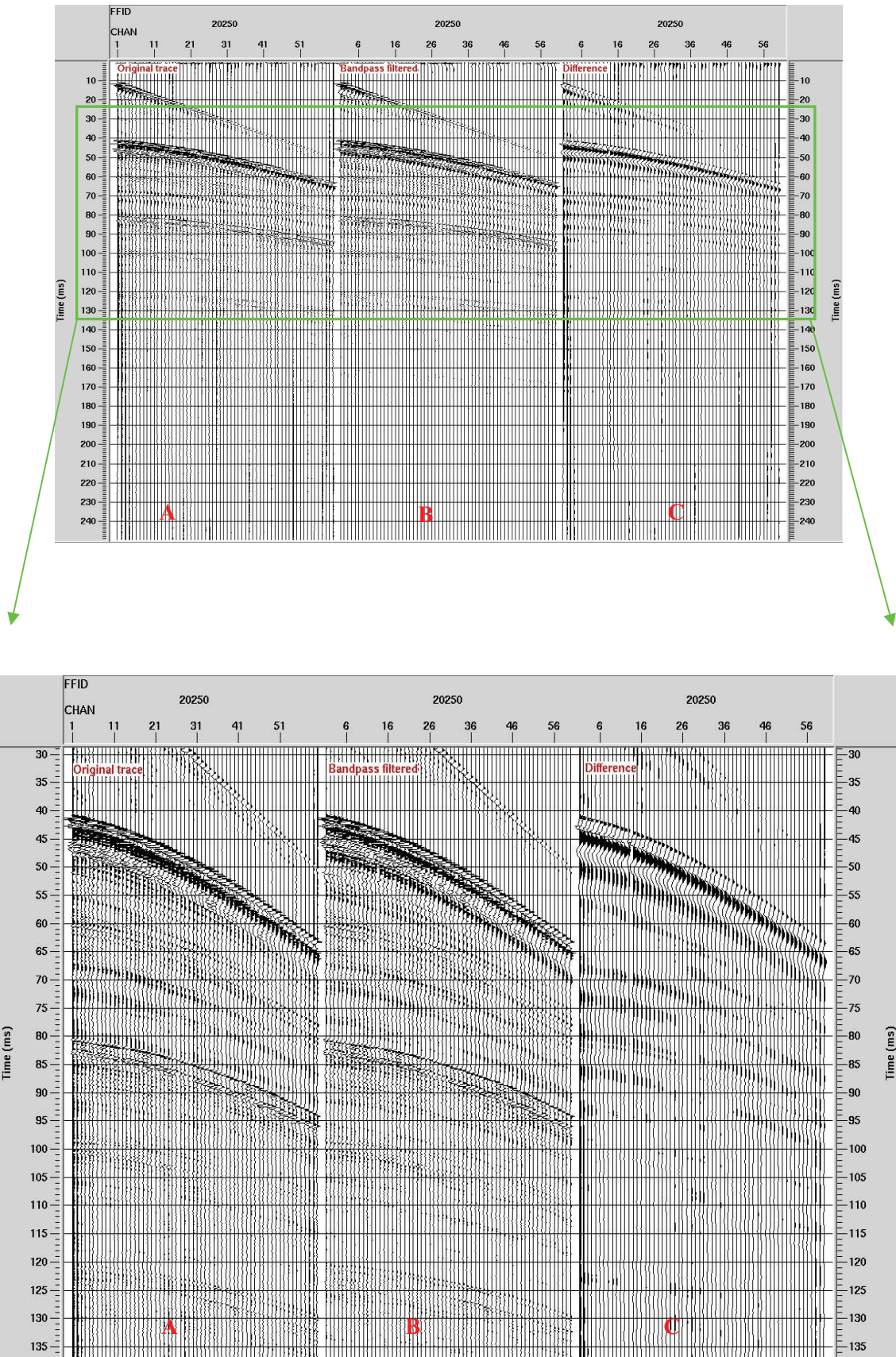


Figure 4.14: Shot record showing the effects of bandpass filtering (Butterworth: 24-150-3500-36). The difference display (C) shows the frequency components that are removed from the gathers after the filter has been applied. The ambient swell noise is sufficiently suppressed (B).

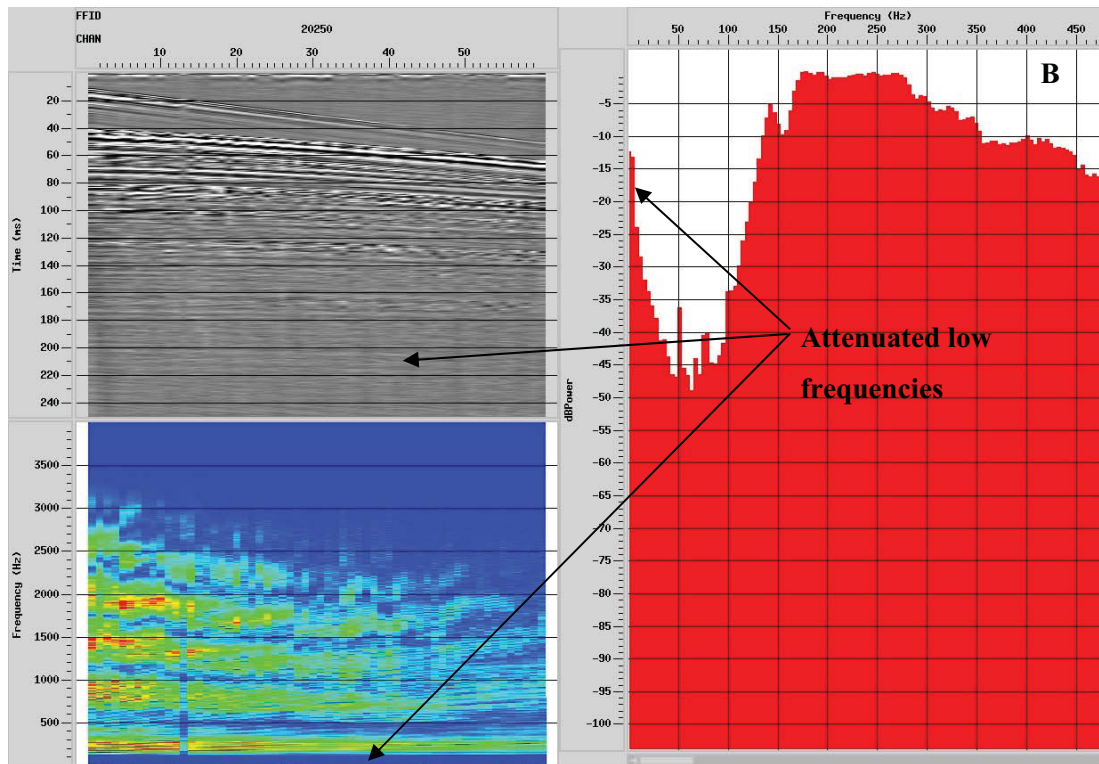
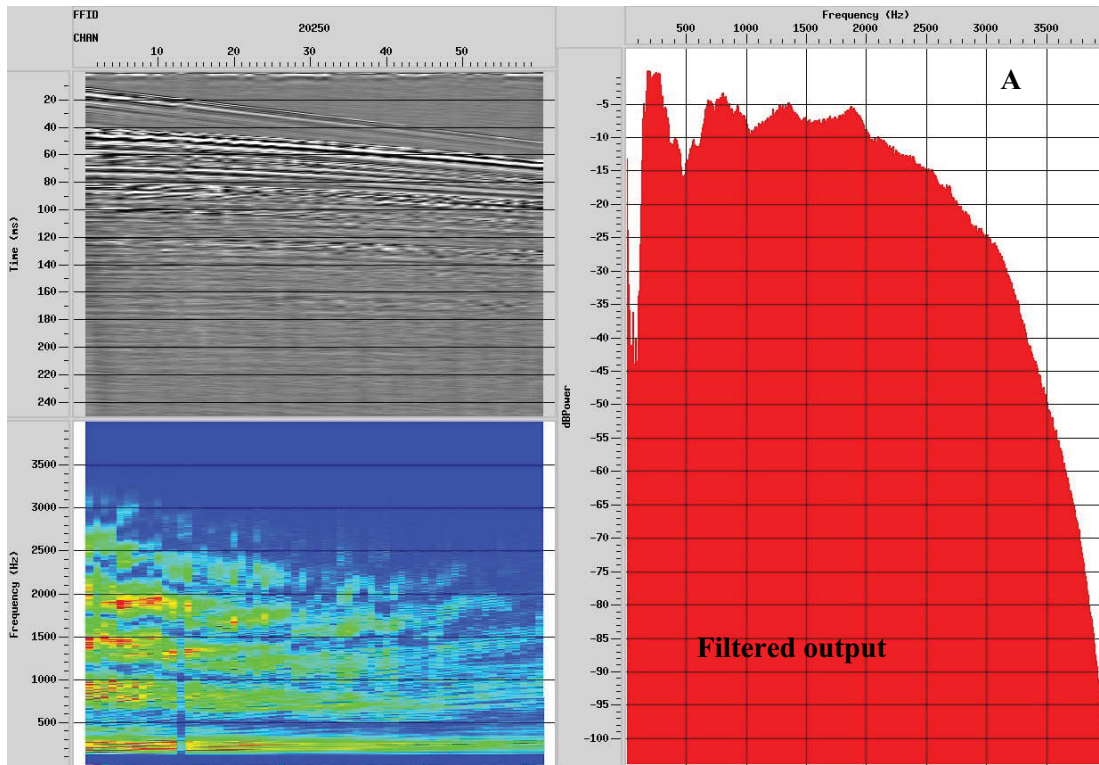


Figure 4.15: Frequency spectrum for a shot record after bandpass filtering applied. This can be compared with figure 4.12 to observe the suppressed lower frequencies. These are not completely removed since this would produce artefacts within the record.

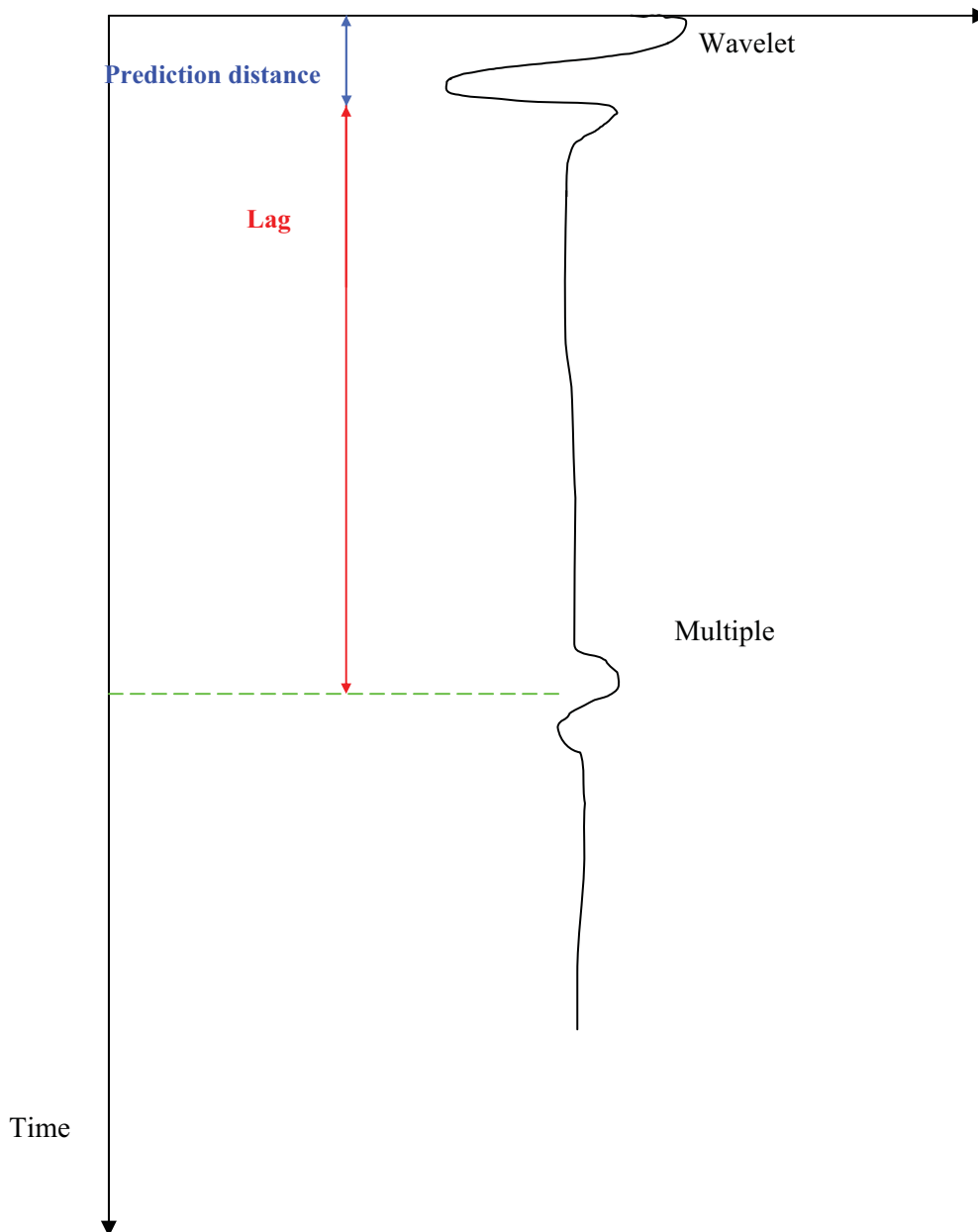


Figure 4.16: An example of an autocorrelation function. The primary energy is contained within the prediction distance. This is omitted from the deconvolution to prevent any primary energy loss. The Lag is the distance to the predictive multiple, which is included in the deconvolution process.

Figure 4.17 displays the autocorrelation function for the seismic data. The wavelet is centred on zero, with the second zero crossing at 1.5ms. There is then a strong peak at 1.6ms and linear energy between 4 and 8ms. Parameter tests can be used to determine the optimum prediction and lag distances that remove these multiple events without causing damage to the primary reflections. Two passes of predictive deconvolution were applied, firstly to tackle the energy between 4 and 8ms, with a prediction length of 3ms and a lag of 8ms (figure 4.18). The second pass of deconvolution should remove any ghost effects with a prediction length of 4ms and a lag of 1.5ms (figure 4.19). The resulting shot records are shown in figure 4.20 with the difference due to predictive deconvolution displayed. A bandpass filter was applied again to the records after the deconvolution to remove any high or low frequency artefacts that the process may cause. The same parameters were used as previously (24-150-36-3500). It is clear that the repetitive multiples are removed resulting in a cleaner record. The wavelet is also compressed which should increase the temporal resolution of the reflections.

Another set of problematic multiples are those generated within the water layer (figure 4.21), due to the very high reflection coefficient and also since water is not very attenuative. These multiples are evident in the record and highlighted on figure 4.20, still remaining after deconvolution is applied. A lag distance of approximately 40ms is needed to remove this energy. Unfortunately the record length is not long enough to model these multiples accurately in the autocorrelation function, so they cannot be removed with deconvolution. The target area for the survey should lie above the first water bottom multiple, so it may not interfere with any target horizons. If these multiples do mask some desired energy, further processing applications can be used to attenuate them.

One problem with deconvolution is that the multiple period does decrease with offset, since the multiples become asymptotic to the primary reflection generated at the same interface. Some residual multiples may therefore remain in the record at very far traces (large offsets). This energy should be removed when the data is stacked together during later stages of processing.

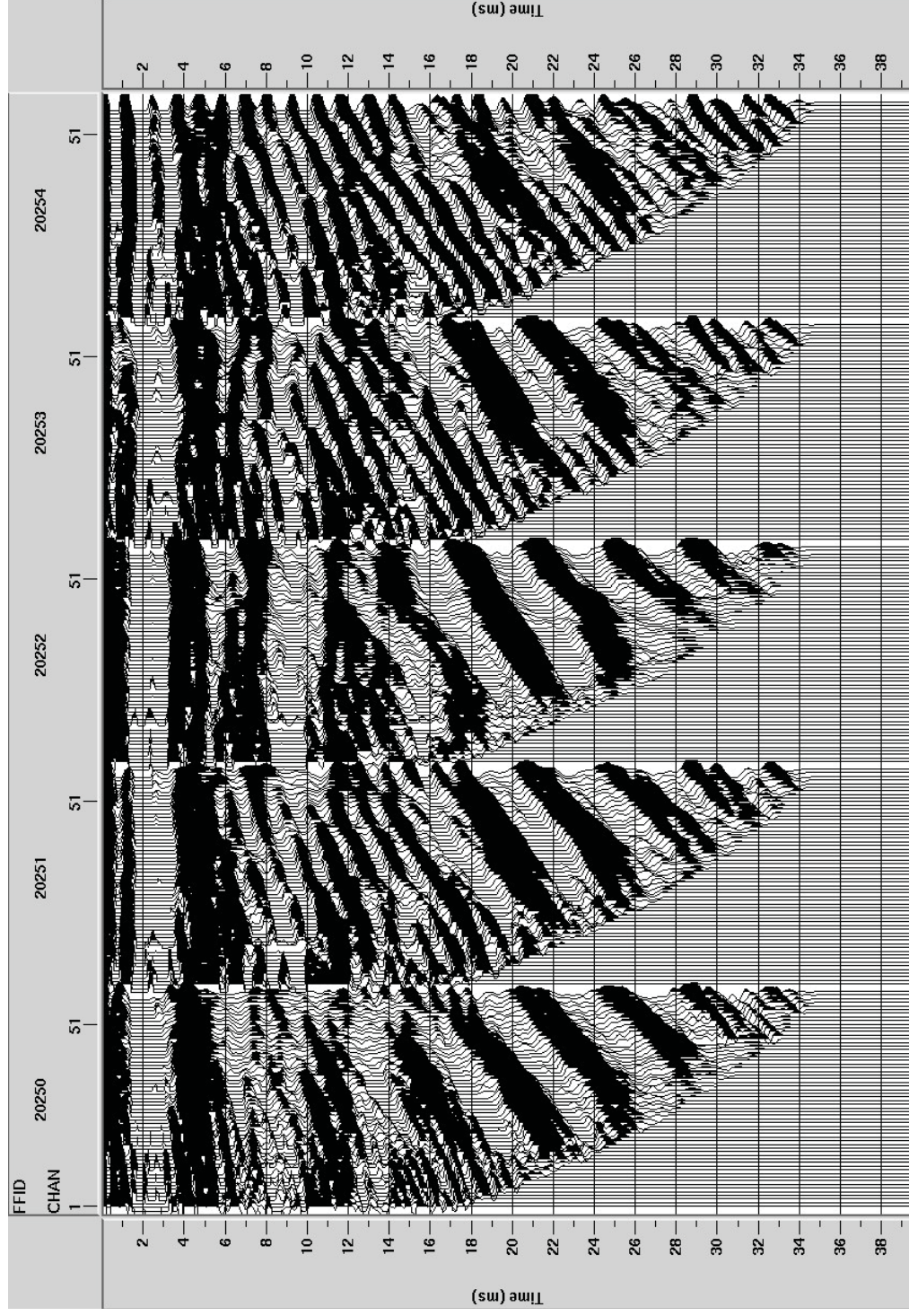


Figure 4.17: Autocorrelation function for 5 shot records. The wavelet at zero time corresponds to the primary reflections. All other energy is repetitive and therefore can be targeted in the deconvolution. There is a band of energy between 4 and 8ms and also energy between 1ms and 2ms, which can be targeted.

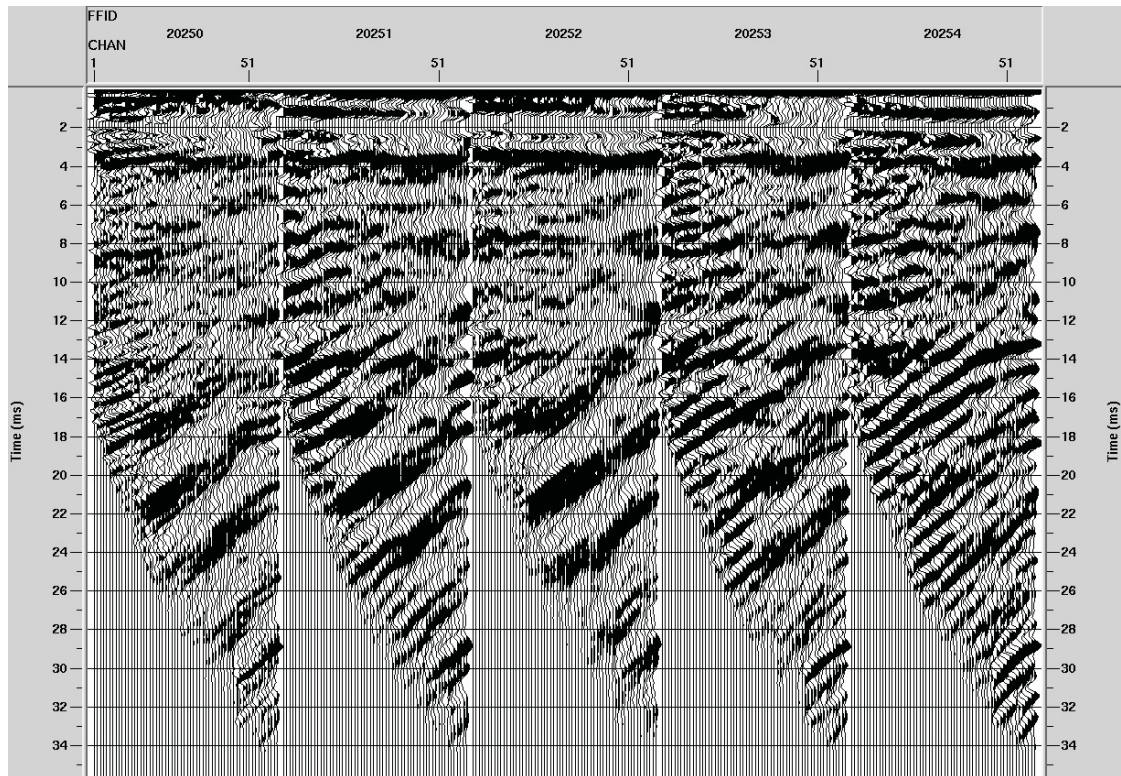


Figure 4.18: Autocorrelation function after one pass of predictive deconvolution (Predictive Distance = 3ms, Lag = 8ms). This pass of deconvolution is targeting any repetitive multiples between 3ms and 8ms (the band identified in figure 4.17).

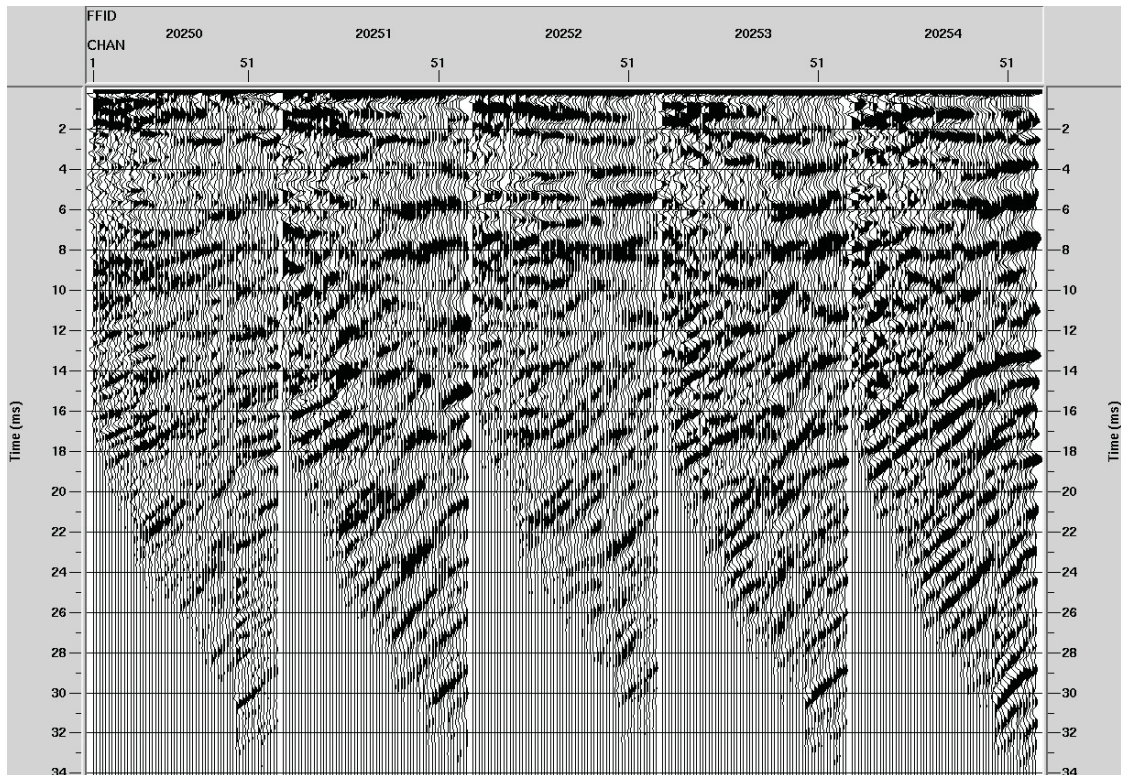


Figure 4.19: Autocorrelation function after two passes of predictive deconvolution (Predictive Distance = 1.5ms, Lag = 4ms). This is targeting the energy identified in figure 4.17 between 1ms and 2ms. Precision is taken so as not to remove any primary energy.

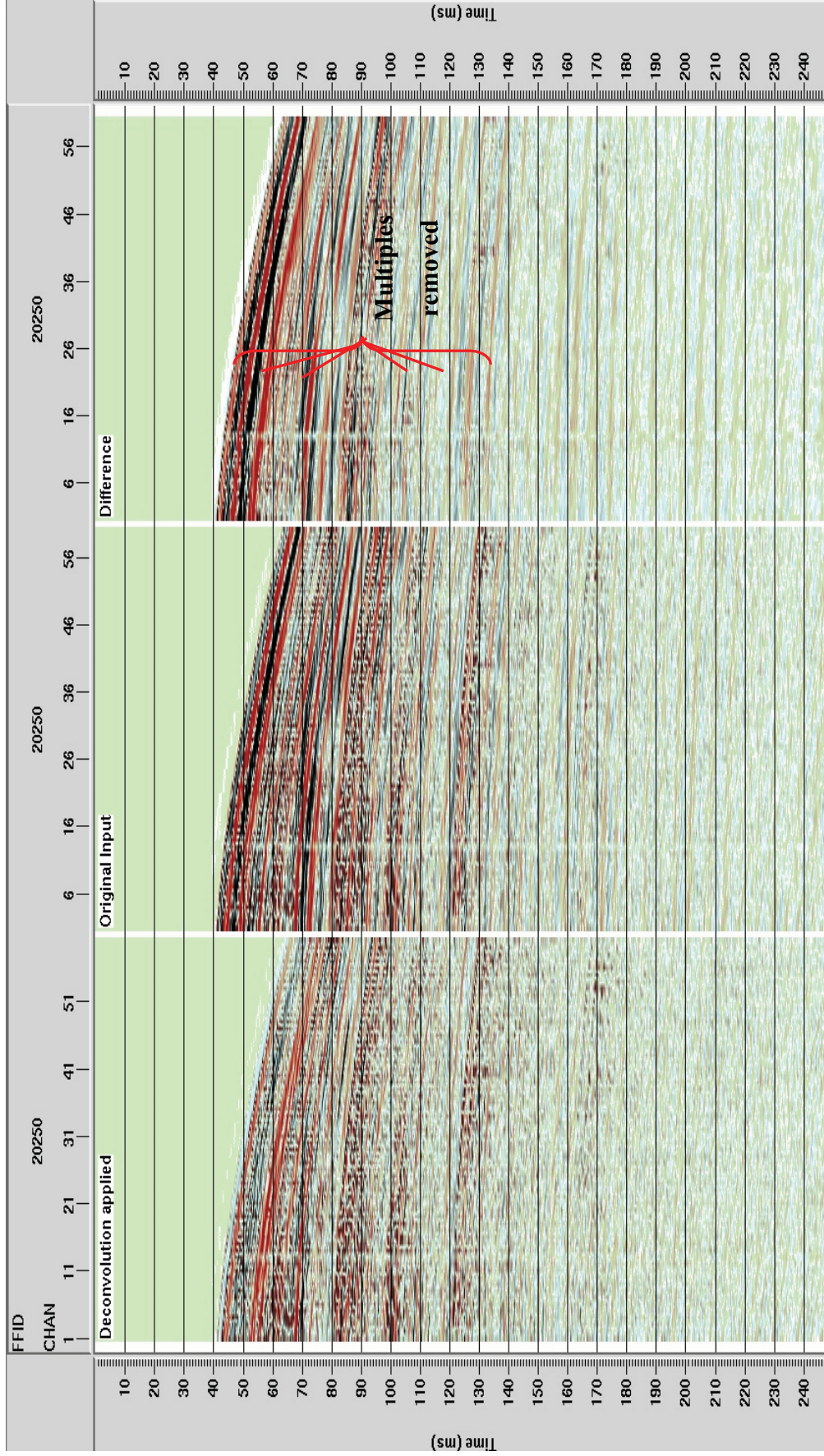


Figure 4.20: Difference display after predictive deconvolution is applied. The predictive multiples have been successfully removed after both passes of deconvolution (panel on right shows energy removed). The resulting record (panel on left) has fewer high amplitude arrivals, especially between 40 and 50ms, which may have been masking weaker primary reflections.

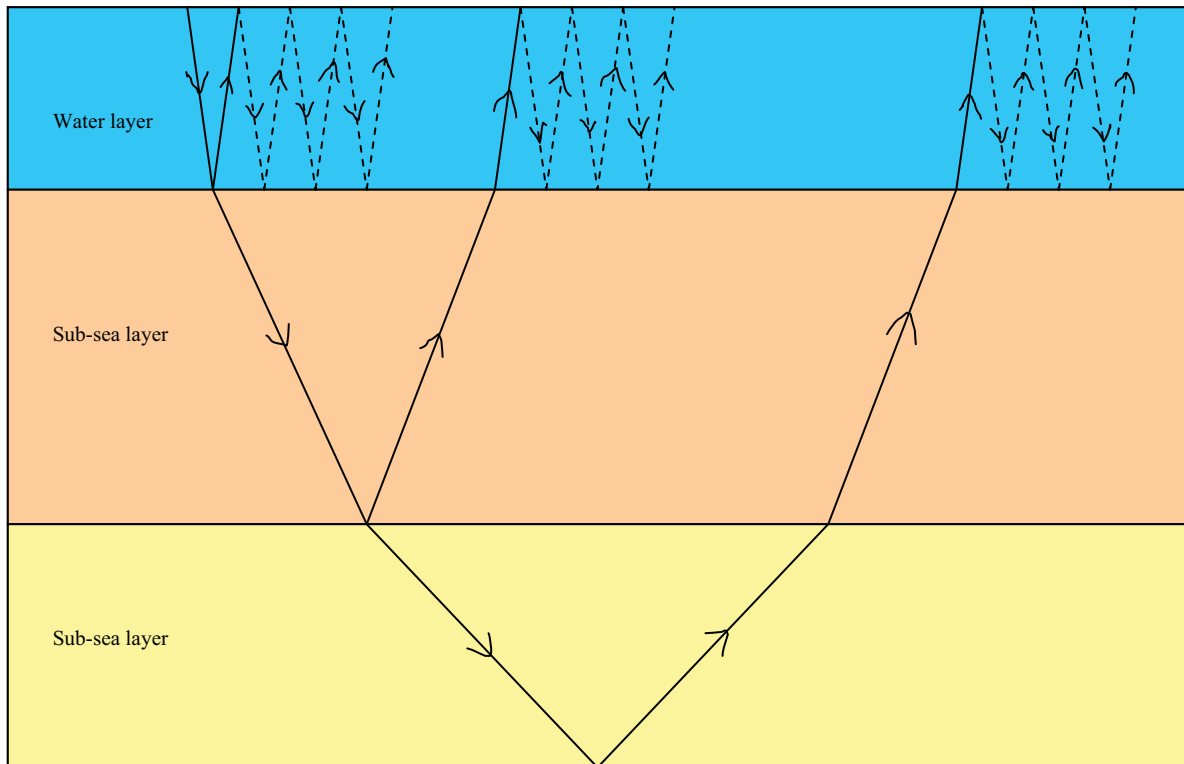


Figure 4.21: Schematic diagram of reverberations in the water column. These can be very problematic since they are high amplitude due to the large density contrast that occurs at the seabed and they appear throughout the shot record. The bold lines identify the primary reflections, with the dashed lines representing the reverberations within the water column.

4.4.3 Main Processing

4.4.3.1 CMP Sorting

The use of the multi-channel recording system allows the data to be sorted into common mid-point (CMP) positions. This allows traces acquired with different offsets to be grouped together into one CMP gather with the reflection point being imaged by several rays instead of one (figure 4.4), giving a multi fold record instead of single fold (figure 4.3). The fold can be determined using the acquisition parameters, and equation 4.5, where n_g is the number of recording channels (60), Δg is the receiver spacing (1m) and Δs is the shot spacing (roughly every 1m). Hence the fold of coverage for this survey was a maximum of 30.

$$fold = \frac{n_g \Delta g}{2 \Delta s} = \frac{60}{2} = 30 \quad \text{Equation 4.5}$$

Since a shot was taken every second, the shot spacing varied making the fold of coverage dependant on the speed of the seismic vessel, which can be related to the weather, sea state and tides. In the English Channel the tides are particularly strong causing large variations in speed, allowing some survey lines to be sampled more than others and hence have a larger fold of coverage.

4.4.3.2 CMP Stacking

The reflections can be enhanced by summing together the arrivals from each CMP to increase the level of signal compared to noise (CMP stacking). The CMP gather is equivalent to a CDP (common depth point) gather only if the reflector is horizontal and the velocities don't vary laterally. In addition to improving the signal to noise ratio, the processing of multi-fold data yields velocity information about the sub-surface.

There are many different types of velocity that can be derived from seismic exploration. Assuming a layered earth the stacking velocity (which is the velocity that yields the best stack) relates to the normal-moveout (NMO) velocity, which can then in turn be related to the root-mean-squared (RMS) velocity. Finally using the RMS velocity, the interval velocity (an average velocity in an interval between two reflectors) can be derived. It is this interval velocity that yields information on the sub-surface since it is dependant on several lithological properties.

4.4.3.3 NMO Correction

In order for the CMP gathers to be stacked coherently, a velocity field must be defined, which is used in the NMO correction. If an accurate NMO correction is applied the primary reflections will be coherently stacked and any lower velocity multiple energy will be under-corrected and will destructively stack.

The NMO correction is defined as:

$$dt = \frac{x^2}{2v_{nmo}^2 t_0} \quad \text{Equation 4.6}$$

This is the amount that needs to be subtracted from travel times to equalise the reflection arrival times at all offsets, which synchronises the reflections ready for stacking (figure 4.22).

P-wave energy is slightly dispersive, which means the energy is dispersed (spread) as it travels through the Earth. Therefore the wavelet recorded at the last channel (far offset) will be slightly larger (lower frequency) than the wavelet recorded at the first channel (near channel). After NMO correcting the reflections some energy in the far offset wavelet will be undercorrected (dip down) and some will be overcorrected (dip up) due to the dispersion. This causes the aligned reflection to be stretched at far offsets, which will cause degradation to the final stacked section. A stretch mute can be applied to mute out any stretched energy caused by the NMO correction.

4.4.3.4 Velocity analysis: CVS

To determine the velocity field of the subsurface, velocity analysis must be used. This is done preliminarily using constant velocity stacks (CVS). The CMP's are stacked together using an NMO correction for a specified velocity. The stack is then displayed and the horizon that is correctly aligned by the V_{nmo} is given that particular stacking velocity.

This method of velocity analysis is very subjective and so is used as a first approximation for further analysis. Figure 4.23 shows the constant velocity stacks for velocities ranging between 1100m/s and 2000m/s for a range of CMP's. Note that ProMAX™ labels CMP's as CDP's, although they are only equivalent for horizontal reflectors (figures show CMP's labelled as CDP's). It is clear from this figure that the energy present in the stacks is coherent between 1500m/s and 1700m/s. This region can then be focussed on in figure 4.24. The seabed reflection is aligned at 1500m/s corresponding to the velocity of water. The seabed multiple is also aligned at this velocity. Reflections can then be identified between 1600m/s and 1650m/s. Deeper reflections that are likely to be higher in velocity are masked by the seabed multiple in this display.

4.4.3.5 Velocity Analysis: Semblance Analysis

Semblance analysis can be used to determine a more accurate velocity field. This makes a contour map of the stacked trace amplitudes by again applying a range of velocities to the CMP gathers. The range of velocities applied was 1300-2500m/s. The program can determine which of the velocities best represents the hyperbolic moveout of each particular reflection in turn. If the velocity is a good match to the reflection hyperbola it produces good correlation and therefore a high amplitude response on the contour map. Poor matches produce poor correlation and give a low amplitude response. The amplitudes are plotted as a function of velocity and zero offset travel time to give the semblance plot (figure 4.25). Velocities can then be determined for reflections at various zero offset travel times and are represented as picks on the semblance plot.

Before using the semblance plots for velocity analysis, supergathers can be constructed to give a better signal to noise response. This stacks together a specified number of CMP gathers, therefore enhancing coherent energy and suppressing incoherent arrivals. The number of combined CMP gathers was chosen to be 101.

The velocity field determined by the CVS is used as an input and the field can then be modified depending on the semblance output. Figure 4.26 represents a semblance plot showing how the correct NMO velocities can be determined. Multiple energy can also be determined as this appears at greater zero offset travel times, but at a lower velocity than the trend suggests. The multiples within the gather can therefore be identified and avoided. Examples of the primary energy (P) and the multiple energy (M) are identified on this figure.

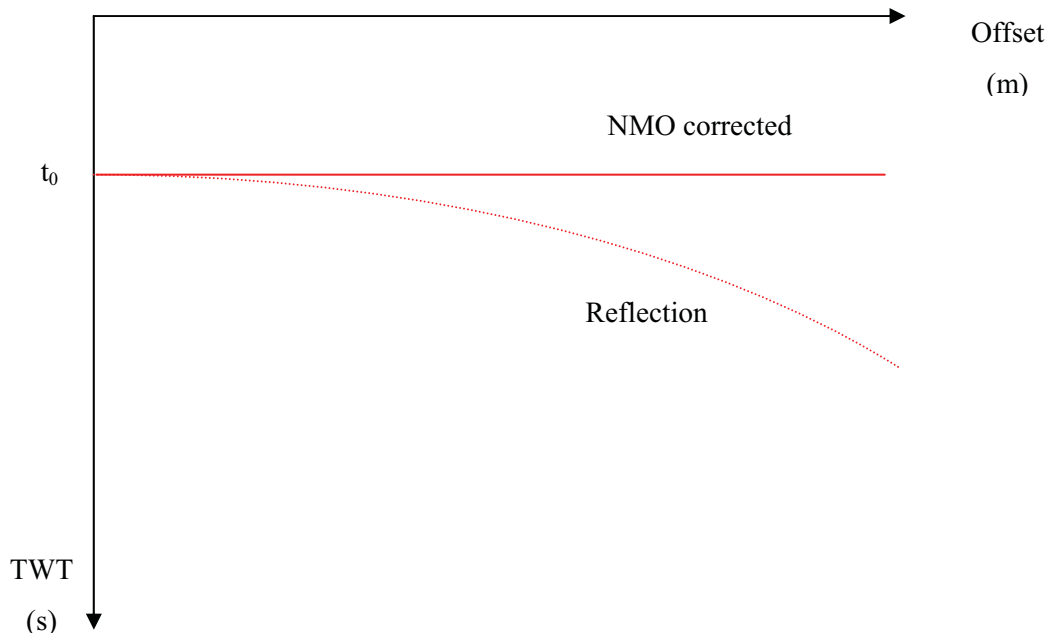


Figure 4.22: Δt needs to be subtracted from travel times to equalise the reflection arrival times at all offsets.

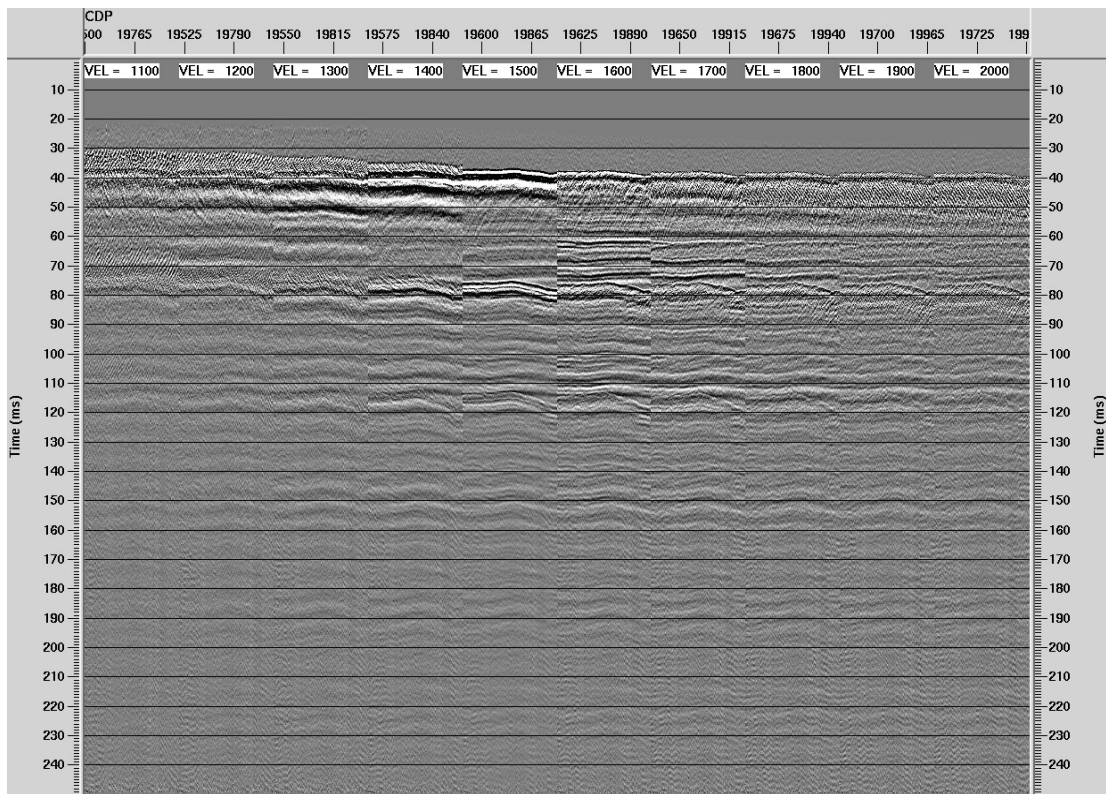


Figure 4.23: Constant velocity stacks with velocities ranging from 1100m/s to 2000m/s. The correct velocity applied to a reflector causes it to be coherent in this image. The CMP range for each panel is 19500-21250.

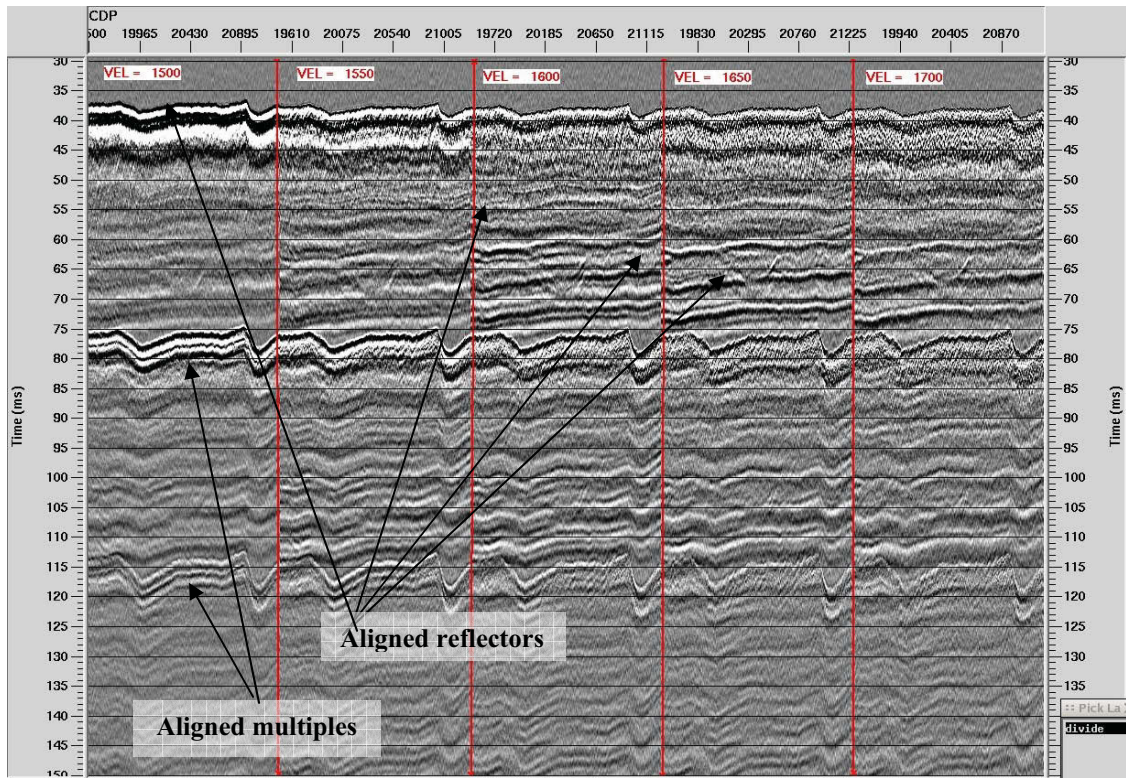


Figure 4.24: CVS showing a zoomed in version of figure 4.23. The figure displays the aligned reflectors and the corresponding velocities for a section of CMP's.

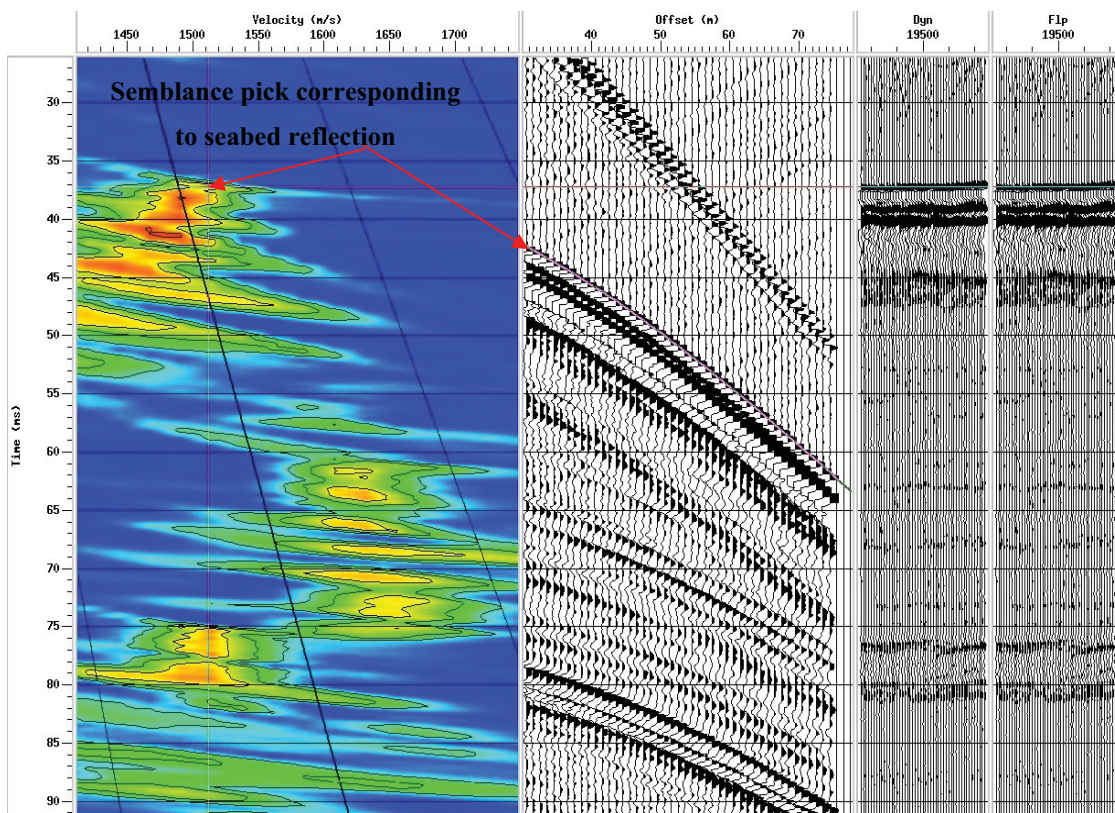


Figure 4.25: The left panel displays the semblance plot as described in 4.4.3.5. The centre panel shows the undercorrected supergathers, and the two panels on the right provide an image of the stack produced by NMO correcting and stacking with the picked velocity field.

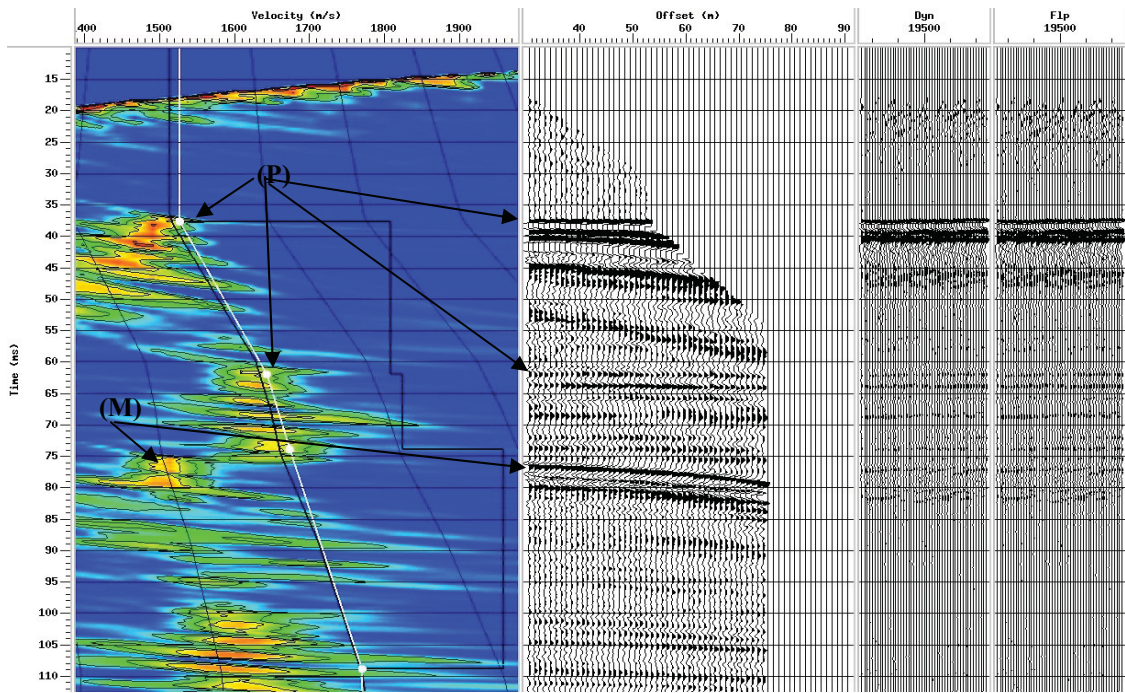


Figure 4.26: Velocity analysis showing primary events (P) and multiple events (M). The centre panel has been corrected using the velocity field picked on the semblance plot (left panel). The primary events are aligned, whereas the multiple events are undercorrected (dip down). An NMO stretch mute has been applied to the corrected data, which mutes out any energy that is stretched to more than 50% of its original shape (as discussed in 4.4.3.3).

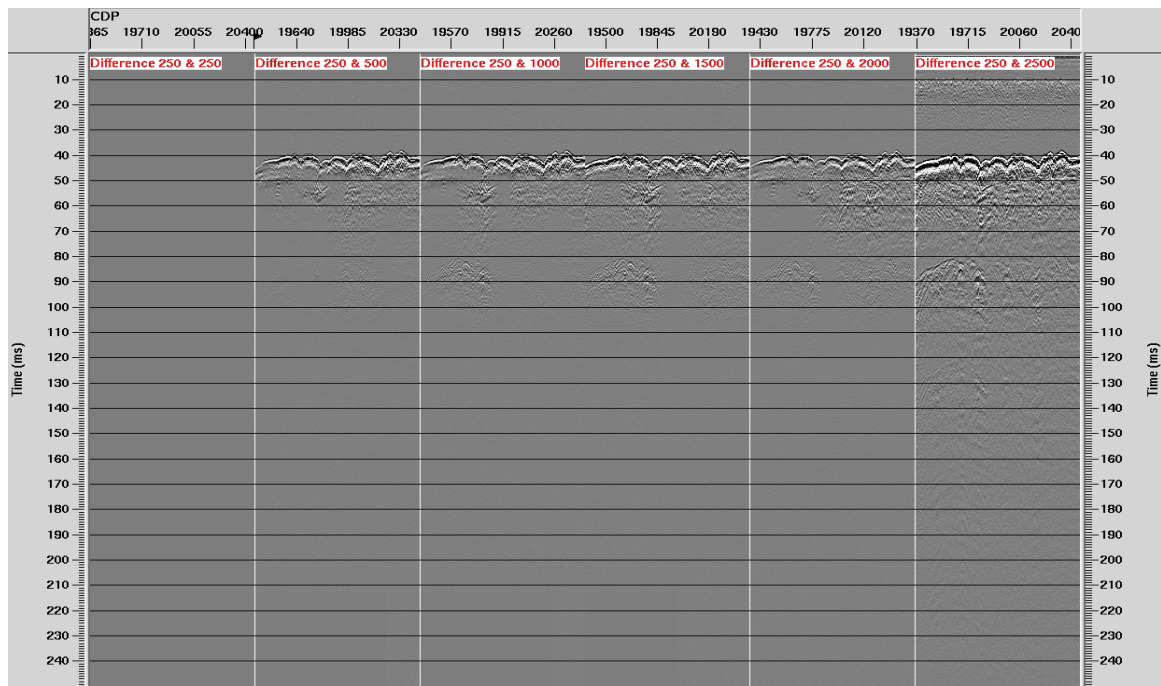


Figure 4.27: Testing velocity analysis frequency. CMP range 19000-20000 A stack was produced using velocities picked at different frequencies (every 250, 500, 1000, 1500, 2000, 2500 CMP's). The panels above show the result after each stacked section was subtracted from the stack produced with velocity analysis every 250 CMP's to observe the effect of reducing the frequency of velocity analysis.

In hydrocarbon seismic surveys where the image targets are deeper and the cables are more than 2km long, velocity analysis is done typically at least 2 to 3 times the cable length. For this particular survey the cable length was 60m, but each line was about 10km therefore velocity analysis every 30m was not suitable. Interpolating between velocity analyses locations can degrade the stack, but as velocity analysis is a labour-intensive process, having locations too close significantly adds to the overhead. The optimum number of velocity analyses locations can therefore be defined as the largest number before the stack is degraded. Comparing stacks with increasing velocity analyses locations can test this. Figure 4.27 shows the difference between velocity analyses every 250 CMP's (~100m) to every 2500 CMP's (~1km). The difference of a stack every 250 with itself is also shown to control any noise that may be introduced with the stack manipulation. The figure shows no noise is introduced, so any differences are due to the reduction in velocity analysis frequency.

It is clear that performing velocity analysis every 2500 CMP's significantly degrades the stack. Figure 4.28 shows a zoomed in version comparing the difference between analyses every 500, 1000 and 1500 CMP's. There is not much difference in primary sub-seabed energy between these stacks, with the most degradation occurring on the seabed reflection. Since this reflection is significantly higher in amplitude than the other recorded reflections, the degradation due to the differing analyses distances is likely to be insignificant. The final conclusion was to perform velocity analysis every 1000 CMP's with the intermediate velocities interpolated.

The velocity field after semblance analysis can then be quality controlled to check no irregularities occur using a velocity viewer. Any large jumps in velocity are assumed to be non-geological and therefore altered to produce a smoother field (figure 4.29).

The velocity field deduced can then be used in the NMO correction to align the primary reflections. Figure 4.30 shows the comparison of the gathers before the NMO correction is applied (A), and the gathers after the correction (B). It is clear to see that the horizons have been aligned with the correction. A stretch mute of 50% was applied to all the NMO corrected gathers to remove any distorted wavelets at far offsets. The NMO corrected CMP's are then stacked together by combining each trace in the CMP to make one trace with constructive amplitudes where coherent energy is present. This technique should enhance the primary reflections that are aligned by NMO, and act to suppress the multiples that are mis-aligned by the correction. The analysis is iterative with energy enhanced or suppressed with every pass. The velocity analysis is completed when further passes do not improve the stack. Figure 4.31 shows an example stack after all velocity analysis has been completed. Even though the primary velocity field applied to produce the stack is accurate, some residual multiple energy remains due to the small amounts of moveout at near offsets (identified on figure 4.30). This means multiple energy cannot be separated from primary events at near offsets using velocity differentiation.

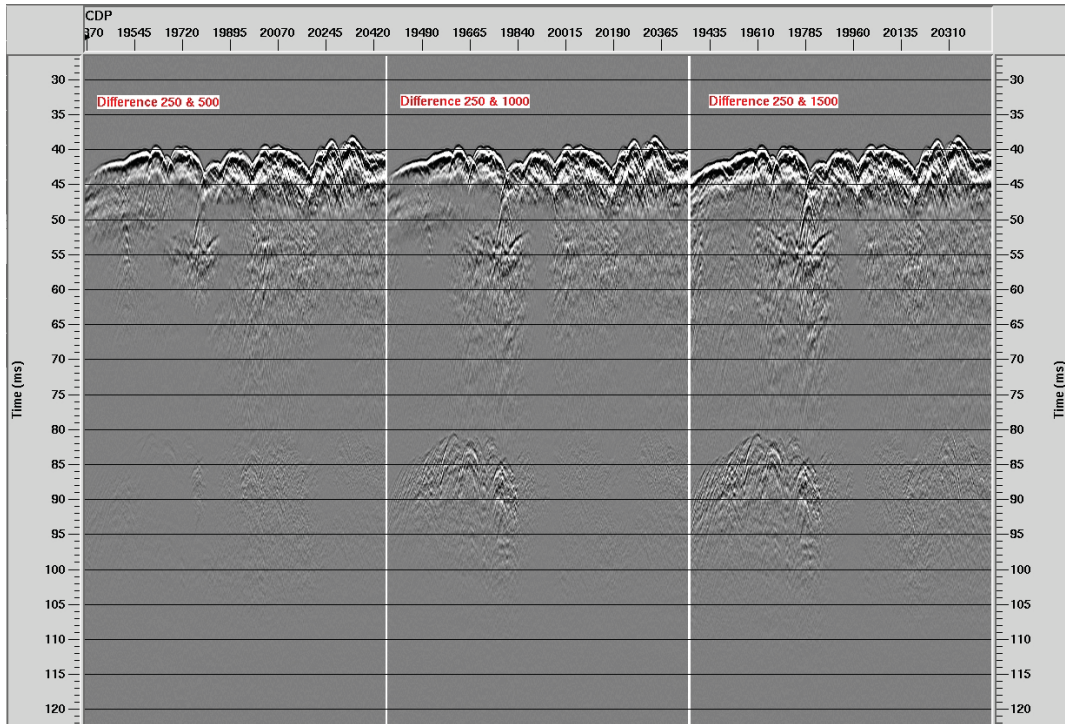


Figure 4.28: Testing velocity analysis locations. This figure shows a zoomed in version of figure 4.27 to help identify the effects of reducing the frequency of velocity analysis. A frequency of every 1000 CMP's was concluded on.

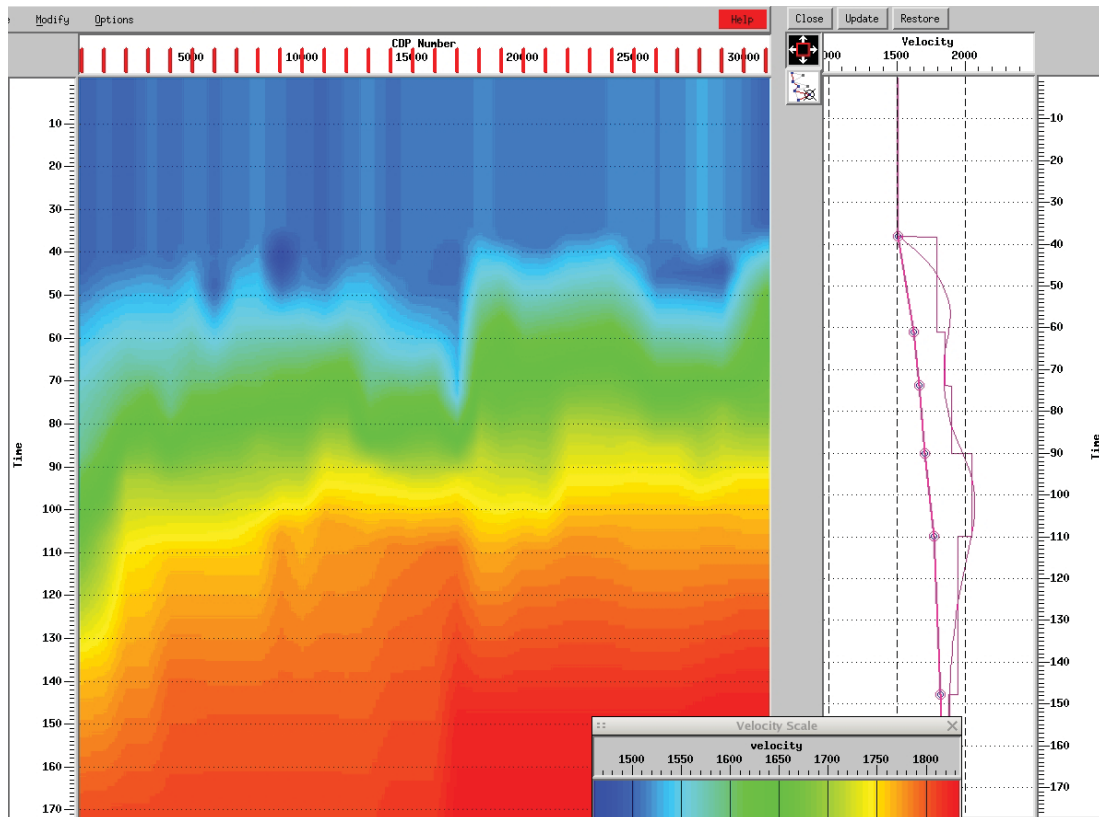


Figure 4.29: Velocity field viewed to check for any irregularities. The red ticks on the x-axis indicate the velocity analyses locations. The panel on the right displays the velocity picks with time, with the interval velocity displayed (calculated using Dix's equation – pink straight lines) and the smoothed velocity (pink curve).

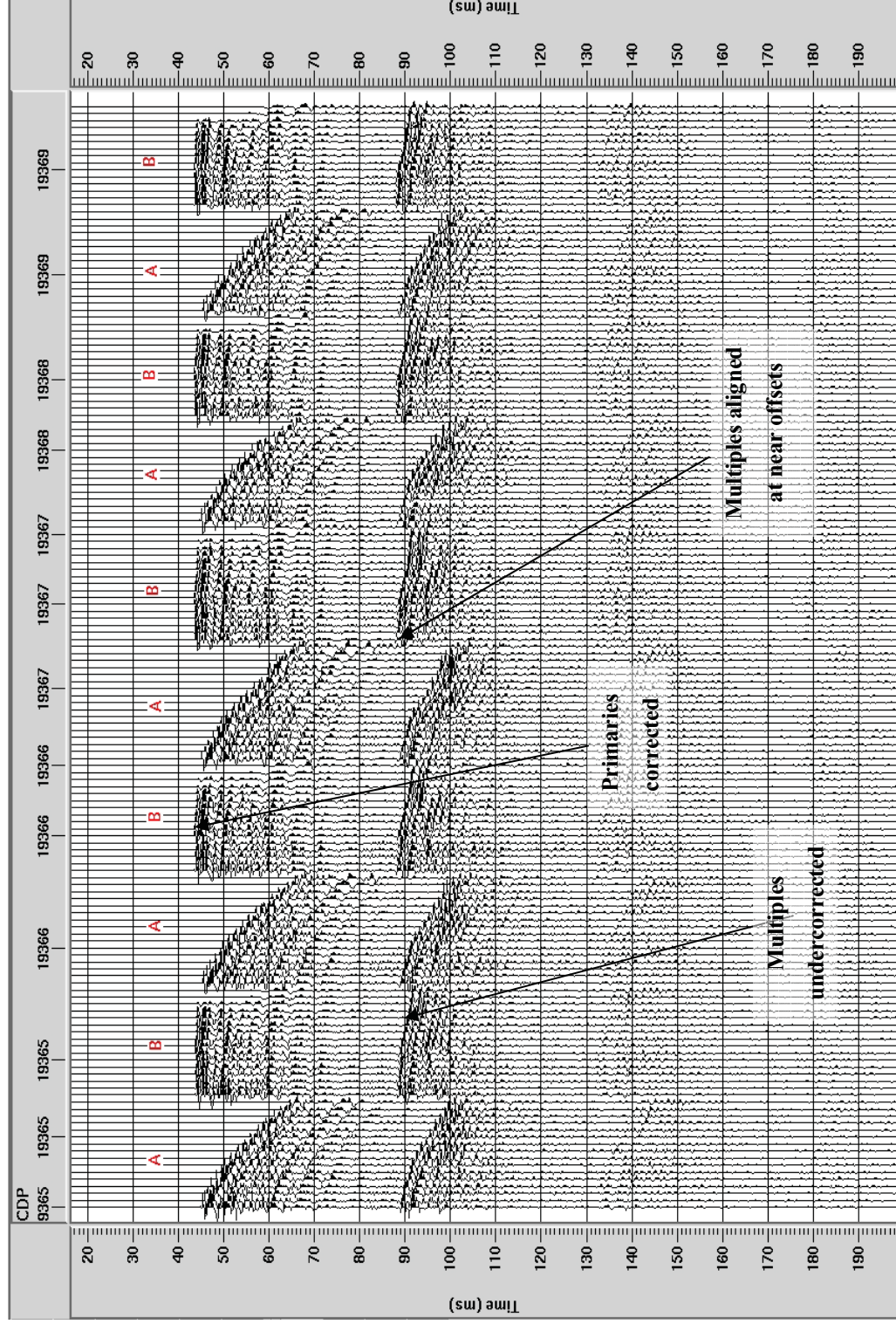


Figure 4.30: Original CMP gathers (A) and NMO corrected gathers (B). The gathers that have been corrected should contain aligned primary reflections and misaligned multiple reflections. The primaries will therefore be enhanced due to stacking, whereas the multiples will be suppressed.

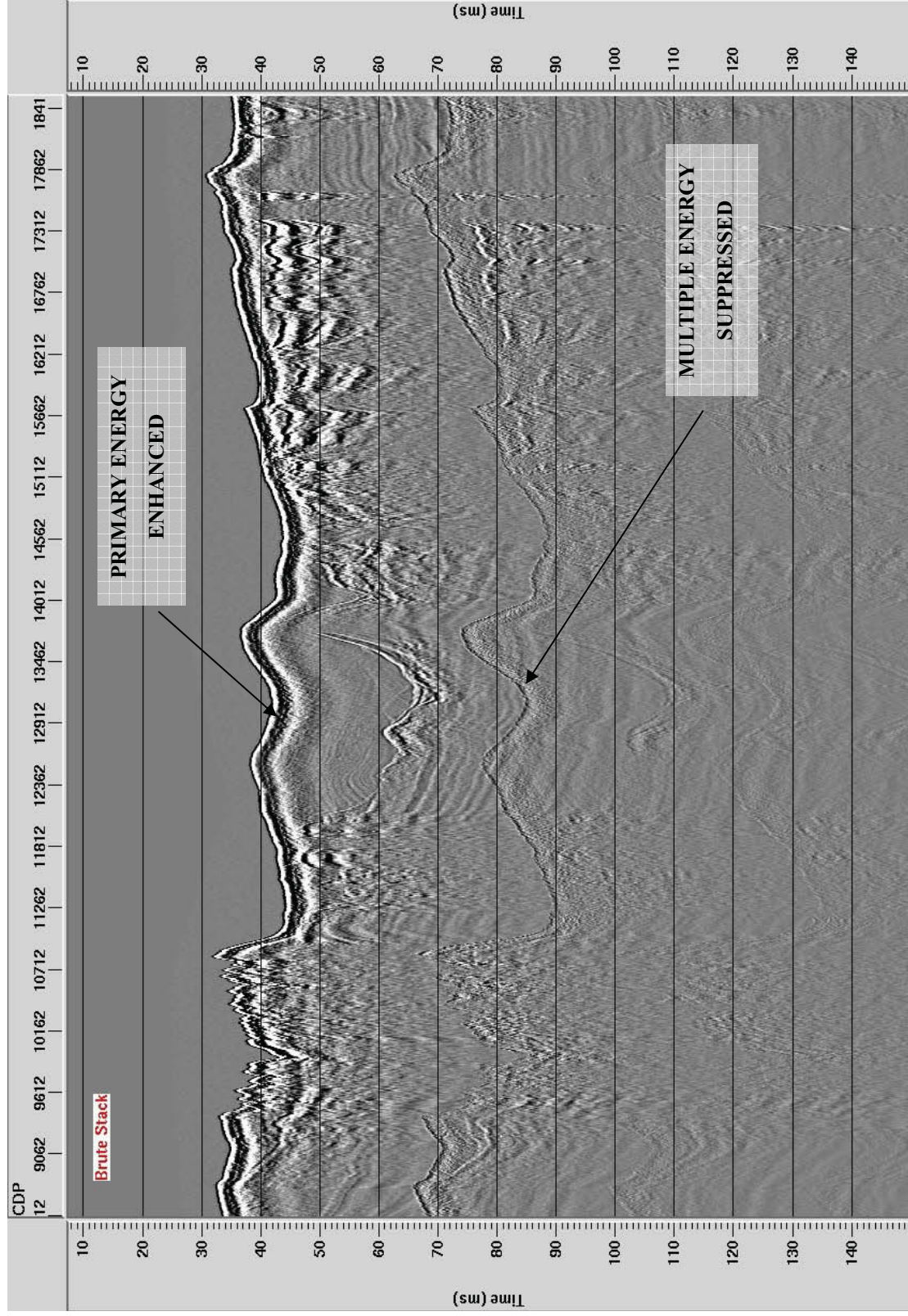


Figure 4.31: Stacked seismic section after velocity analysis has been completed. The primary arrivals are enhanced and the multiple arrivals are suppressed.

4.3.2 Post-stack Processing

As shown previously, some residual multiple energy remains in the stacked section, which degrades the stack and causes any imaging beneath this multiple to be tenuous. Tests were made to see if it was possible to design post-stack processes to suppress this energy further. The residual multiples were partly due to the small differential NMO between the P-wave velocity for water and the low velocity shallow sediments. There was also the added factor that the dipping near surface structure resulted in a lower apparent NMO velocity as explained in equation 4.7, where θ is the dip of the reflector.

$$v_{nmo_app} = v_{nmo} \sin \theta \quad \text{Equation 4.7}$$

4.3.2.1 FK Demultiple

Since the multiple energy is lower in velocity than the primary energy it masks, a filter based on the velocities can be designed. The data can be transformed into the frequency-wavenumber (fk) domain to be imaged. This allows separation of events due to their frequency and velocity, with the velocity determined as the gradient of a straight line in the FK domain, as shown in equation 4.8.

$$v = f\lambda = \frac{f}{k} \quad \text{Equation 4.8}$$

By NMO correcting the gather using a velocity function that is between the correct velocities for the primary and multiple events, the multiples will be undercorrected (still dip down in the t-x domain) whereas the primary events will be overcorrected (dip up in the t-x domain), as shown in figure 4.32. This will result in a negative velocity for the primary reflections and a positive velocity for the multiples, resulting in the different energy mapping onto two different quadrants. A polygon filter can then be designed to reject any signal within it. The filter was designed to remove the positive quadrant of the FK domain, which would represent the multiple energy (figure 4.33).

Figure 4.34 displays the effect of the filter. Some multiple energy has been successfully removed, but residual multiple energy still contaminates the deeper stack. This is due to the small velocity moveout that occurs at near offset traces, which makes the separation of multiple and primary energy problematic. The difference display shows that although some multiple energy is removed, the signal is also degraded due to the filter. Since the target area lies above the seabed multiple, the FK filter was not applied as it caused degradation of the stack rather than an improvement.

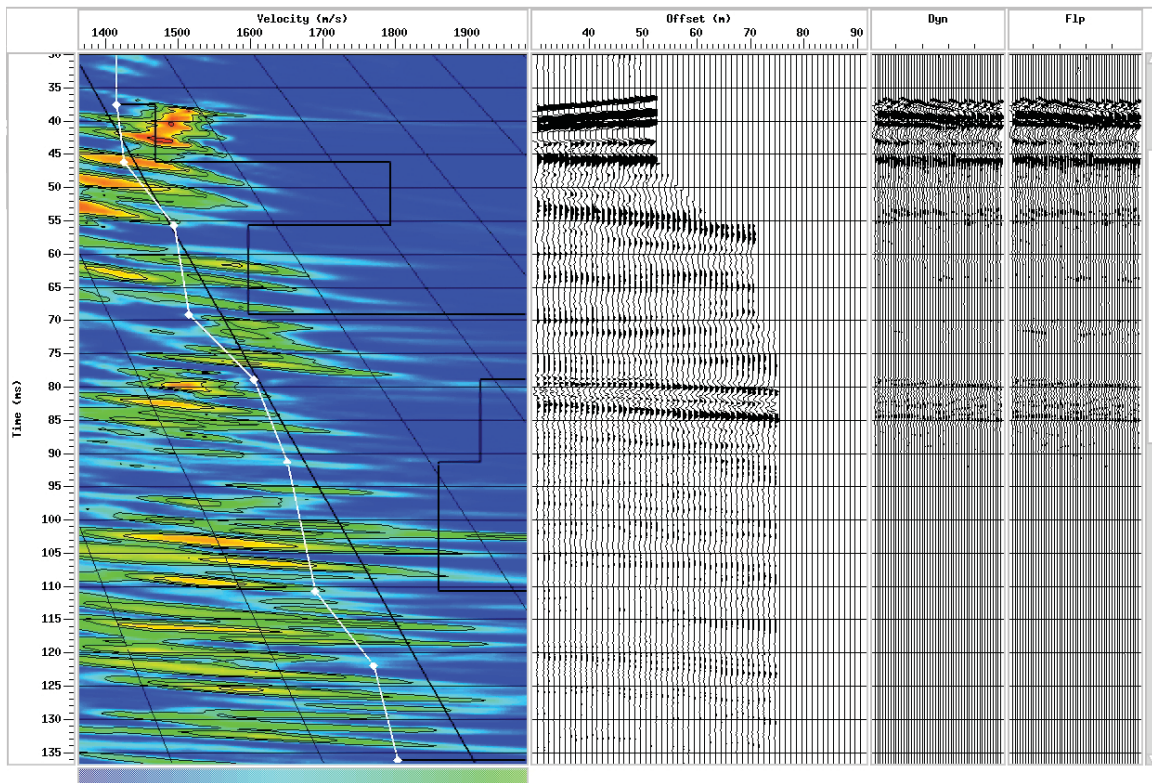


Figure 4.32: Intermediate velocity function picked to separate multiple energy from primary events. The intermediate velocities will then undercorrect (dip down) the multiple energy and overcorrect (dip up) the primary energy. This is observed in the centre panel.

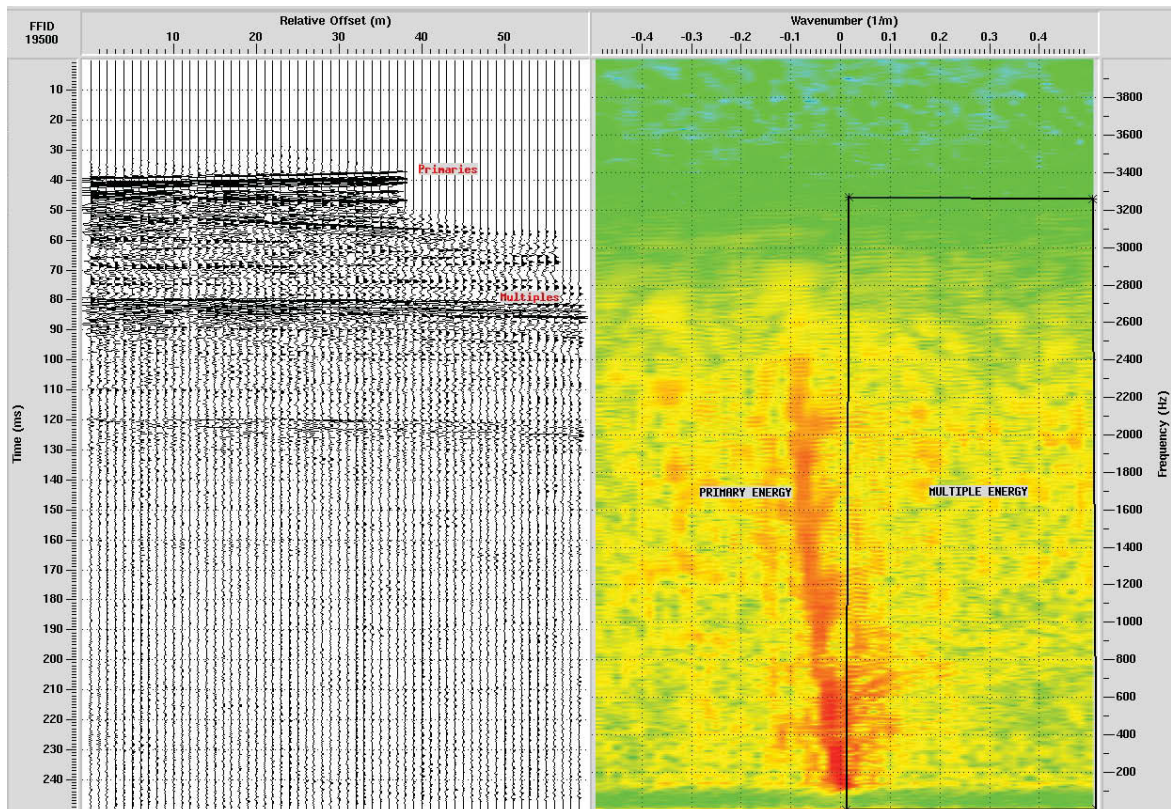


Figure 4.33: FK filter designed to remove multiple energy. This energy is dipping down after NMO correcting (as in figure 4.32) and therefore will appear in the positive quadrant of the FK domain. The filter shown here will reject energy within it.

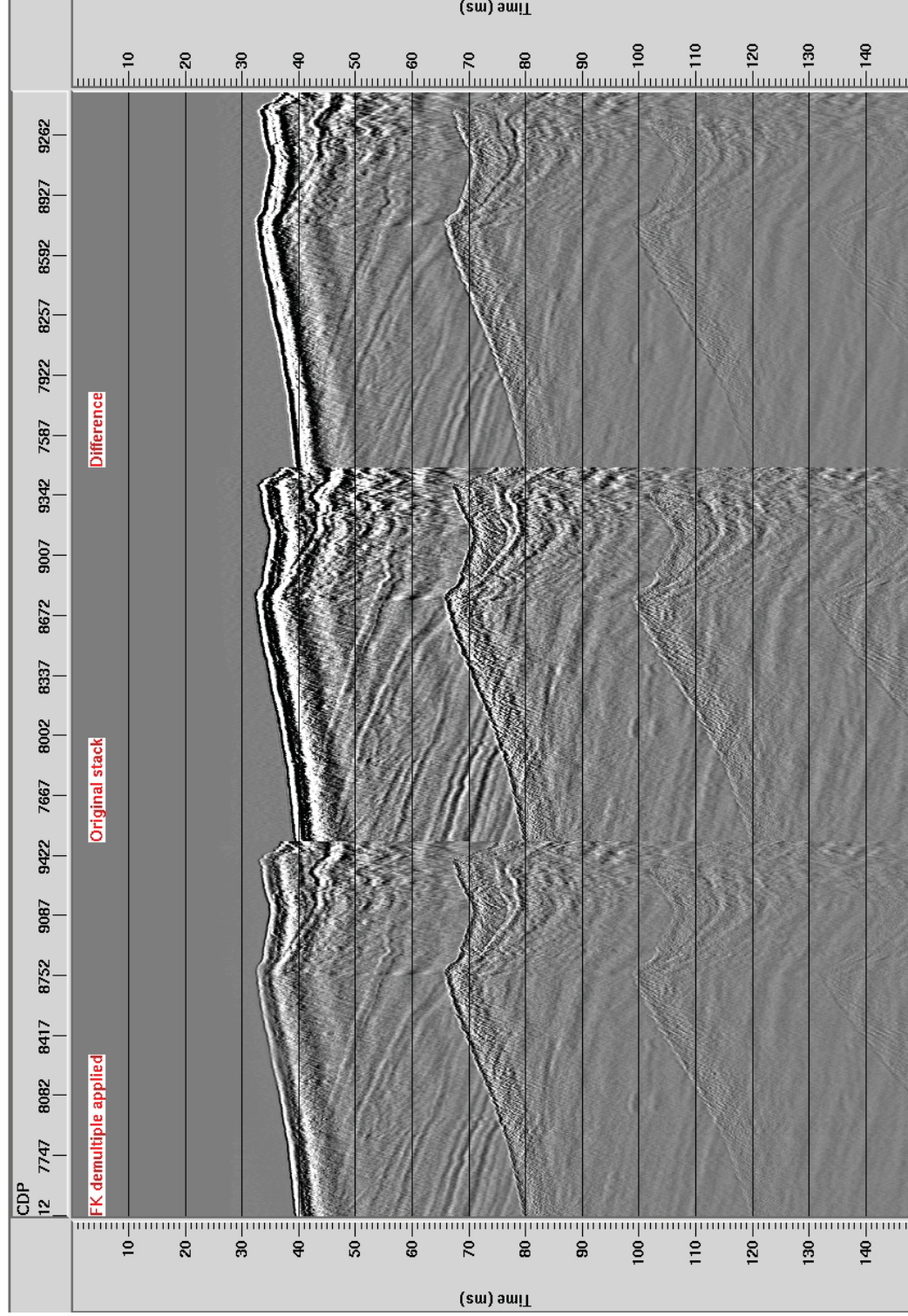


Figure 4.34: Effects of applying FK demultiple to CMP range 6336-9627. The left panel has been filtered and the right panel displays the effect of applying the filter.

4.3.2.2 Migration

The stacked section has had multiples and ambient noise suppressed, but still contains several diffraction events due to irregularities on reflectors. The most problematic regions are the areas that have been dredged by the aggregate companies and therefore have disturbed seabed reflectors (figure 4.35). The diffractions caused by this surface appear as steeply dipping energy and could be masking events below. Also identified on figure 4.35 are ‘bow-tie’ artefacts caused by the small wavelength undulations of the seabed.

Similarly, there are several high amplitude irregular sub-surface reflectors, which are identified on figure 4.36, also causing several diffraction events, which could be obscuring deeper horizons. Migration can be used to remove this steeply dipping energy by collapsing the diffraction curves. Migration also moves dipping reflections to their true subsurface positions thus increasing spatial resolution and producing an improved image of the subsurface.

Stolt migration was used, which is performed in the frequency domain and has the effect of; shortening, steepening and moving reflectors in the up dip direction. On figure 4.37 the radial line represents a dipping reflector from the origin to point B in the FK domain. After migration has been applied this radial line now maps onto another radial line from the origin to point C. The horizontal wavenumber k_x is unchanged, but the dip angle θ and frequency ω do alter.

Figure 4.38 and 4.39 represent the dredged area and high amplitude channel area that had problematic diffractions present before migration. The figures show the effect of applying migration, which successfully removes the steeply dipping artefacts caused by the diffractions. The bow-tie effect mentioned previously is also now transformed into a synclinal feature.

4.3.2.3 Depth Conversion

Having the section as a function of depth instead of two-way travel time allows the horizons to be correlated with any well data and provides a more accurate image of the subsurface. Depth conversion converts the final stacked section from two-way time into depth using the velocity field determined previously. Figure 4.40 shows the section with depth, where the seabed reflection can be identified at approximately 30m depth, with the channel feature extending to depths of 55m.

4.3.2.4 Geophysical Logging of Vibrocores

A selection of the vibrocores collected in the survey area in June 2003 (discussed in chapter 5) can be interpreted using a multi-sensor core logging (MSCL) system at the Southampton Oceanography Centre (SOC). This non-destructive logging device provides information on the P-wave velocities and the densities (therefore the impedance), the magnetic susceptibility, and the P-wave amplitude of the sample at specified depths. Three vibrocores were selected to log; 8, 9, and 10 (see Appendix B).

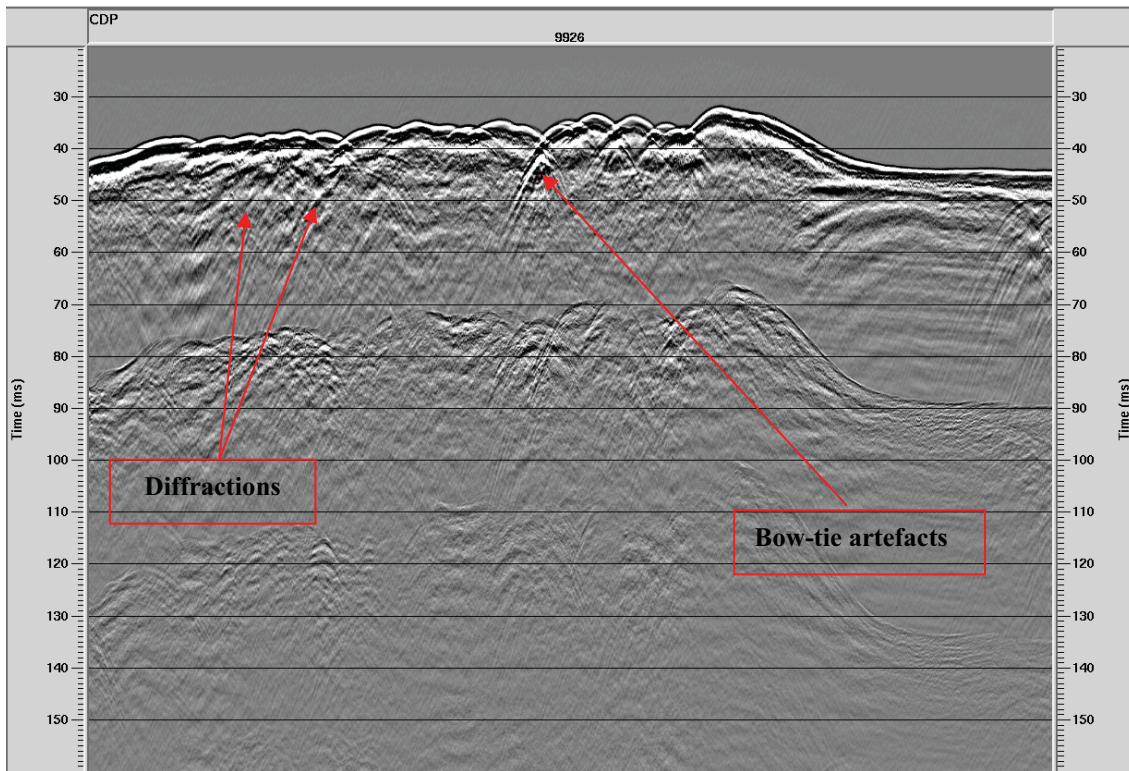


Figure 4.35: A stacked seismic section showing diffractions occurring due to dredged site within the area.

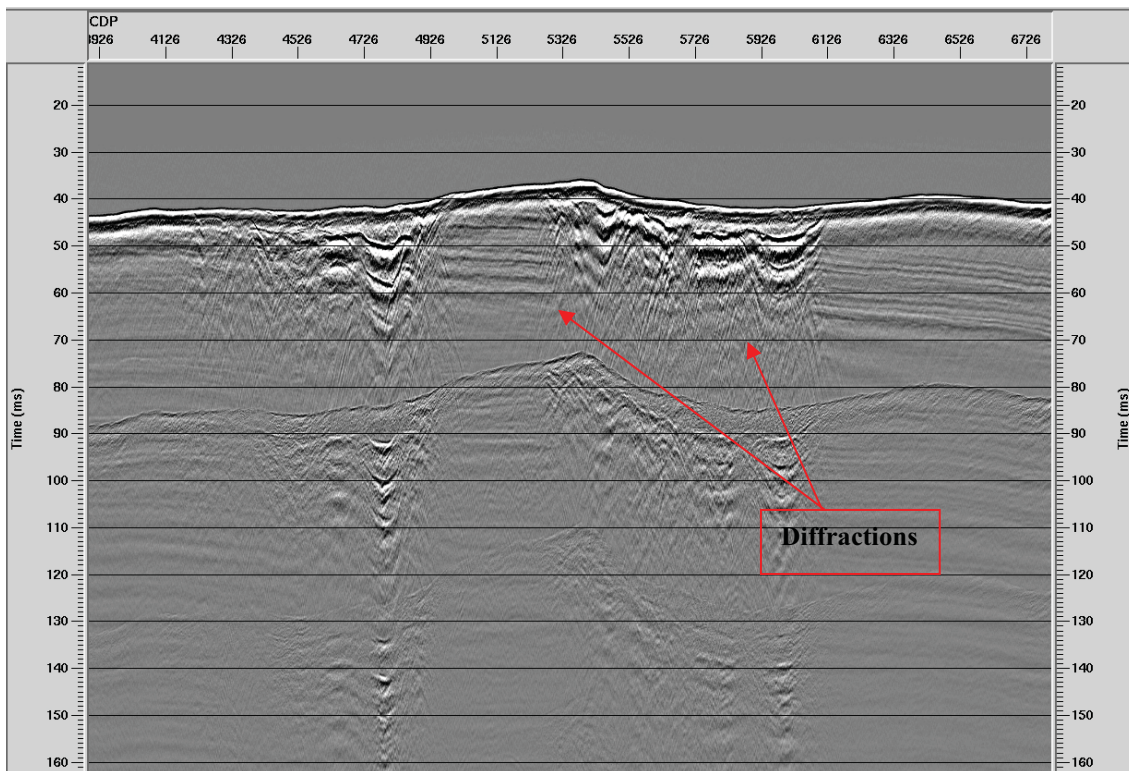


Figure 4.36: A stacked seismic section showing diffractions due to high amplitude truncated reflector.

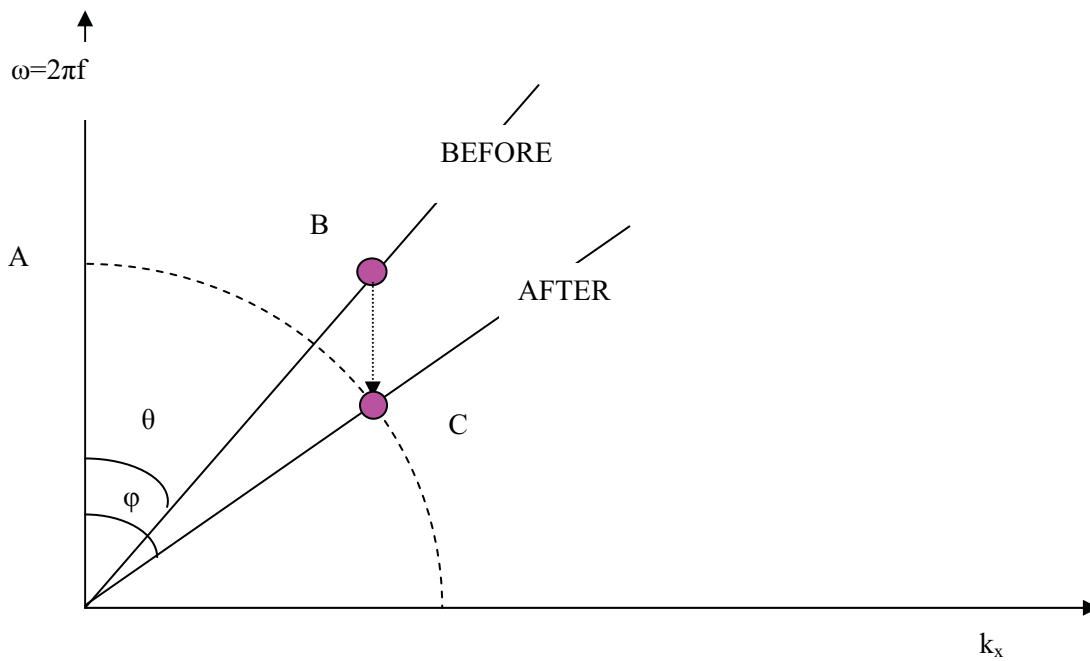
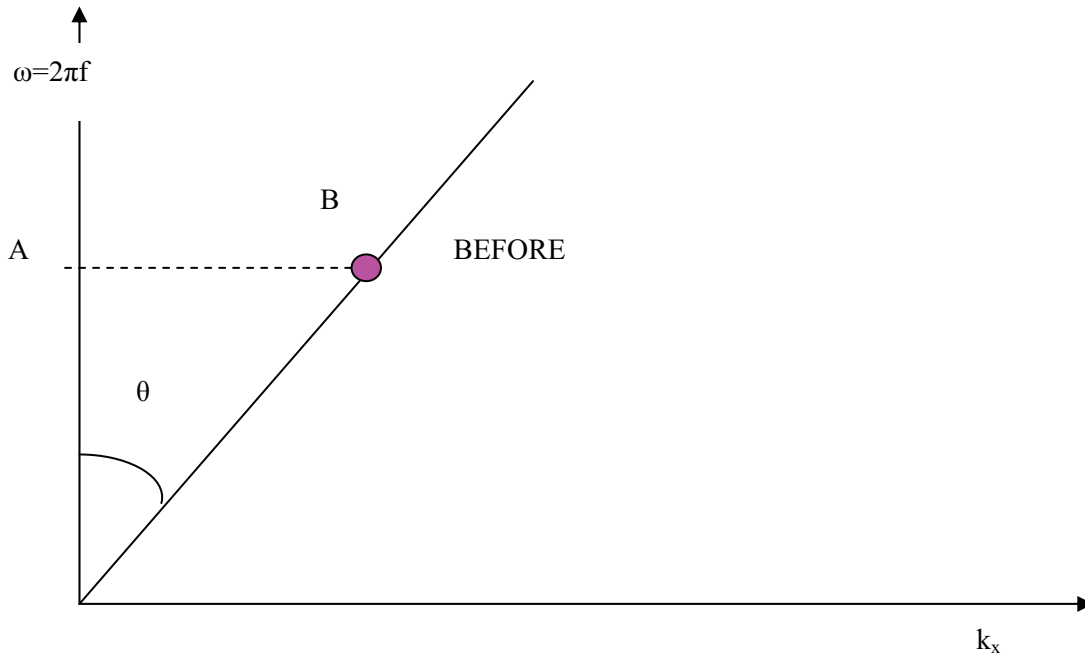


Figure 4.37: Migration in the FK domain. Migration has the effect of moving events up dip whilst keeping the wavenumber constant.

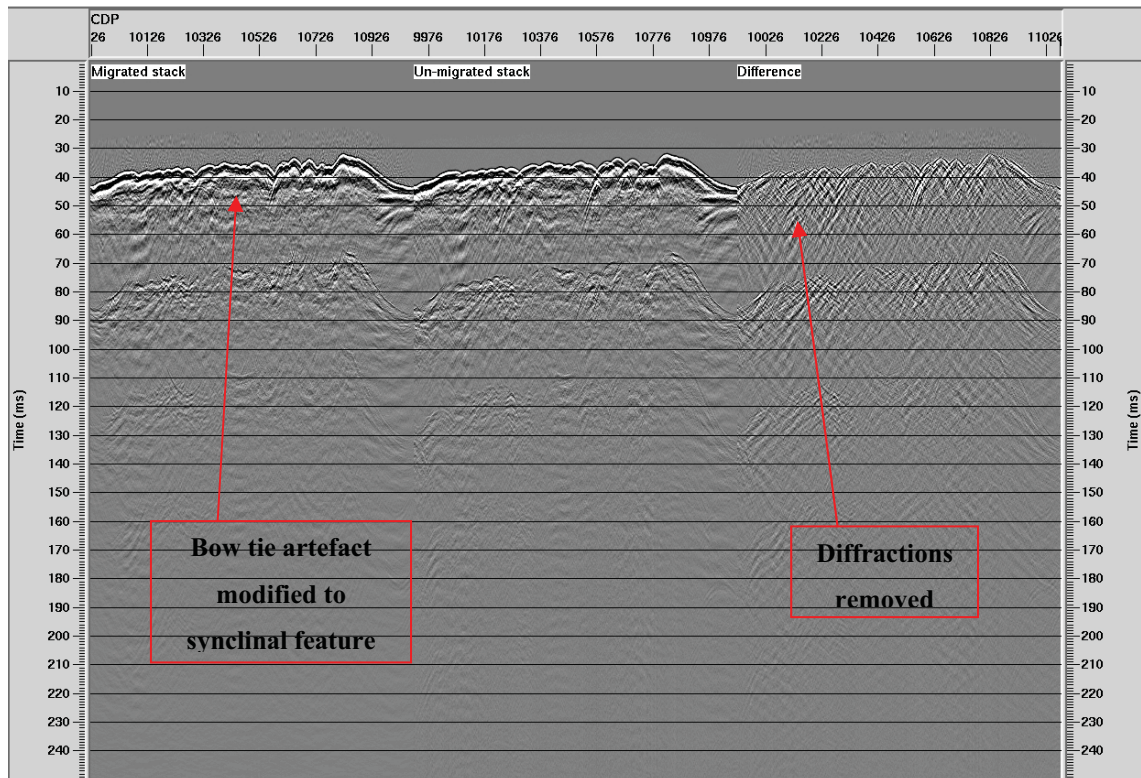


Figure 4.38: The stacked seismic section as imaged in figure 4.35, showing the effects of migration over the dredged area.

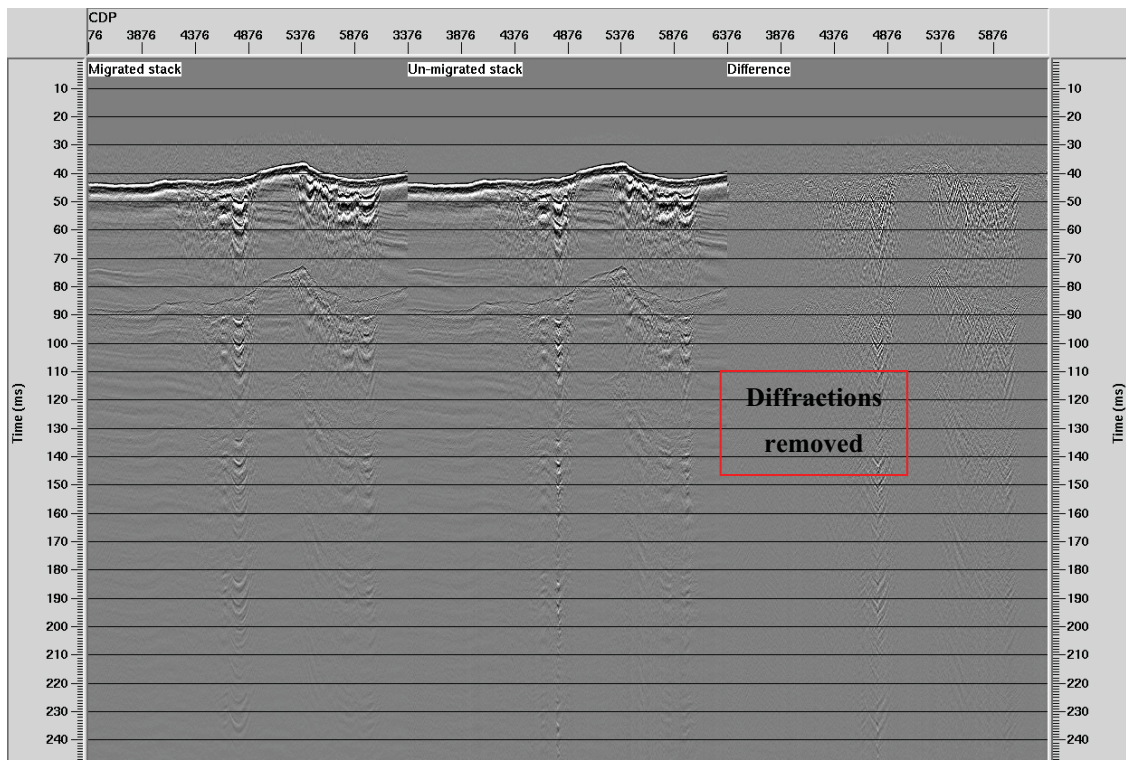


Figure 4.39: The stacked seismic section as imaged in figure 4.36, showing effects of migration over channel area.

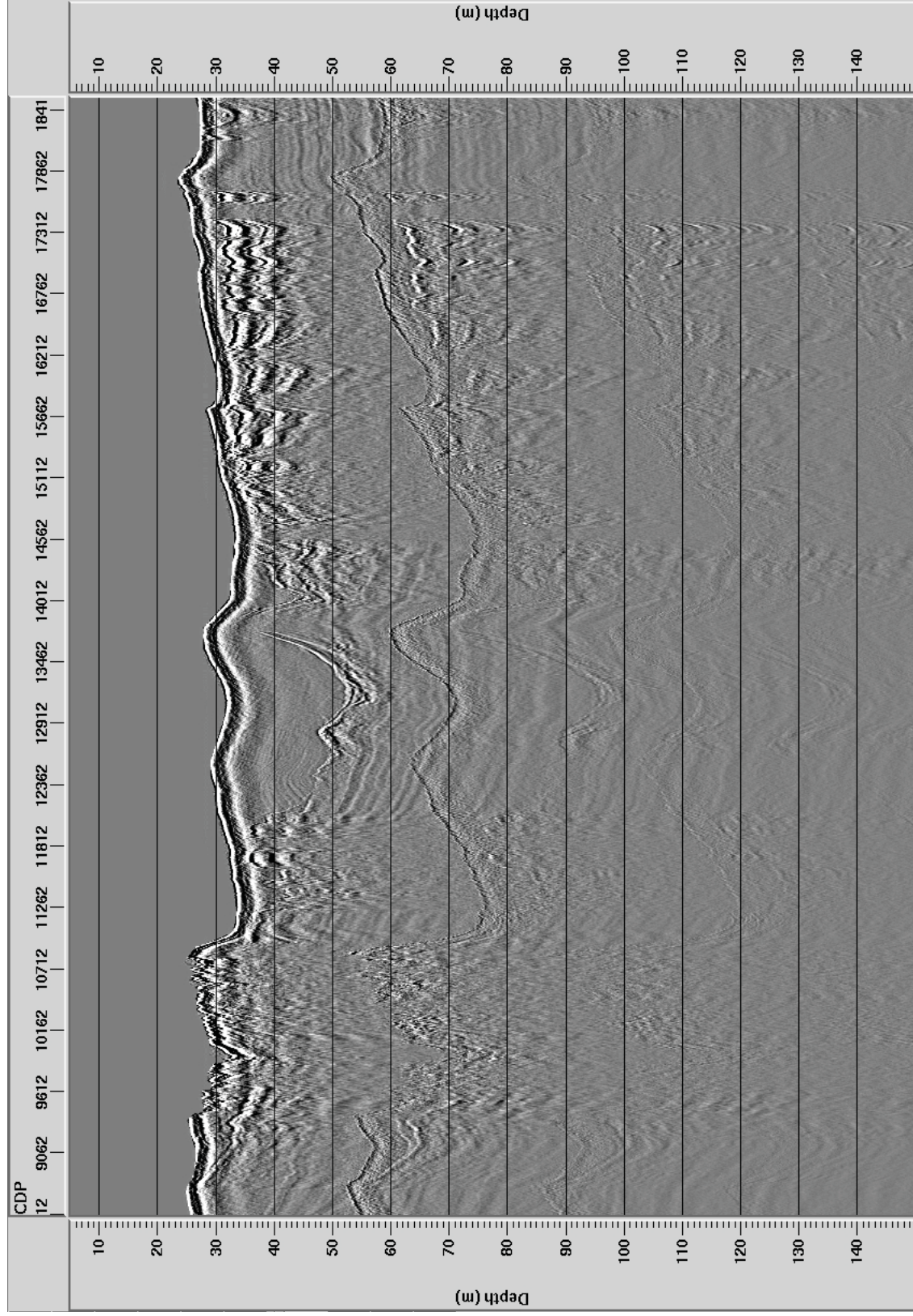


Figure 4.40: Depth converted stacked seismic section for line 5.

Problems were encountered however, since the cores were logged in December 2003 and had therefore been in storage for 6 months. The result of this delay caused the core samples to dry out and become un-representative of the sub-surface that they were extracted from. Additionally the P-wave transmitter within the MSCL system couldn't transmit P-wave energy through air. Hence in regions where air had replaced pore fluids, the logging device returned a null response (zero P-wave amplitude). This dramatically affected the results. No P-wave velocities were returned from core 8, and limited velocities were determined from core 9 and 10. Figure 4.41 shows the velocity variation with depth for cores 9 and 10. The different lithologies are also identified on the figure as interpreted from the cores in figure 4.42. The velocities all lie around 1600m/s with a slight increase corresponding to the mud lithology. There is no other real correlation with depth or lithology. Figure 4.43 shows the density variations with depth for the two cores. We would expect an increase in density with depth corresponding to compaction, but again there is no evident correlation with depth or lithology. It was therefore concluded that the condition of the vibrocores is imperative in producing significant results from the MSCL system. The optimum results would be obtained either by down-hole logging (expensive and time consuming) or immediate logging on the vessel. The long period of storage after collecting the cores was significant enough to dry out the samples and cause logging and interpretation to be unreliable.

4.4 DATA ASSESSMENT AND INTERPRETATION

Figure 4.44 shows the final processing flow developed for the data. The previous analogue surveys that were acquired in the study area by the aggregate companies were processed to stage 1 in the flow. All the new digital lines were processed to stage 2, however because of time constraints, only a selection of priority lines were fully processed to stage 3.

4.4.1 Comparing sections throughout processing

Figure 4.45 shows how the processing affects the imaging within a channel section. The aggregate companies processed their seismic data to stage 1. After the first stage of processing the channel is identifiable due to the high amplitude base reflector, which is likely to be coarse sediments such as gravels, but it is difficult to distinguish any internal stratigraphy. It is also difficult to determine the shape of the sides of the main channel, and secondary, smaller channels either side of the main cut. After the second stage of processing, the quality is comparable to digitally processed single channel data. Again the channel cut is clear, but although the ghost effects have been removed, internal stratigraphy and the structure beneath the cut are still tenuous to interpret. Finally after the full processing sequence has been applied to the data (stage 3), it is clear the image has improved considerably.

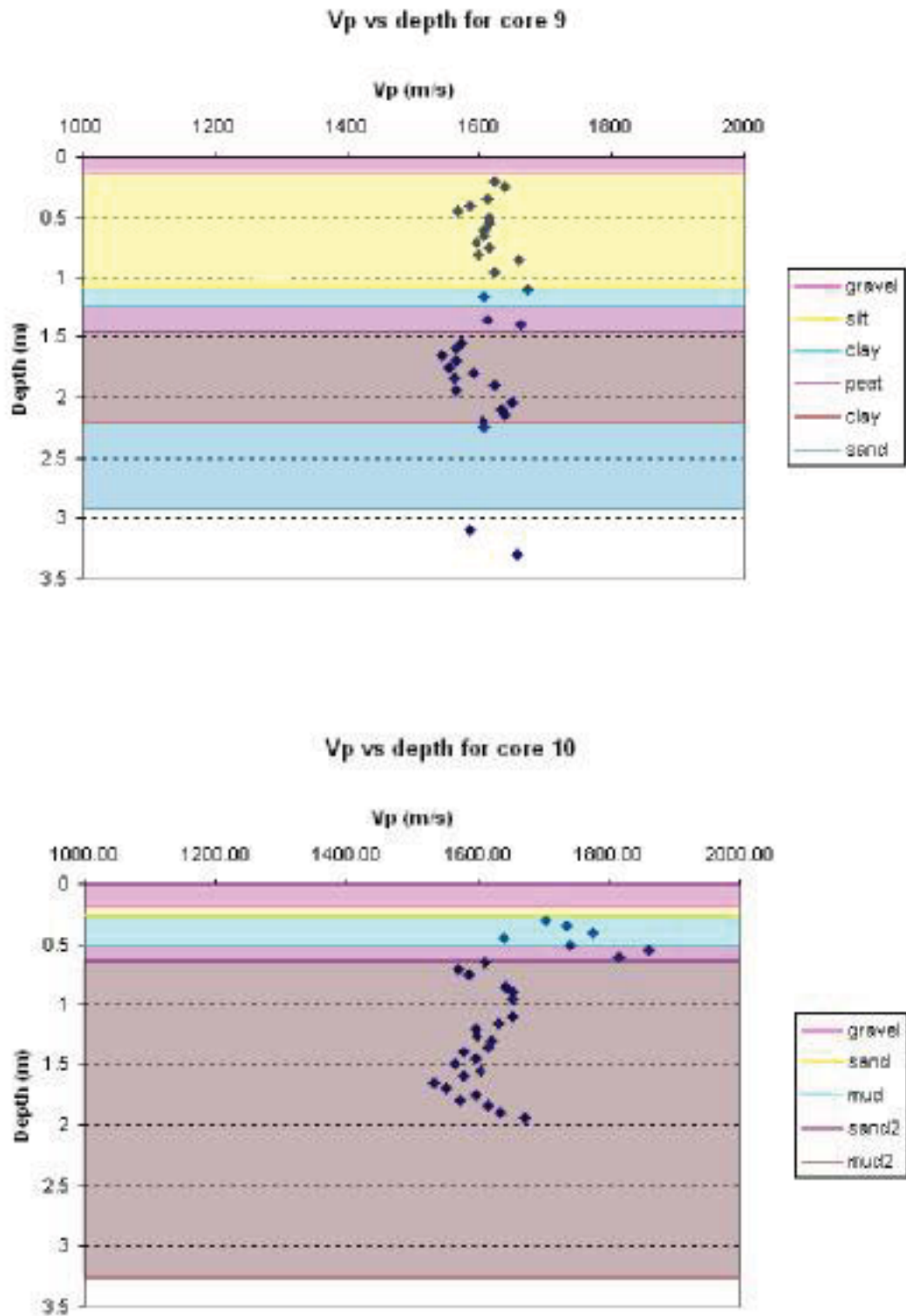


Figure 4.41: P-wave velocity as a function of depth for vibrocores 9 and 10. The shaded regions show interpreted lithologies.

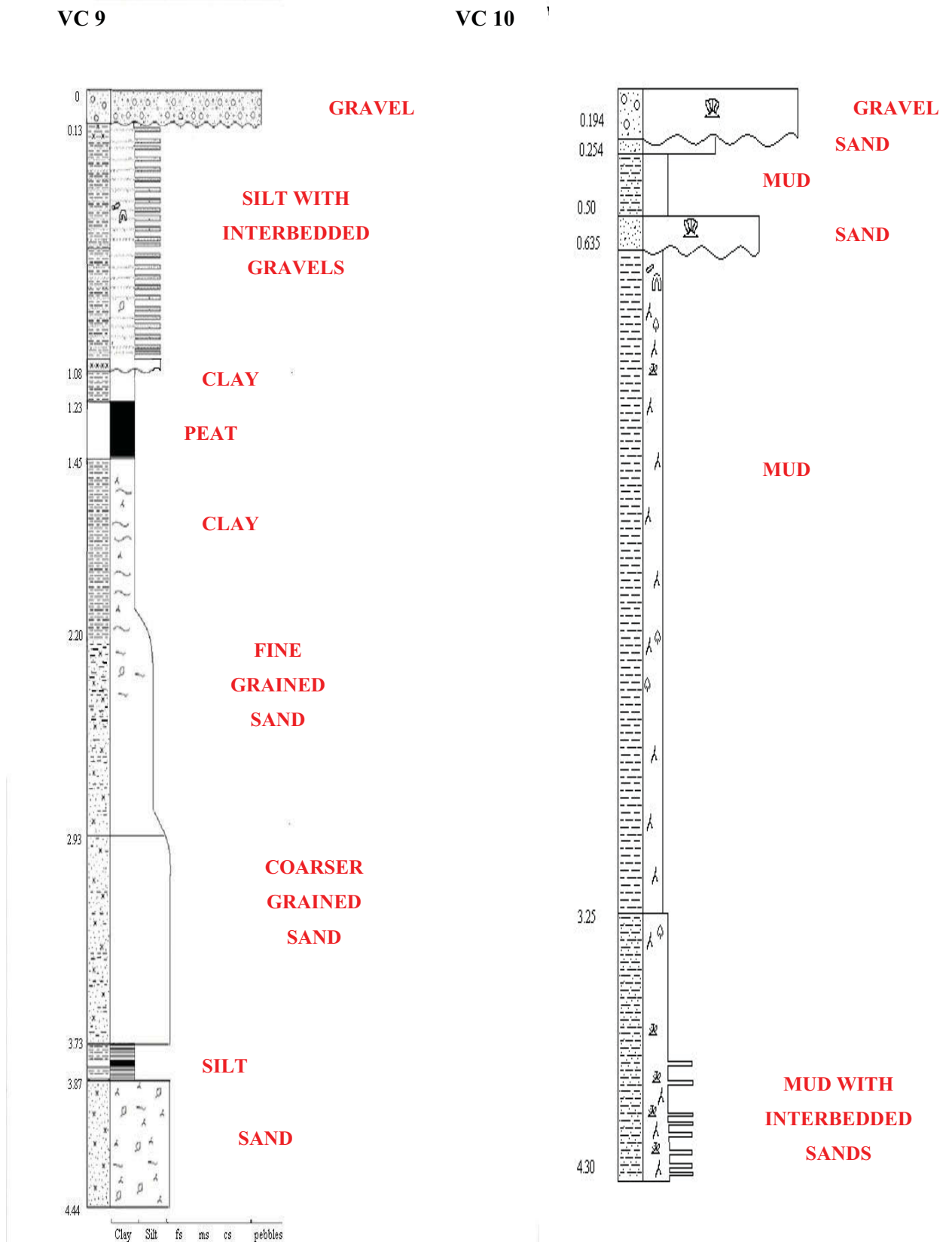


Figure 4.42: Sedimentary logs of vibrocores 9 and 10 used in figure 4.41 and 4.43. The numbers on the y-axis represent depth in metres, with the x-axis representing grain size, increasing to the right.

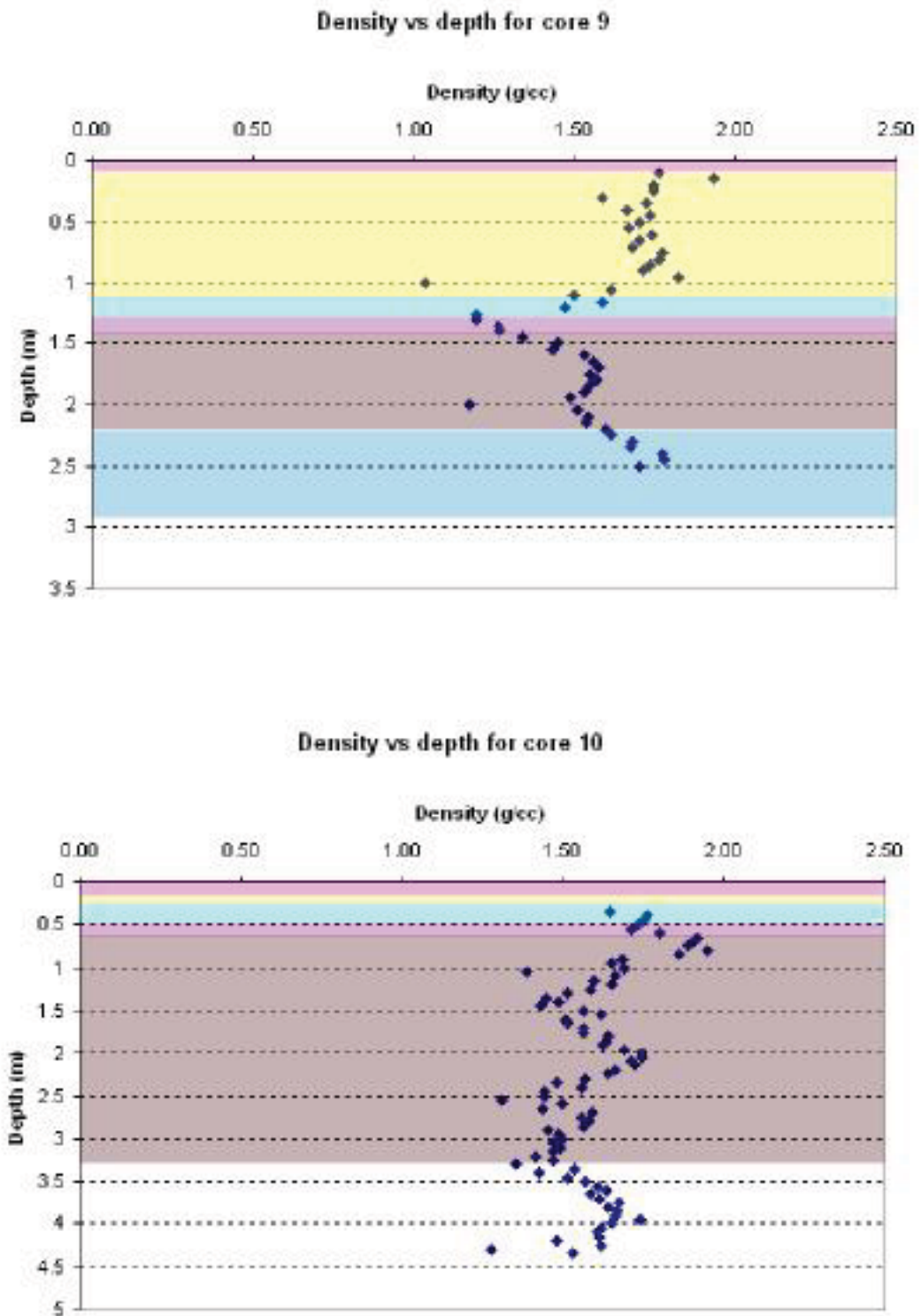


Figure 4.43: Density as a function of depth for vibrocores 9 and 10. The shaded regions are the lithologies interpreted as shown in figure 4.41.

The base of the channel can now be seen to extend further with the steep dipping horizon on the right, now interpreted not as the base of the channel, but as a later channel cut. Additionally, internal structure interpreted as distinct infilling events can now be identified. There are several dipping horizons, which can be interpreted as the fine infilling of sediment within the channel.

4.4.2 Base channel picks

To successfully map the course of the fluvial system offshore, all the survey lines were processed to stage 2 (figure 4.44), to reduce coherent and ambient noise. Single channel sections were then produced for each line by combining the first channel from each shot gather. These figures were studied to identify any channel features. Figure 4.47 shows an example of a few single channel sections from the 2003 seismic line, with their locations and shot numbers shown on figure 4.46. As is apparent some lines were more problematic than others, mainly due to the weather. The survey lines acquired in the northern region of the study area contain more problematic seabed multiples since they are in shallower water. Removing this high amplitude coherent noise was more complex in these regions due to less differential NMO between the shallower sediments and the water velocity, which caused degradation of the seismic image. The southern regions were in deeper water and consequently the sediments had a higher P-wave velocity due to compaction, therefore the differential NMO between the sediments and the water was larger. This allowed for more successful multiple suppression.

The quality of the image is also very dependent on the sea-state. Table 4.1 shows the weather observations for each survey line. Days when the weather was poor resulted in a drastic decrease in quality of the recorded seismic image. The rising and falling of the tide also had an effect on the recorded quality. When the vessel was sailing against the tides, the speed was reduced dramatically. This resulted in a reduction in shot spacing (Δs – chapter 4.4.3.1), which would increase the fold of coverage of the data. Consequently, this would increase the quality of the data. Similarly, when the vessel was sailing with the tides, the speed was increased and therefore the shot spacing increased. This resulted in a reduction of fold and a reduction in recorded quality accordingly.

Using the single channel images, any apparent channel feature was picked within ProMAX™ to produce a set of tables containing the location and two-way time (TWT) to the channel. Examples of the channels are shown in figure 4.48. These channel picks were then combined with picks from the previous surveys to identify the course of the palaeo-Arun from its onshore mouth at Littlehampton to where it meets the northern palaeochannel. This interpretation is discussed in chapter 5.

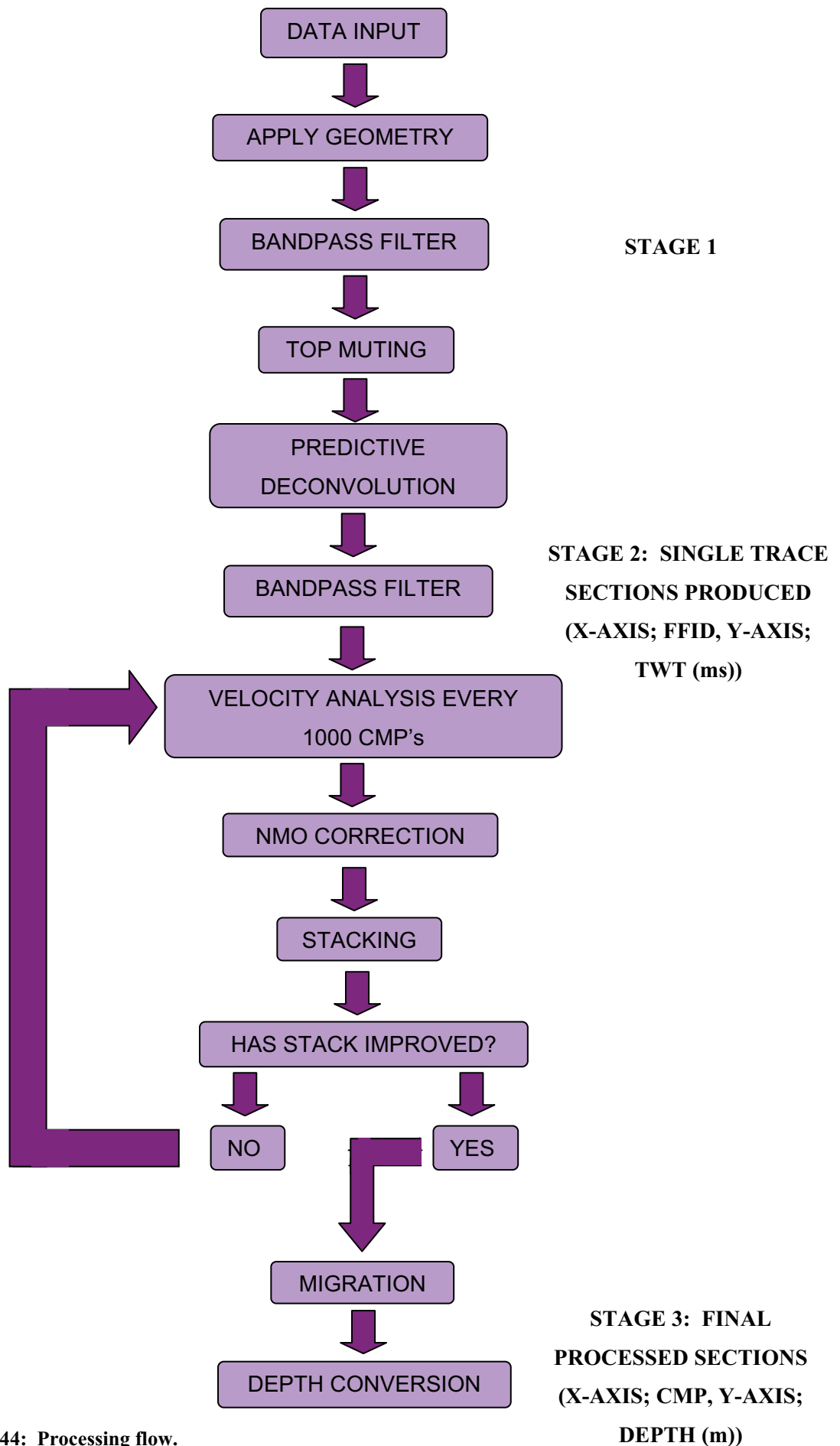


Figure 4.44: Processing flow.

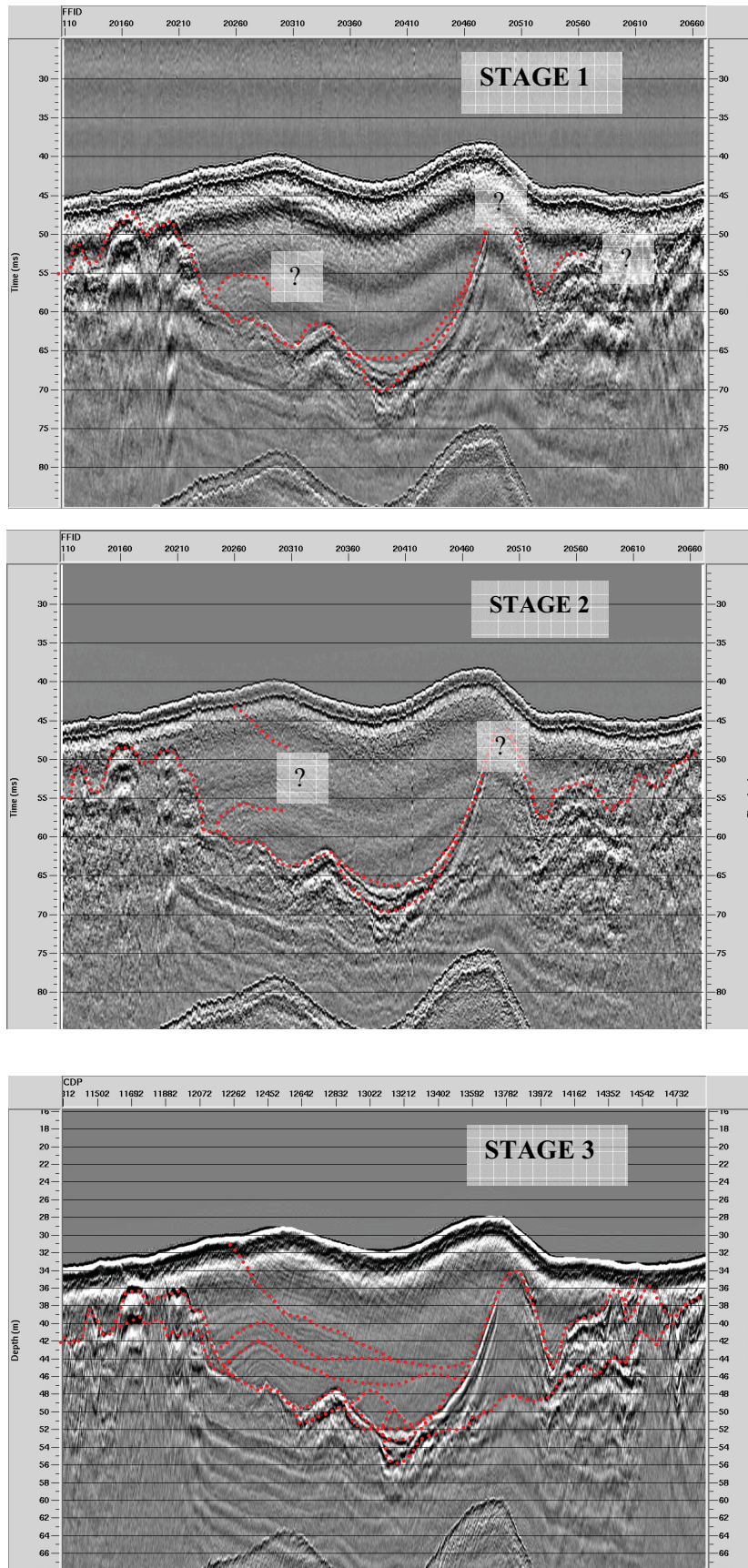


Figure 4.45: Channel imaged after different stages of processing.

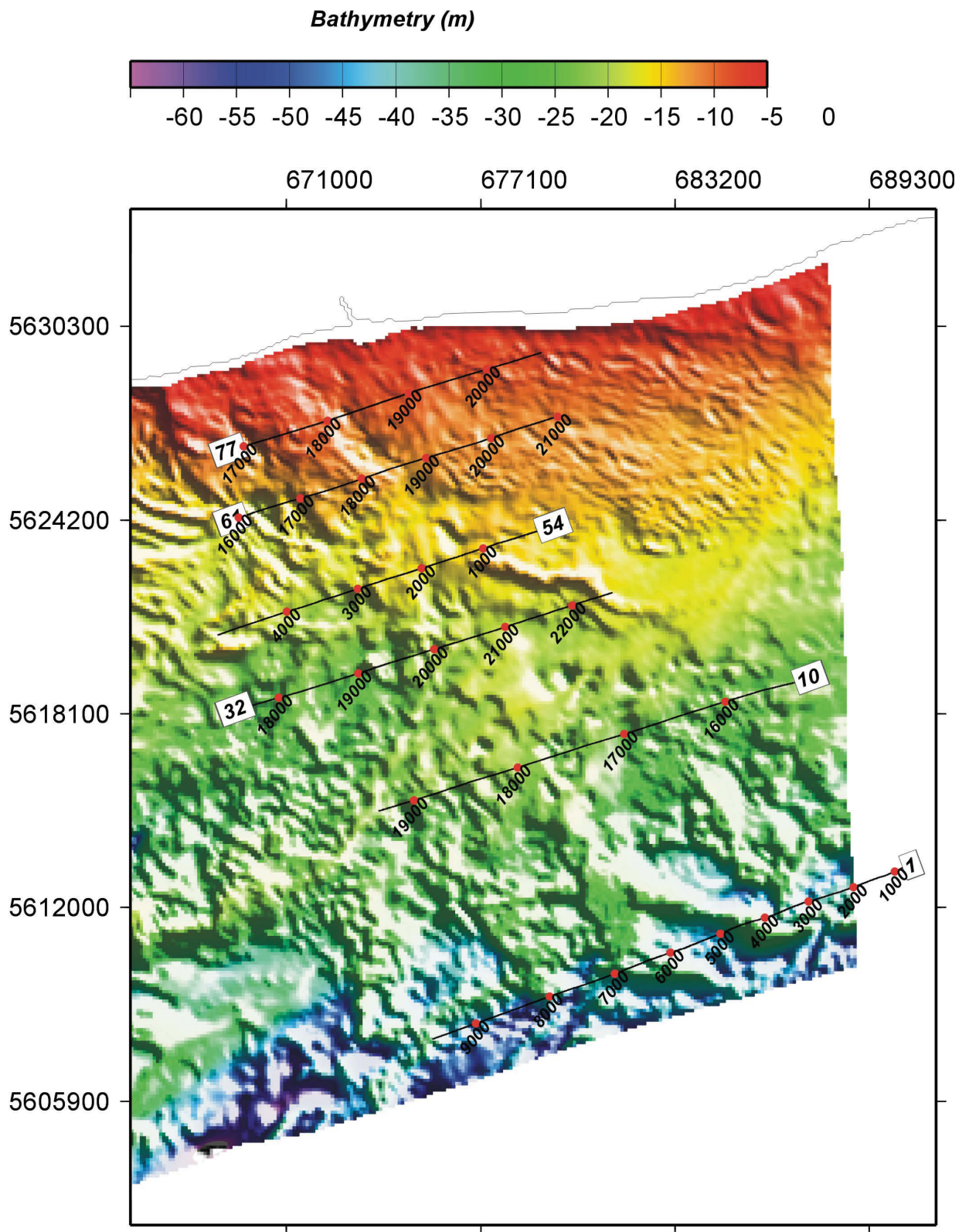


Figure 4.46: Location of six example lines used in Figure 4.46. The lines have their shot (FFID) number labelled every 1000. The seismic lines are superimposed on the singlebeam bathymetry data. The coastline is also identified as the thin black line above the bathymetry data, showing the mouth of the Arun onshore fluvial system.

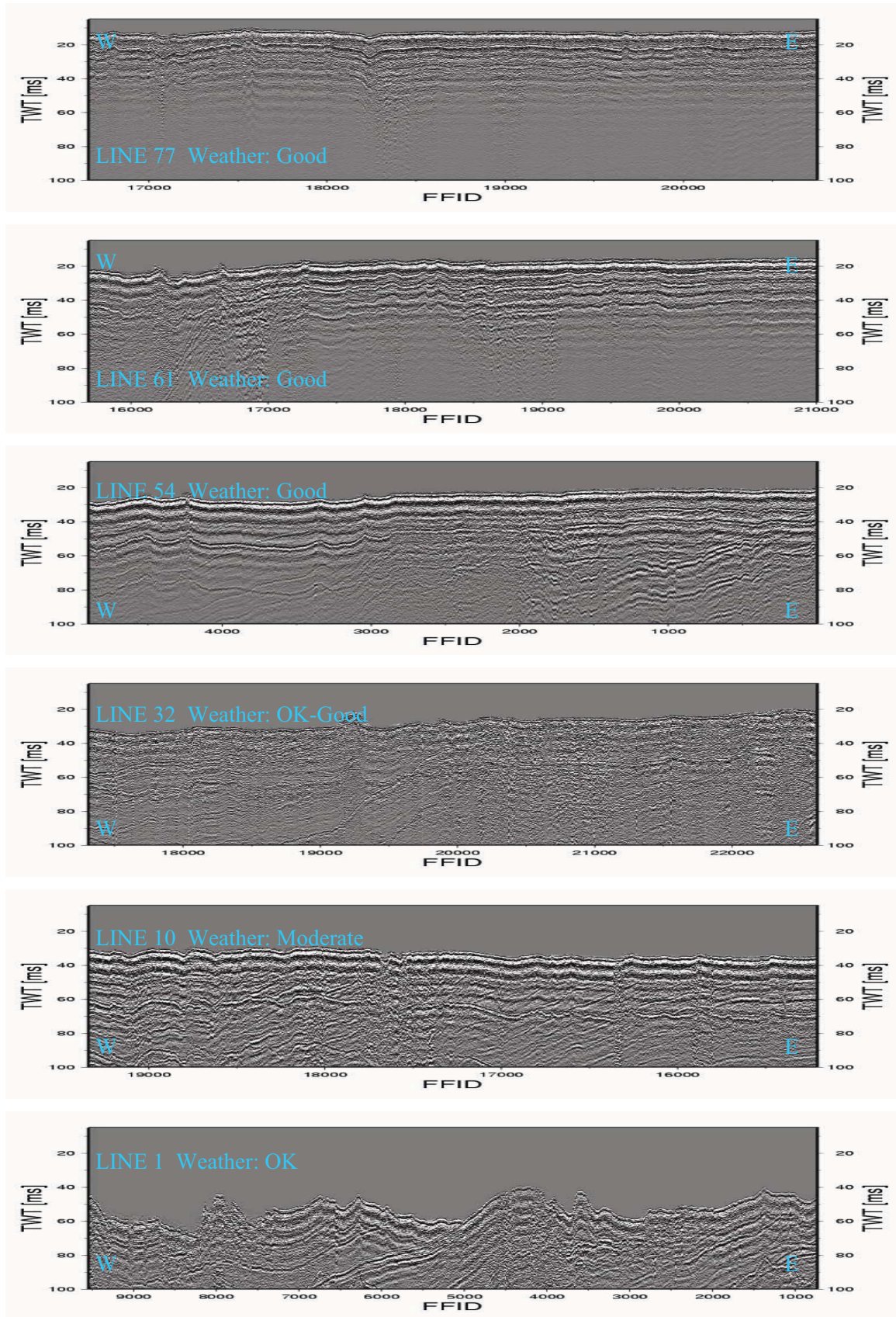


Figure 4.47: Six examples of single channel sections, comparing the quality of the lines due to weather and sea-state variability. The figure also indicates the problematic multiples associated with the shallow survey areas.

4.4.3 Resulting multi-channel sections

Figure 4.50 illustrates the fully processed seismic lines for the southern part of the study area. The valley is focussed on and followed north across the different lines as shown in figure 4.49. Following the main channel northwards shows the complexity of the fluvial system. Note that not all the lines cross the channel perpendicularly. Annotated in red are different cut and infill events that can be identified due to the multi-channel processing. The overall trend appears to be a fine infill of sediments with a coarse gravel base. There are deep incisions representing the main channel that cut to depths of 30m. Either side of these deep incisions are broader channels (5m deep), which have a terraced-like geometry.

4.4.4 Comparison between 2003 boomer and previous studies

The channel section seen on line 5 (figure 4.50) is also imaged with the previously acquired analogue seismic data. Four other surveys intersect the new survey line as shown in figure 4.51. The imaged channels can therefore be compared to give a qualitative evaluation of the differences in the sections due to acquisition and processing techniques. The survey parameters for each line can be shown in table 4.2.

Figure 4.52 shows the channel section imaged using the 4 analogue surveys (note that the lines are not co-incident). The display parameters used for analogue data are critical to the quality of the paper record. The application of AGC, TUG and other trace scaling processes and the power source was not known.

Figure 4.53 shows the direct comparison between the fully processed 2003 data and the 1999 analogue data. The 1999 dataset provides excellent imaging of the shallow internal interfaces that are not easily identifiable on the 2003 data. However after 15ms below the seabed reflector there is little energy recovered except the high amplitude gravel base of the channel. The 2003 dataset has problems resolving near surface reflectors, but it does provide an improved image of the deeper interfaces. It also images beneath the seabed multiple, providing understanding of the bedrock control in the area. This Tertiary bedrock structure is important to image as it controls and constrains the fluvial system as discussed in chapter 3 and 5.

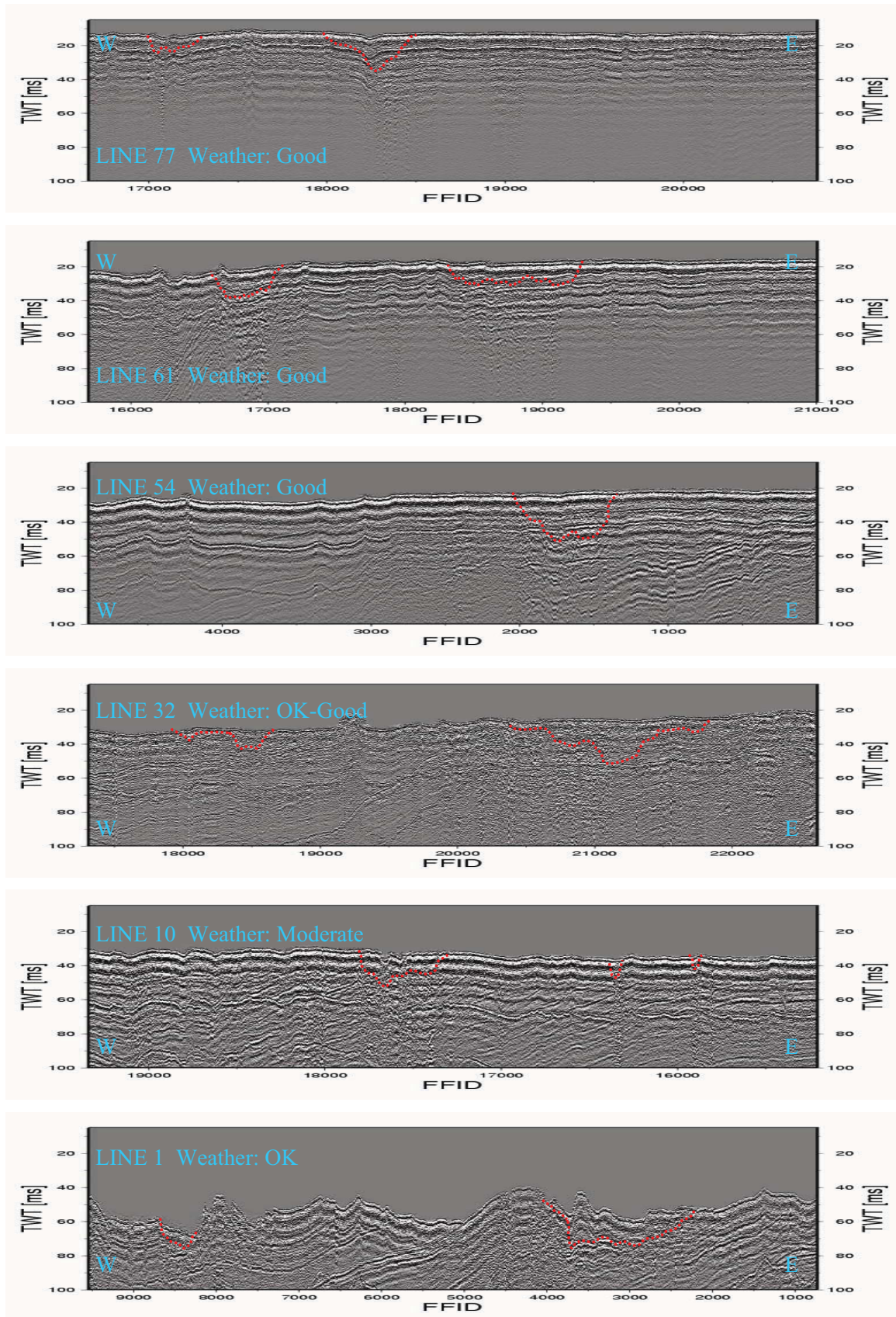


Figure 4.48: Single channel sections shown in figure 4.46, with base reflector picked (red line).

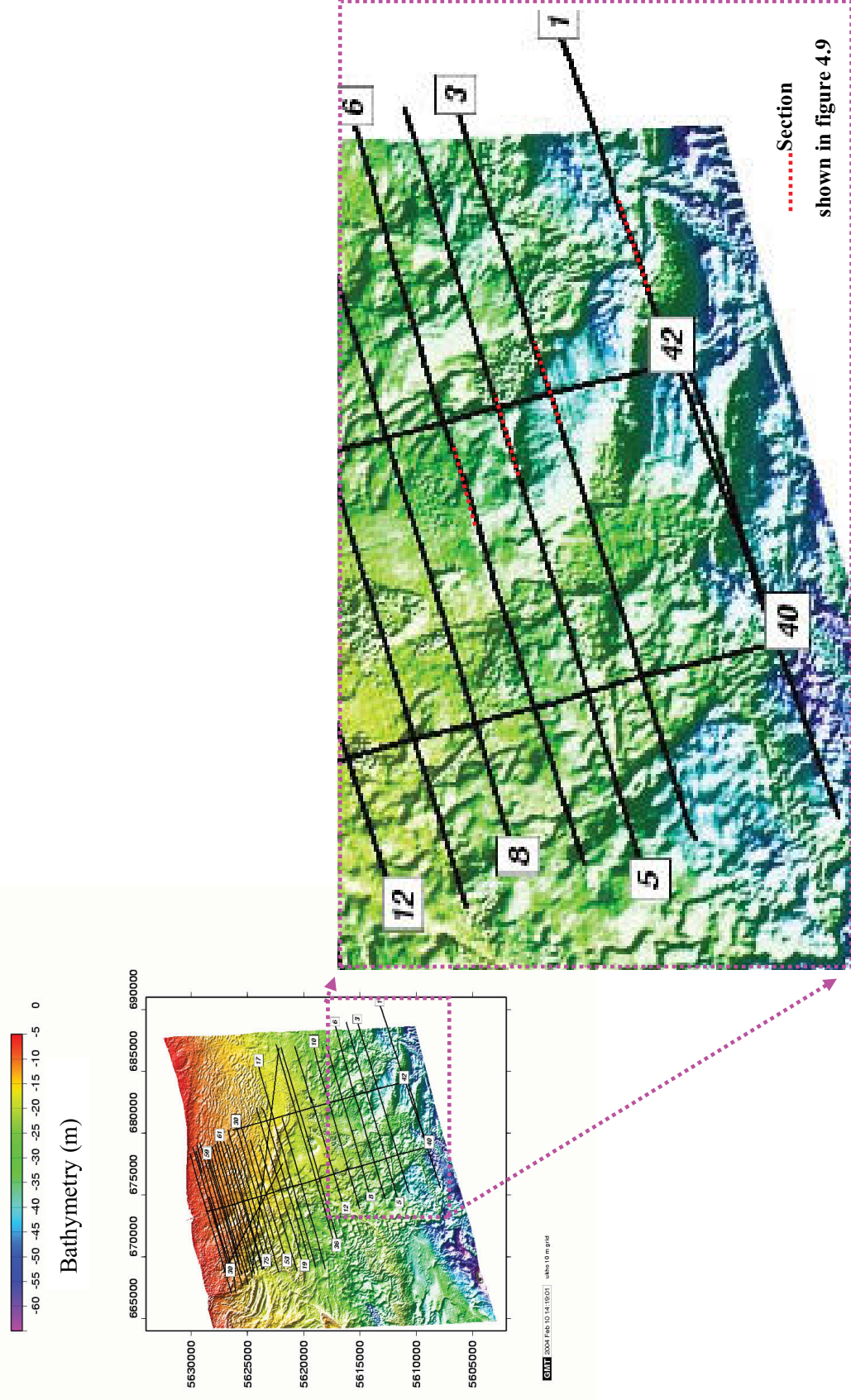


Figure 4.49: Location of seismic reflection lines fully processed and imaged in Figure 4.49.

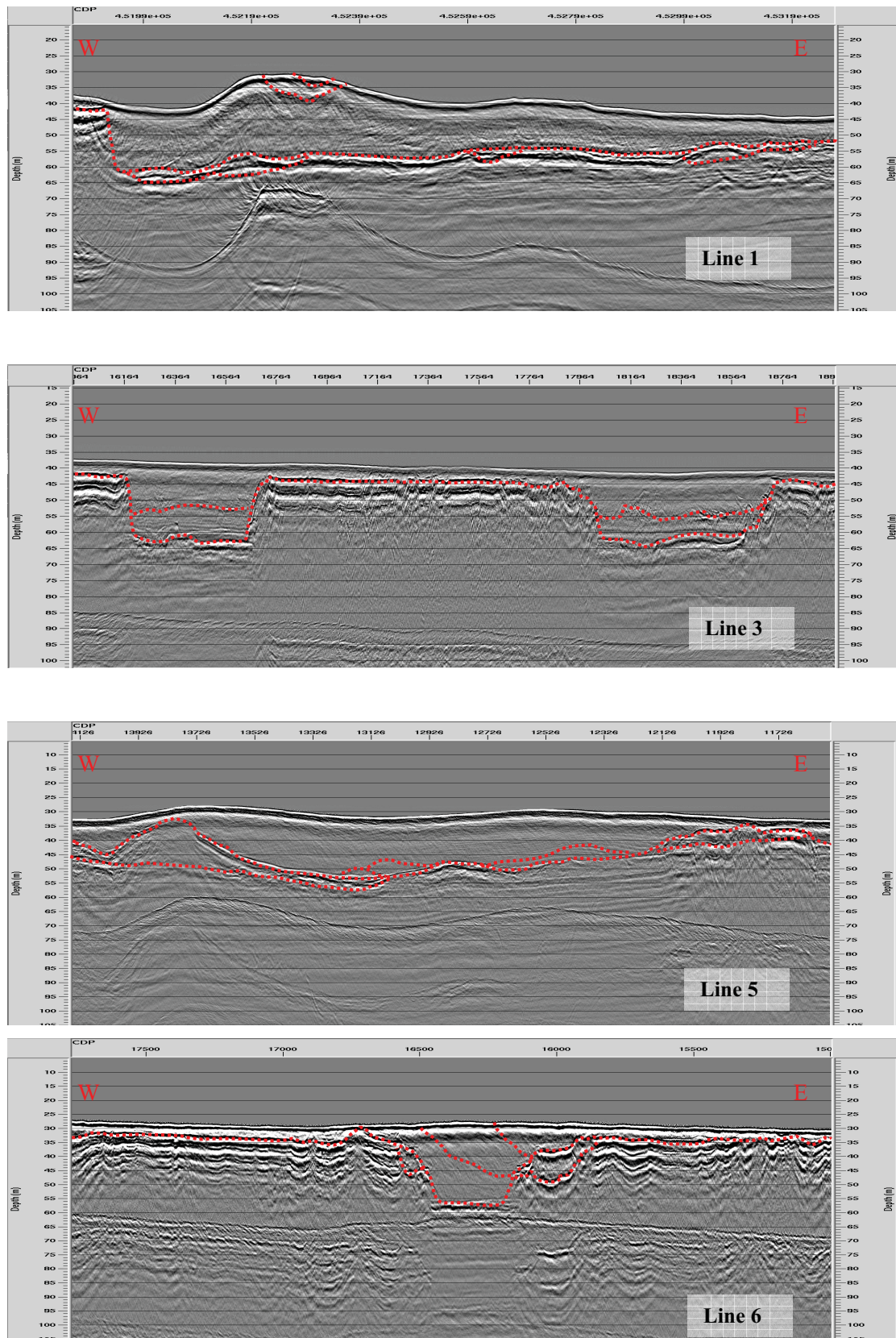
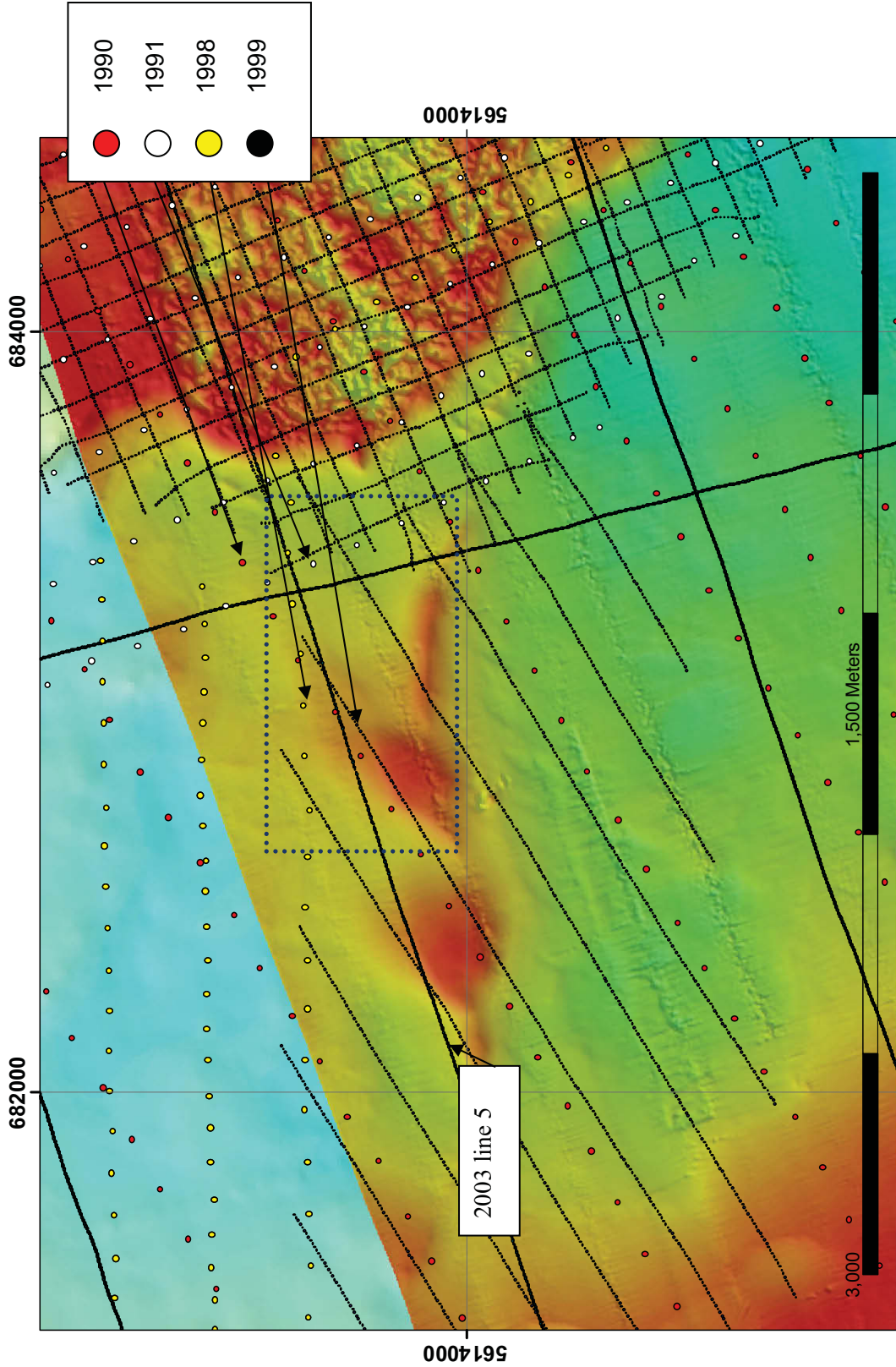


Figure 4.50: Mapping the palaeo-Arun fluvial system northwards. See Figure 4.48 for line locations.

The vertical exaggeration is x13 for each display.



682000 Figure 4.51: Location of compared lines shown in figure 4.49.

The seismic shown lies within the blue box.

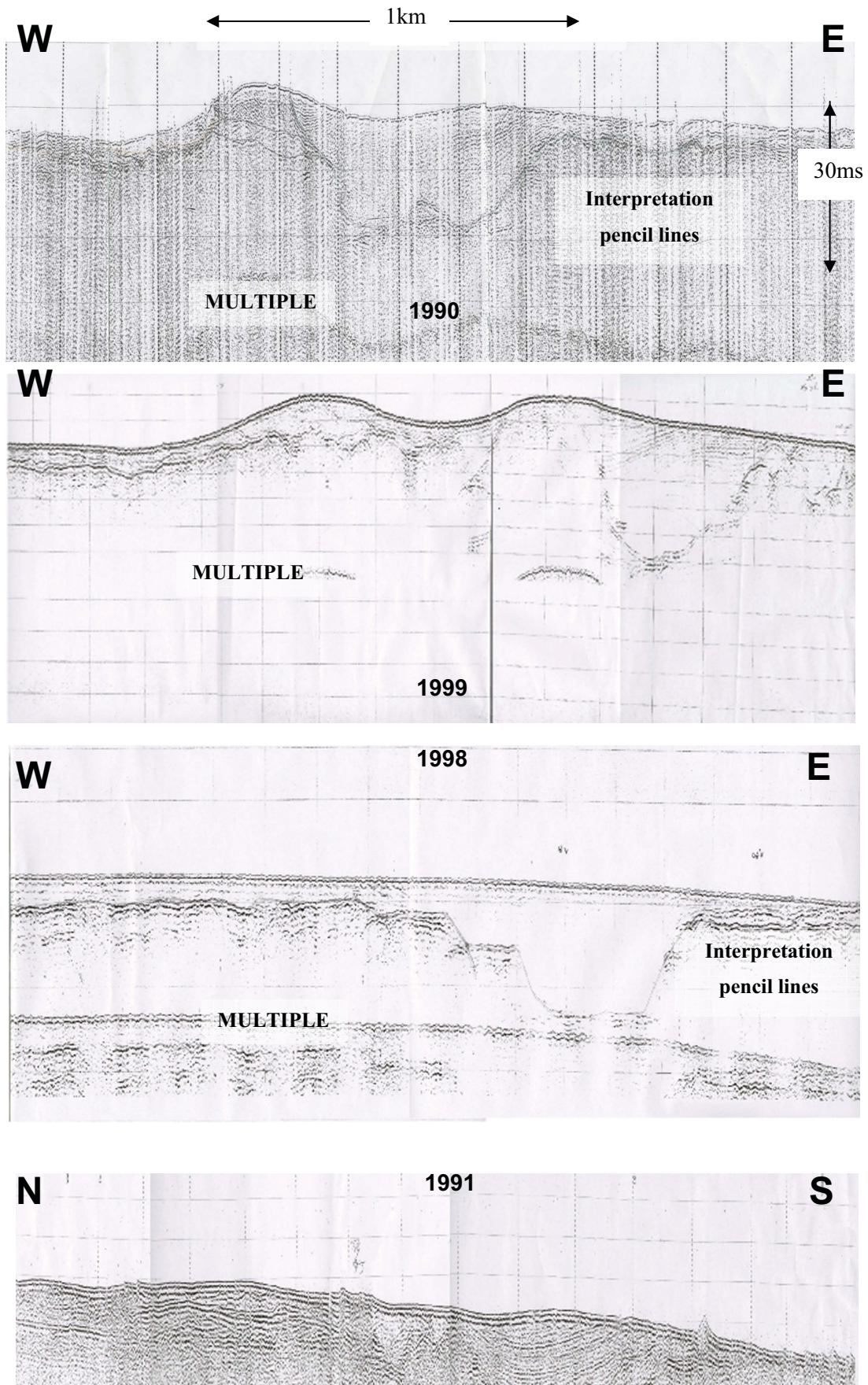


Figure 4.52: Comparison between analogue data. Scale on the first image is valid for all surveys. The vertical grid lines correspond to the shot frequency for each survey (table 4.3), except for 1998 and 1999 that indicate every 10 shots. The horizontal grid lines indicate TWT (10ms (90 & 98) or 5ms (91 & 99)).

Survey	Single or multi channel	Frequency Range (Hz)	Shot Interval (m)	Record length (ms)
1990	Single	700-2000	150m	125
1991	Single	1200-2000	120m	62
1998	Single	800-3500	10m	125
1999	Single	1000-2500	10m	125
2003	Multi	150-2000	1s (every 1-2m: variable due to vessel speed)	250

Table 4.2: Acquisition parameters for seismic reflection surveys acquired over 13 years

4.4.5 Archaeological Implications

The now-submerged shelf that was exposed during the previous glacial lowstand is likely to yield physical and cultural remains of Palaeolithic humans. The reconstruction of the palaeo landscape for the study area reveals potential locations of archaeological resources relating to early humans.

Terrestrial data indicate a direct relationship between areas of high archaeological resources and geomorphic features, which served either as a source of fresh water or as a topographic high (C.E.I. 1977). Such geomorphic features within a fluvial system include flood plains, river terraces, ponds and bays, and are likely to keep sites preserved prior to marine transgression. The additional rapid transgression to the present day coastline also acts to preserve any archaeological sites, as the area would not suffer from long periods of shoreface erosion (Stright 1986).

Using this information, possible archaeological resources could be located using the new processed boomer seismic lines. Figure 4.54 displays the seismic image of such possible locations, which exhibit high potential for the occurrence of preserved archaeological sites. Identified are the fill terrace depositional units as mentioned in 4.4.3. The new data allows these terrace features to be defined, increasing accuracy of the image and aiding the location of potential archaeological sites.

There is also potential for evidence of archaeological resources at the contact between the coarse basal gravels, representing the base of the fluvial channel, and the fine-grained sediments infilling the channels, representing estuarine deposition during marine transgression. The rapid marine transgression caused little erosion to such areas, allowing primary archaeological materials to be buried within the vicinity of their original location.

The processed data also allows for accurate delineation of the basal gravel lag and the valley base, which could contain secondary archaeological materials, re-worked and deposited by the fluvial processes affecting these areas over the past thousands of years. Using the new data permits more precise mapping of such features and allows their distribution and location to be more accurately identified.

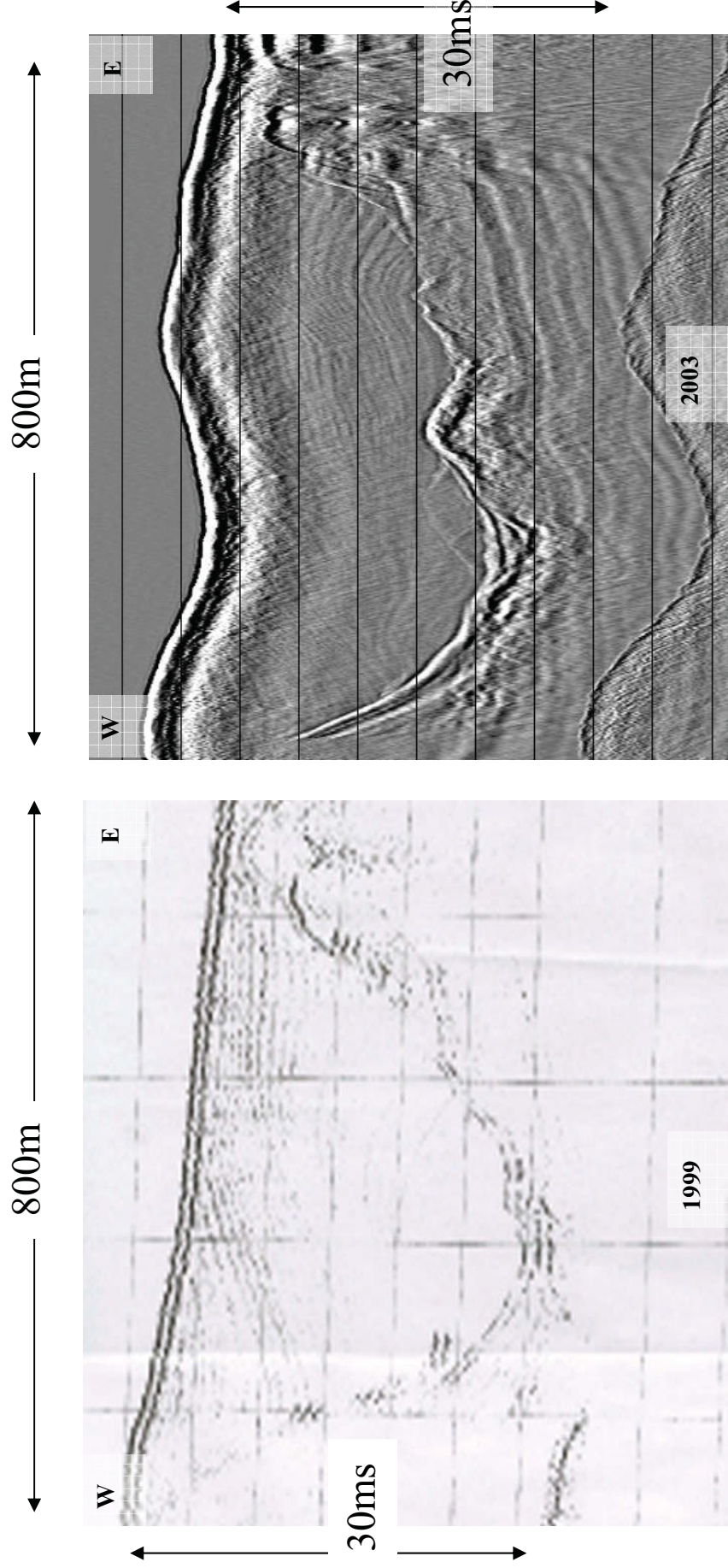


Figure 4.53: Comparison between analogue and digitally processed datasets. The Horizontal grid lines on both panels indicate every 5ms, with both panels having a vertical exaggeration of x20.

4.5 DISCUSSION

It is clear from the comparison of the different seismic surveys over the years that processing drastically improves the quality of the seismic image. It allows both coherent and ambient noise to be suppressed, which could be masking low amplitude events. The target for the 2003 dataset was to image and map the offshore palaeo-Arun system. This required high frequencies to resolve the fine detail within the channel. However as mentioned previously (4.4.1), higher frequencies are attenuated more than lower frequencies, and therefore cannot penetrate as deep within the subsurface. This is demonstrated by the 1999 dataset, which used high frequencies (up to 2500Hz) and resolved very fine detail in the shallow channel, but couldn't transmit energy far enough to provide information on the deeper sections of the channel.

The target therefore needs to be considered before designing the acquisition of the survey. The target for the aggregate companies was the first few metres of subsurface, which their surveys accurately imaged. The target for this survey was the base channel as well as the internal stratigraphy infilling the channel, therefore lower frequencies were needed. However the lower frequencies used to image deeper events caused temporal resolution to be lost and resulted in deterioration within the shallow regions of the channel.

The source frequency is therefore very significant and controls the detail imaged by the surveys. The processing vastly improves the image recorded, but if the frequency content is not correct for the survey target no amount of processing will improve the resolution.

Although this survey did record frequencies up to 3000Hz, the data was primarily below 2000Hz, which caused a loss of resolution within the channel fill. The lower frequencies allow penetration up to depths of 150m. This provides an image of the full extent of the channel and also the Tertiary bedrock beneath the channel. Figure 4.55 shows the location and shot points of the two north-south lines that were acquired in the area, with Figure 4.56 showing the single channel sections for both lines. These lines clearly show the extent of the penetration and the complexity of the structure in the region, which as discussed in chapter 3 and 5, is an important control over the valley geometry and hence the fluvial system. It is therefore imperative that the geometry and orientation of faults and folds within the area are adequately imaged. Processing of the new boomer data has enhanced the image of the deeper horizons and allowed such structure to be shown (Figure 4.56)

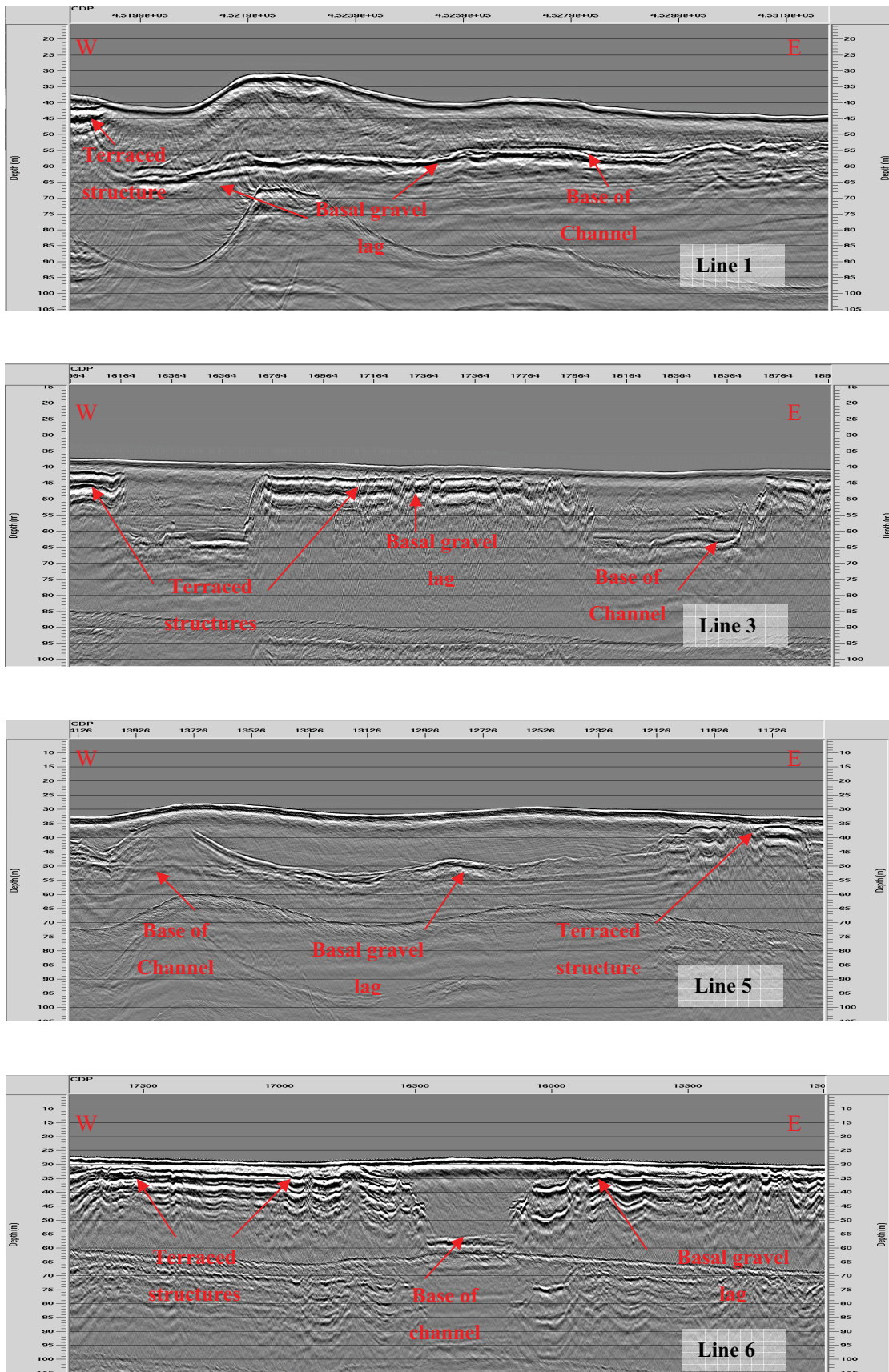


Figure 4.54: Figures shown in 4.49 with archaeological interpretation. Annotated are the locations of possible archaeological resources within the fluvial system.

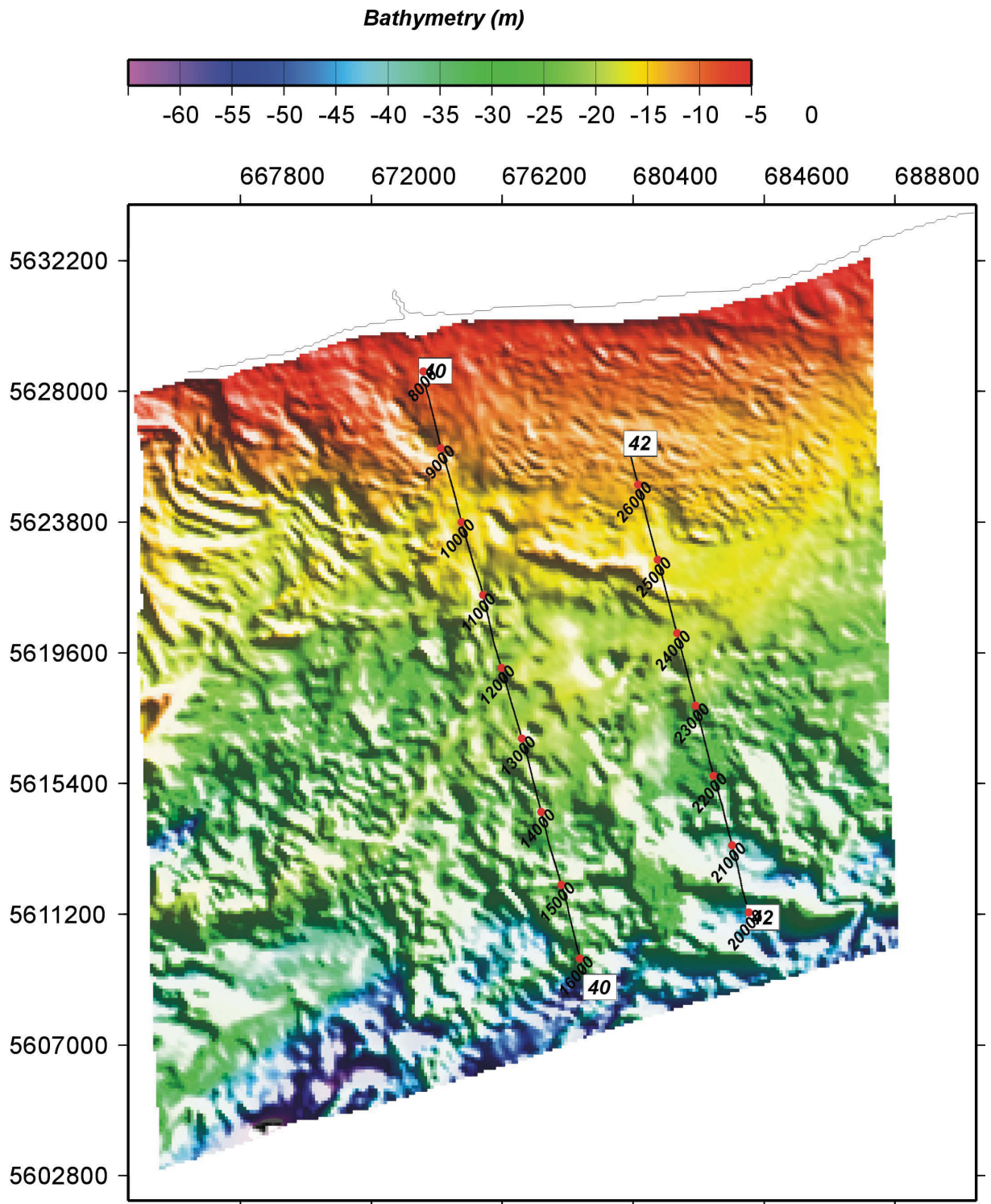


Figure 4.55: The location of the two north-south trending seismic reflection lines acquired in the study area (line 40 and line 42). Shot positions are annotated every 1000. The image is superimposed on the singlebeam bathymetry data, with the coastline position also shown (thin black line).

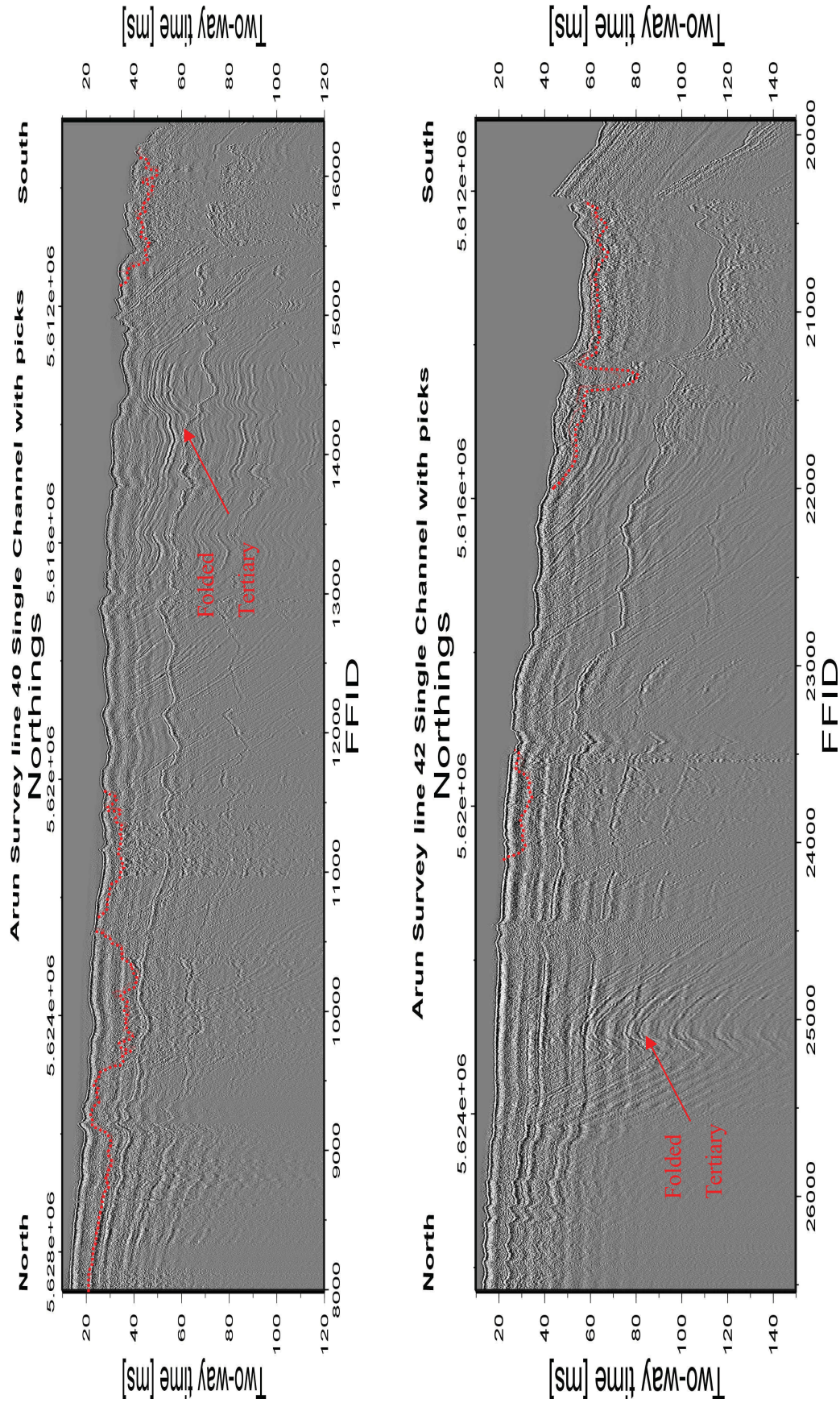


Figure 4.56: Single channel N-S seismic lines showing the extent of penetration and folding of Tertiary bedrock. Dipping reflectors can be traced across the two seabed multiples to the bottom of the section. The channels are interpreted in red.

4.6 SUMMARY OF CHAPTER

Over 650km of high resolution seismic reflection surveys were acquired in April 2003 with the aim of imaging an area of sub-bottom stratigraphy offshore of the Sussex coast. The lines were acquired using a boomer source (frequency range 500-3000Hz) and a recording streamer of 60 hydrophone channels. This allowed for multi-channel processing with velocity determination and depth conversion, permitting comparisons between logged data and seismic sections.

Previous surveys had been completed in the area by aggregates companies, using a boomer source and a single channel receiver. These surveys were in analogue form (paper) and therefore further processing could not be achieved.

The newly acquired lines however were digitally recorded and processed to improve the quality and enhance the reflected arrivals. The comparison between the analogue datasets and the new digitally processed data show the improvements due to post-acquisition processing.

All the new boomer lines had a frequency filter (Butterworth bandpass: 24-150-36-3500) applied to them to reduce the effect of low frequency ambient noise, mainly due to the weather and wave motion. Deconvolution and trace muting was also applied to remove problematic multiples, such as the ghost arrival and high amplitude linear energy, such as the direct wave and refractions.

The use of a multi-channel recording system allowed the data to be transformed from the usual time-offset (t-x) domain, into common mid-point (CMP) bins. Velocity analysis was then performed on these CMP's to determine the velocity structure of the sub-surface. Once the velocities were established, the CMP's could be aligned using the NMO correction and stacked together to produce a seismic stacked section.

Further processing was also applied to the stacked section in the form of migration. This process was performed to suppress any diffracted events that occurred due to undulating and truncated surfaces. The diffractions were especially problematic in the channel areas and therefore needed to be tackled to aid interpretation of the fluvial system.

After completion of the digital processing, the resulting sections were used to locate and constrain any possible archaeological sites. Key areas included:

- Base of channel
- Basal gravel lag
- Terrace structures

- Sediment contact between fluvial (coarse gravels) and transgressive (fine sands) sediments.
- Flood plain locations

The digitally processed data has allowed accurate location of these areas and improved the quality of the reflected horizons by suppressing unwanted high amplitude energy and enhancing the signal.

The channel base was accurately mapped to constrain the course of the Arun palaeo-valley offshore Littlehampton to where it joined the northern palaeo-channel some 20km south. The onshore-offshore correlation was achieved due to the densely spaced survey lines in the northern region of the study area. The interpreted channel picks were then combined with base channel picks from the previous analogue surveys in the area to provide a comprehensive image of the fluvial system for the whole study area.

Comparing the new seismic reflection data with images from the aggregates surveys reveals the improvement due to digital processing. Problematic multiples could be suppressed allowing easier and more accurate interpretation of the enhanced reflectors.

The newly acquired dataset had a lower frequency content than the previous surveys, which resulted in a reduction of resolution in the shallow Quaternary structure. This meant that previous seismic surveys with higher frequency content could resolve more shallow detail and constrain individual cut and infill events within the fluvial channel. The reduction in resolution in the shallow deposits was compensated however, since high frequencies are attenuated more than lower frequencies in the sub-surface therefore the previous surveys could only image to about 30m depth below the seabed. The lower frequency content of the new data provided greater penetration to depths of up to 150m, which allowed deeper Tertiary reflections to be imaged. The data improved the imaging of potential archaeological sites, but also allowed the underlying Tertiary structure to be analysed. This complex structure, including folding and faulting beneath the fluvial system, would have controlled and constrained the course of the Arun palaeo-river and therefore the distribution of archaeological sites. It is therefore extremely important to image and understand the Tertiary structure within the area, which the newly acquired data demonstrates efficiently.

4.7 REFERENCES

- Bevan, B.W.** 1991. The search for graves. *Geophysics*, **56**: 1310-1319.
- Bushe, K.E.A.** 2003. *PSSP Extraction using Towed Streamer Data*. M.Sc. Thesis, Leeds University, Leeds.
- (CEI), C.E.I.** 1977. Cultural resources evaluation of the northern Gulf of Mexico continental shelf.
- Clark, A.J.** 1986. Archaeological geophysics in Britain. *Geophysics*, **51**: 1404-1413.
- Milkereit, B., Mueller, C., Theilen, F. and Bohlen, T.** 2001. Toward High-resolution 3-D marine Seismic Surveying Using Boomer Sources. In: *EAGE 63rd Conference & Technical Exhibition*, pp. 1-5, Amsterdam, The Netherlands.
- Nissen, S.E., Combes, J.M. and Nekut, A.G.** 1999. Acquisition, processing and analysis of shallow high resolution seismic data from the outer continental shelf and upper slope, offshore Louisiana. *Journal of Sedimentary research*, **69**.
- Palmer-Felgate, A. and Pye, J.** 2003. Cruise Report: Joint multibeam, chirp, sidescan and boomer seismic survey of Arun palaeo-river system 7th March - 25th April, Imperial College, London.
- Parasnis, D.S.** 1997. *Principles of Applied Geophysics*. Chapman and Hall, London.
- Sheriff, R.E. and Geldart, L.P.** 1995. *Exploration Seismology*. Cambridge University Press.
- Stright, M.J.** 1986. Evaluation of archaeological site potential on the Gulf of Mexico continental shelf, using high-resolution seismic data. *Geophysics*, **51**.
- Telford, W.M., Geldart, L.P. and Sheriff, R.E.** 1976. *Applied Geophysics*. Cambridge University Press.
- Yilmaz, O.** 1987. *Seismic Data Analysis*, **1**. Society of Exploration Geophysicists.